ABSTRACT

The Seismo-Lineament Analysis Method (SLAM) Applied to the
South Napa Earthquake and Antecedent Events

Victoria E. Worrell, M.S.

Chairperson: Vincent S. Cronin, Ph.D.

Earthquake data from the M 6.0 South Napa Earthquake of 24 August 2014 and other local seismic events were utilized in the Seismo-Lineament Analysis Method (SLAM) to locate seismogenic faults in the Napa Valley. Focal mechanism solutions and the corresponding uncertainties were used to generate seismo-lineaments. Geomorphic analysis and field work located surficial fault-related damage, which was analyzed for trends with previously mapped surface ruptures. GPS strain was calculated in the area to determine regional stress before, during, and after the South Napa earthquake. The seismo-lineament produced for the South Napa earthquake included the areas of known surface rupture after the M 6.0 event. Results also suggest that data from previous earthquakes, especially the M 4.9 Yountville earthquake of 2000, could have been used to identify the western portion of the West Napa fault zone as seismogenic before the South Napa earthquake.

The Seismo-Lineament Analysis Method (SLAM) Applied to the South Napa Earthquake and Antecedent Events

by

Victoria E. Worrell, B.S.

A Thesis

Approved by the Department of Geosciences

_____

Stacy C. Atchley, Ph.D., Chairperson

Submitted to the Graduate Faculty of
Baylor University in Partial Fulfillment of the
Requirements for the Degree
of

Master of Science

Approved by the Thesis Committee

_____

Vincent S. Cronin, Ph.D., Chairperson

_____

Jay Pulliam, Ph.D.

_____

Markus Hunziker, Ph.D.

Accepted by the Graduate School

August 2016

_____

J. Larry Lyon, Ph.D., Dean

Page bearing signatures is kept on file in the Graduate School.

TABLE OF CONTENTS

CHAPTER FIVE

LIST OF FIGURES

Figure Page

LIST OF TABLES

ACKNOWLEDGMENTS

I would like to give the greatest of thanks to the following people for the immense support I received during the completion of this thesis. First of all, thank you to Dr. Vince Cronin for his guidance through this entire process. I appreciate the opportunity to work as his graduate student during my time at Baylor University, and I would have been so lost without his guidance and advice through this time. I would also like to extend thanks to the many institutions that provided financial assistance for the Petroleum Fellowship at Baylor, and special thanks to the Geological Society of East Texas for additional financial support. Thank you to Dakota Draper, my supportive and determined field assistant. Many thanks to the City of Napa for providing me with data about water-line rupture after the South Napa earthquake. I would also like to thank my parents for their immense support through all of the years of my education, even as I moved half-way across the country. Thank you to my husband, John, for being my backbone during this process. Your support and love mean more to me than I could put into words. Most importantly, I have to give the greatest of thanks to my savior, Jesus Christ, for creating this beautiful Earth that we have the privilege of studying every day.

To my mom, my dad, and John. Without your love and support, none of my accomplishments would have been possible.

"Accept the challenges so that you can feel the exhilaration of victory."

- *General George S. Patton*

CHAPTER ONE

Introduction

The Browns Valley section of the West Napa fault was not considered to be active before the M 6.0 South Napa earthquake of 24 August 2014 (Bryant, 2000a; Bryant, 2000b). Wesling and Hanson (2008) investigated the West Napa fault by using stereo aerial photographs at varying scales and field mapping. They interpreted geomorphic features observed in the rural and suburban areas of central Napa to indicate more recent Quaternary activity than had been documented previously. Wesling and Hanson were able to characterize some strands of the West Napa fault that were previously unknown. Some of the strands that ruptured during the South Napa earthquake correlated with these newly-mapped sections of the West Napa fault, but were not considered hazardous prior to the M 6.0 event (USGS, 2015e).

The West Napa fault passes through the Napa Valley and cuts through 2 km of late Pleistocene to Quaternary aged sediments under the valley floor (Wesling and Hanson, 2008; Brocher et al., 2015). The valley is located at the southernmost end of the Mayacamas Mountains and extends from the north at Calistoga to just south of Napa. Bedrock is primarily mapped in the foothills around the basin; deposits range from the Lower Cretaceous Great Valley Sequence (although some Jurassic to Cretaceous aged Franciscan Complex deposits are locally mapped in the surrounding hills) to the Quaternary alluvial and fluvial deposits of the Napa River and its tributaries (Wesling and Hanson, 2008; fig 1).

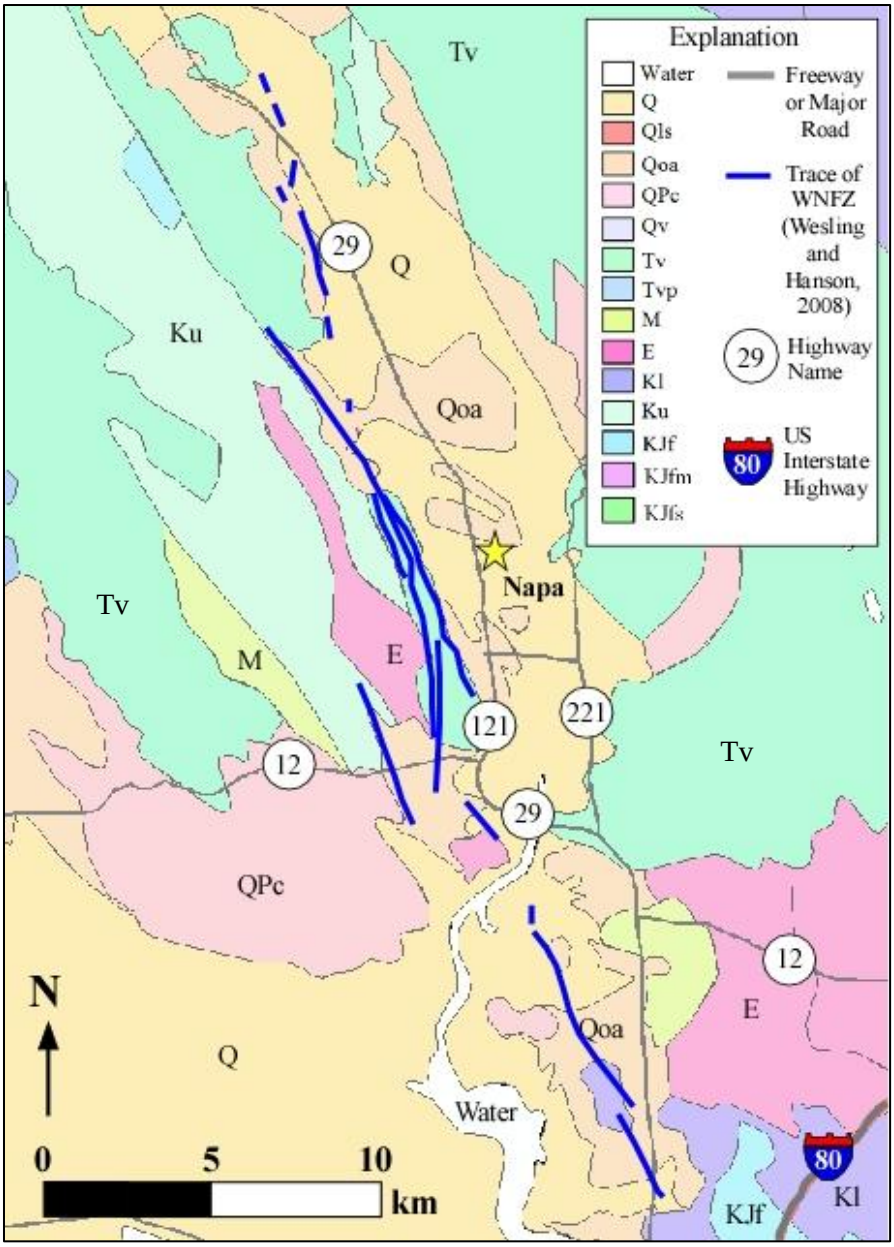

Figure 1. Previously mapped strands of the West Napa fault (Wesling and Hanson, 2008). Basemap data is from ESRI (2015). Geology from Jennings et al. (1977). Geologic Explanations: **Q** – Alluvium, lake, playa, and terrace deposits; unconsolidated and semi consolidated; **Qls** – Selected large landslides; **Qoa** – Older alluvium, lake, playa, and terrace deposits; **QPc** - Pleistocene and/or Pliocene sandstone, shale, and gravels deposits; mostly loosely consolidated; **Qv** – Quaternary volcanic flow rocks; minor pyroclastic deposits; **Tv** – Tertiary volcanic rocks; **Tvp** – Tertiary pyroclastic volcanic rocks; **M** - Miocene marine sandstone, shale, siltstone, conglomerate, and breccias; moderately to well consolidated; **E** - Eocene marine shale, sandstone, conglomerate, and minor limestone; mostly well consolidated; **Kl** – Lower Cretaceous sandstone, shale, and conglomerate; **Ku** – Upper Cretaceous sandstone, shale, and conglomerate; **KJf** – Blueschist and semi-schist of the Franciscan Complex; **KJfm** – Franciscan Complex – metamorphic rocks; **KJfs** – Franciscan Complex – mélange;

The San Francisco Bay area is characterized by many active faults, including the San Andreas fault zone, which is an important part of the transform plate boundary between the North American and Pacific plates (Atwater, 1970). The San Andreas fault system has several active splays north of the Parkfield segment in west-central California that are roughly parallel to one another, including the San Andreas, Hayward, Rogers Creek, Franklin, West Napa, and Green Valley faults (fig. 2). Many devastating earthquakes have occurred within this system of active faults. The 1857 M 7.9 Fort Tejon earthquake created a 350 km long surface rupture along the San Andreas fault (SCEDC, 2013), and the M 7.8 San Francisco earthquake of 1906 resulted in 477 km of surface rupture (Lawson et al., 1908). Data from the 1906 earthquake inspired the elastic-rebound theory used in modern seismological models (USGS, 2012).

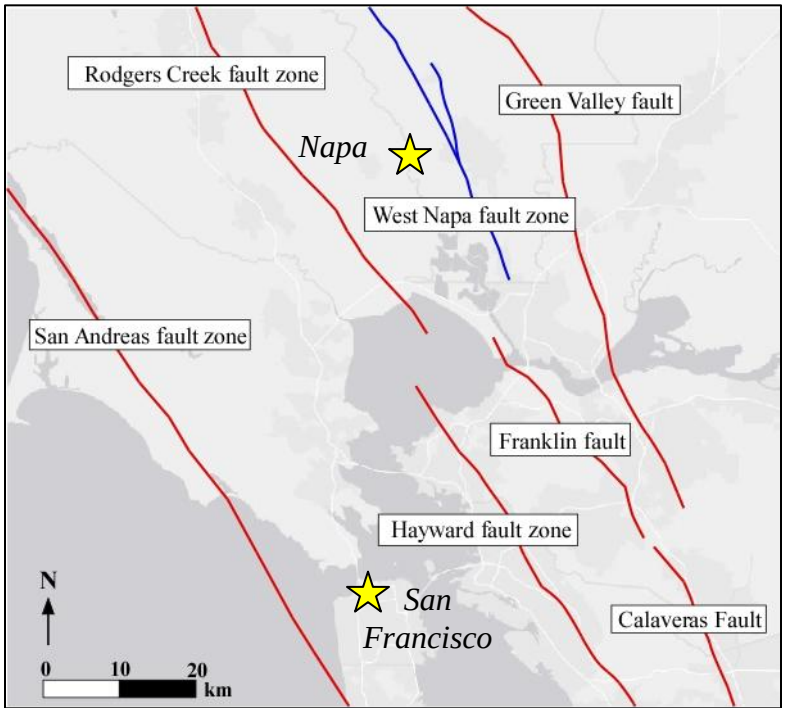

Figure 2. Major faults in the San Francisco Bay area. Fault data is from California Geological Survey (2015). Basemap is from ESRI (2015).

Napa and the surrounding areas were in a state of emergency after the South Napa earthquake (Williams et al., 2014). The seismicity damaged unreinforced masonry buildings in the downtown area of Napa, cracked roads in the suburban and downtown areas of Napa, and destroyed many residential homes (USGS, 2015e). Gas, water, and electric lines were ruptured during the earthquake. Millions of dollars of damage occurred through the area, and many people were injured. One death was recorded because of injuries sustained during the earthquake (EERI, 2014). It is necessary to have better characterization of faults that can produce such great seismicity in order to mitigate damages like these in the future. Better characterization of active faults in the study area will allow for faults to be identified as seismogenic.

Seismogenic faults are those that have produced earthquakes within the recent past. Bryant and Hart (2007) explain that an active fault is defined in the state of California as having displaced the ground surface within approximately the last 11,000 years. Traditional methods of fault characterization are not necessarily the most efficient means of locating active faults in this area. Trenching completed by Wesling and Hanson (2008) in the Napa area revealed the presence of recent fault activity, but shrinking and swelling of soil impeded the ability to determine age and number of faulting events. Cronin et al. (2008) developed a method that allows for identification of potentially seismogenic faults with use of publicly available focal mechanism and hypocenter data: the Seismo-Lineament Analysis Method (SLAM).

SLAM provides potentially valuable information that other fault-investigative and field techniques cannot provide in areas where potential surface traces are obscured by soil, vegetation, or urban cover. SLAM has been used to locate seismogenic faults in

multiple studies, including in the Santa Monica Mountains in southern California (Bayliss, 2007; Millard, 2007; Seidman, 2007), the Northern Arizona Seismic Belt (Lancaster, 2011), and the Tahoe-Truckee area of California and Nevada (Lindsay, 2012; Reed, 2014). SLAM has also proven successful for locating unknown faults in cases where earthquake data did not spatially correlate with known faults. The South Napa earthquake was well located using regional seismograph networks, and there are well-mapped surface ruptures (Morelan et al., 2015; fig. 3), so this is an excellent opportunity to test the effectiveness and utility of the Seismo-Lineament Analysis Method. Data from the M 6.0 South Napa earthquake, as well as from 3 smaller-magnitude events that also occurred on 24 August 2014, are analyzed using SLAM to determine if the results correlate with the surface rupture recorded immediately after the South Napa earthquake.

This thesis seeks to evaluate whether information from smaller-magnitude, antecedent earthquakes could have been used to identify the unmapped strand of the West Napa fault zone as seismogenic before the M 6.0 South Napa earthquake. Five smaller-magnitude earthquakes ($M < 4.0$) that occurred in the Napa area prior to 24 August 2014 are investigated to see if their seismo-lineament solutions spatially correlate with the surface ruptures from the South Napa earthquake along the trace of the active strands of the West Napa fault.

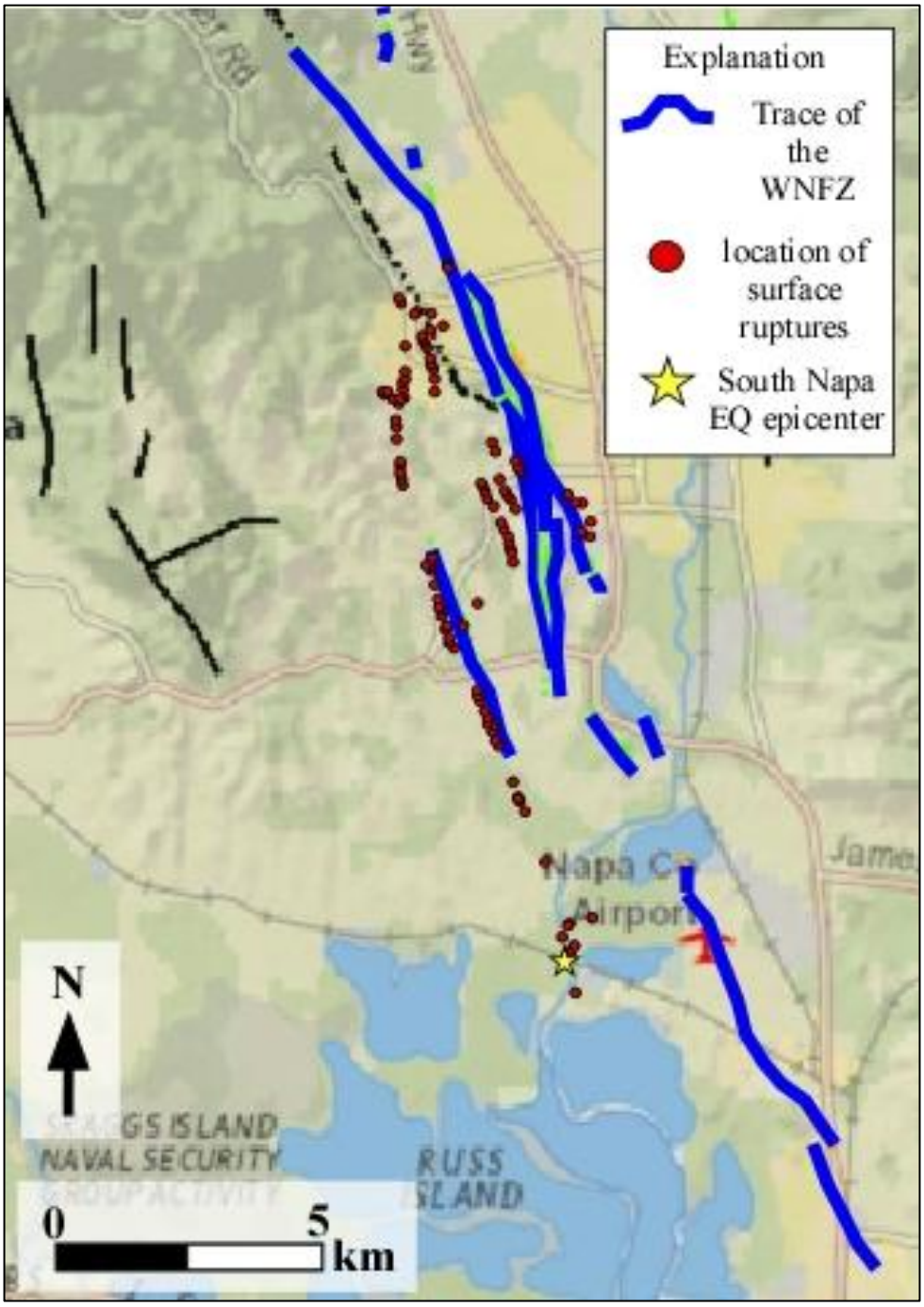

Figure 3. Surface ruptures of the South Napa earthquake compared to the previously-mapped sections of the West Napa fault zone (Miller, 2014). Surface rupture data is from the USGS, California Geological Survey, and Morelan et al. (2015). Basemap is from USGS (2015d).

CHAPTER TWO

Background

The West Napa fault is divided into two main sections: the southern Airport section and the northern Browns Valley section (fig. 4; USGS, 2015d). The sections were first mapped by Weaver (1949), but were named the West Napa fault zone by Helley and Herd (1977). Both sections of the fault are dextral strike-slip faults. The average strike of the Browns Valley Section is 342°, with dips ranging from 75° to 90° (Bryant 2000a, 2000b). The Browns Valley displayed most recent deformation in the Late Quaternary (<130 ka). The Airport section has an average strike of 334°, with vertical dips, and was most recently deformed in the latest Quaternary (<15 ka; Bryant 2000a, 2000b). No earthquakes with M > 6.0 are associated with the West Napa fault zone (Wesling and Hanson, 2008).

The South Napa earthquake resulted in right-lateral strike-slip movement along the Browns Valley strand of the West Napa fault. Geoscientists inferred that the South Napa earthquake occurred along the West Napa fault immediately after the main shock because it is the only strike- slip fault in the area (USGS, 2015d). The epicenter of the South Napa earthquake lies approximately 1.7 km west of the nearest known trace of the fault (Brocher et al., 2015). Other larger-magnitude events have occurred in the area in recent years. Figure 5 displays all the earthquakes adjacent to the West Napa fault from January 1996 to January 2016. The M 4.9 Yountville earthquake of 2000 was located approximately 12.6 miles northwest of the South Napa earthquake epicenter along the

north-northwest trend of the West Napa fault zone, and was initially reported to have occurred along a western strand of the Browns Valley Section of the West Napa fault zone. The event produced minor damage to buildings in downtown Napa and injured 25 people (Miranda and Aslani, 2000).

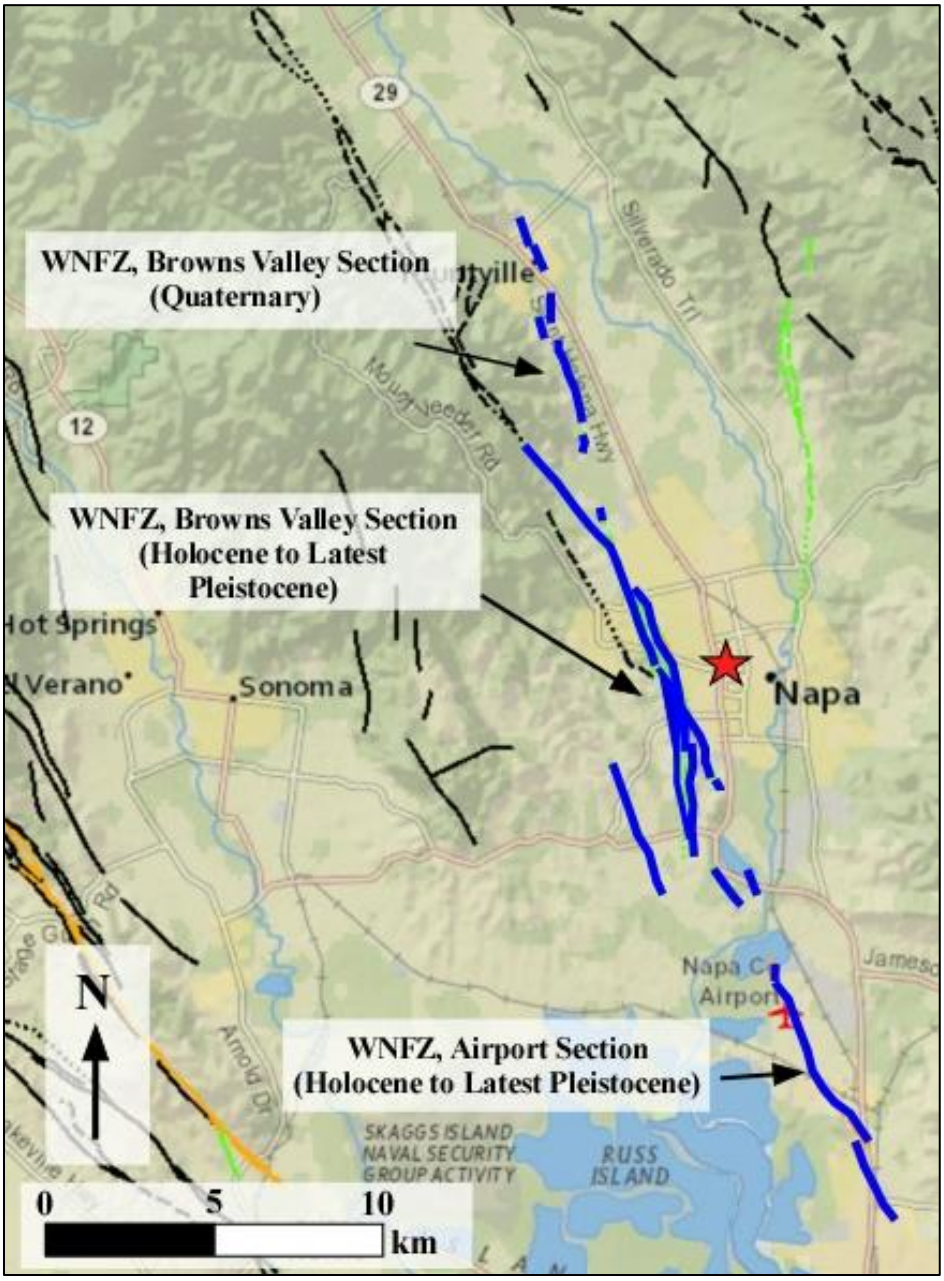

Figure 4. Sections of the West Napa fault zone. Basemap is from USGS (2015d).

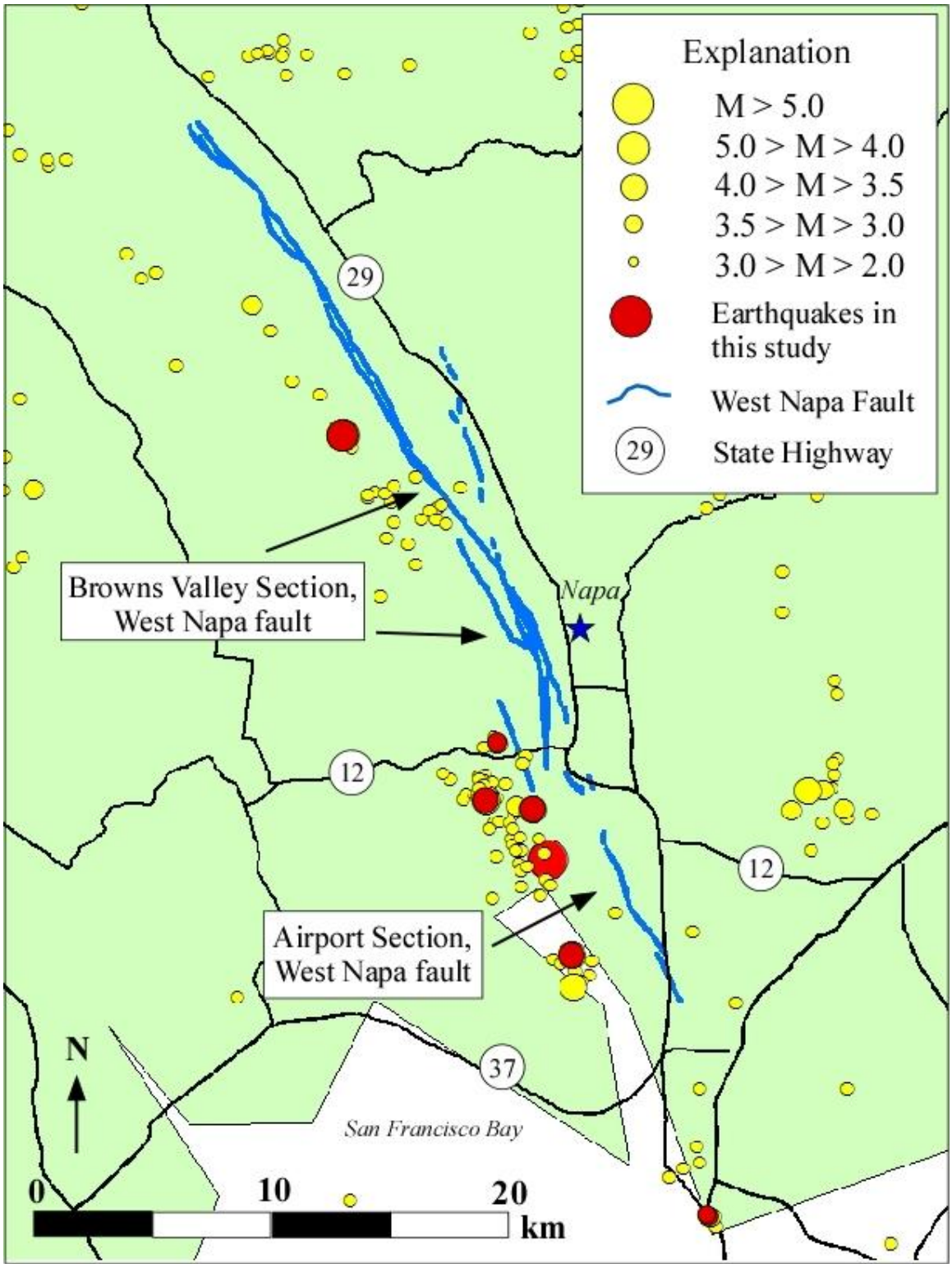

Figure 5. Locations of earthquakes adjacent to the West Napa fault from1 January 1996 to 1 January 2016. Fault location from Jennings (1994). Earthquakes from USGS (2015a).

Very little annual slip has occurred along the strands of the West Napa fault in the past (Figuers, 1991; Geomatrix, 1998; Unruh et al., 2002; Kelson et al., 2005; Wesling and Hanson, 2008). No known creep occurred from 1979-1999 (Galehouse and Lienkaemper, 2003), but slip has been measured more recently. The California Department of Conservation (2015) indicates a slip rate of 1 (± 1) mm/yr of slip along the West Napa fault, and Bryant (2000a) indicates a slip rate from 0.2 to 1.0 mm/yr along both the Browns Valley and Airport sections of the fault. Slip of the fault is determined through geomorphic studies of the area and general orientation of the West Napa fault zone (Bryant, 2000b). Up to 20 cm of slip was observed in surface ruptures created during the South Napa earthquake (Morelan et al., 2015). An unusual amount of afterslip occurred in the days following the event, which increased the total slip to 46 cm (Brocher et al., 2015). This event provided researchers the unique opportunity to observe surface rupture and test various reconnaissance methods (Morelan et al., 2015; Barnhart et al., 2015). In this study, the locations of surface ruptures collected immediately after the event are compared to the results of a seismo-lineament analysis.

CHAPTER THREE

Methods and Analytical Techniques

Earthquake Data Acquisition

The area of this study is bounded by latitudes 38° 40’ 30” N and 38° 04’ 00” N and longitudes 122° 49’ 00” W and 122° 04’ 30” W (approximately 42 miles north-to-south and 41 miles east-to-west, or 1697 mi²). The size of the study area was calculated by computing the lateral distance from the epicenter of the South Napa earthquake to the surface trace of a gently inclined nodal plane so that all possible seismo-lineament solutions could be observed. A $\frac{1}{3}$ arc-second digital elevation model (DEM) with ~ 10 meter resolution was used as a base map for this study. The DEM was obtained from the US National Map Viewer (USGS, 2015c) in ArcGRID format, then converted to an ASCII DEM. The conversion workflow is described in video format by Chris Breed of the Center for Spatial Research at Baylor University (available at http://croninprojects.org/Vince/SLAM/SLAMWorkflow.html). The DEM was then thinned and cropped for use in the SLAM code in accordance with the SLAM workflow (Cronin, 2014c). No map stitching was necessary for this study, as the entire study area fit within the boundaries of the single DEM. Appendix A contains all SLAM codes utilized in this study (also available via http://croninprojects.org/Vince/SLAM/CurrentBaseCodes.html).

The focal mechanism solutions, hypocenter locations, and uncertainties in strike and dip of nodal planes for all earthquakes in this study were obtained from the Northern

California Earthquake Data Center earthquake catalog (NCEDC, 2015). Earthquake information for each event in this study is presented in Tables 1 and 2. Events are labeled in Table 2 according to the date and time of the earthquake (yyyyMMddhhmm). Focal mechanism solutions utilized in this study are mapped in Figure 6.

Table 1. Earthquake and Hypocenter Location Data

Year	Mo.	Day	Hr	Min	Sec	Lat. (°N)	Long. (°E)	Depth (km)	Mag	EH1 (km)	EH2 (km)	EH1 az (°)	EZ (km)
2014	8	26	12	33	16.94	38.17058	-122.28996	10.183	3.9	0.026	0.026	90	0.026
2014	8	24	12	47	12.58	38.23362	-122.33619	7.961	3.6	0.02	0.02	90	0.021
2014	8	24	10	21	45.51	38.23206	-122.31974	9.121	3.81	0.014	0.014	90	0.014
2014	8	24	10	20	44.15	38.20666	-122.29787	8.919	6.02	0.028	0.028	90	0.029
2012	2	16	17	13	20.82	38.07991	-122.22500	5.886	3.54	0.031	0.022	90	0.041
2012	2	16	2	9	14.29	38.07697	-122.22435	5.941	3.55	0.026	0.023	90	0.036
2000	9	3	8	36	30.22	38.37731	-122.40205	8.226	4.9	0.029	0.018	83	0.029
1990	10	14	2	6	21.16	38.04987	-122.23091	7.296	3.5	0.02	0.012	60	0.029
1990	6	11	9	7	26.32	38.3674	-122.39333	7.56	3.5	0.022	0.016	83	0.029

Earthquake data from NCEDC (2015); relocated hypocenters and given uncertainties by Waldhauser (2015).

Table 2. Fault Plane Solutions and Uncertainties

Origin Date and Time yyyyMMddhhmmss	Dip Direction (°)	Dip Angle (°)	Rake (°)	Strike Uncertainty (°)	Dip Uncertainty (°)	Rake Uncertainty (°)
201408261233	085	90	180	5	38	25
201408241247	274	81	-155	13	35	25
201408241021	090	90	-90	40	25	50
201408241020	075	85	-170	5	10	25
201202161713	330	80	0	10	40	25
201202160209	055	90	180	10	45	25
200009030836	240	90	165	3	15	5
199010140206	240	90	155	8	38	15
199006110907	238	80	170	8	30	25

Focal mechanism uncertainties from NCEDC (2015).

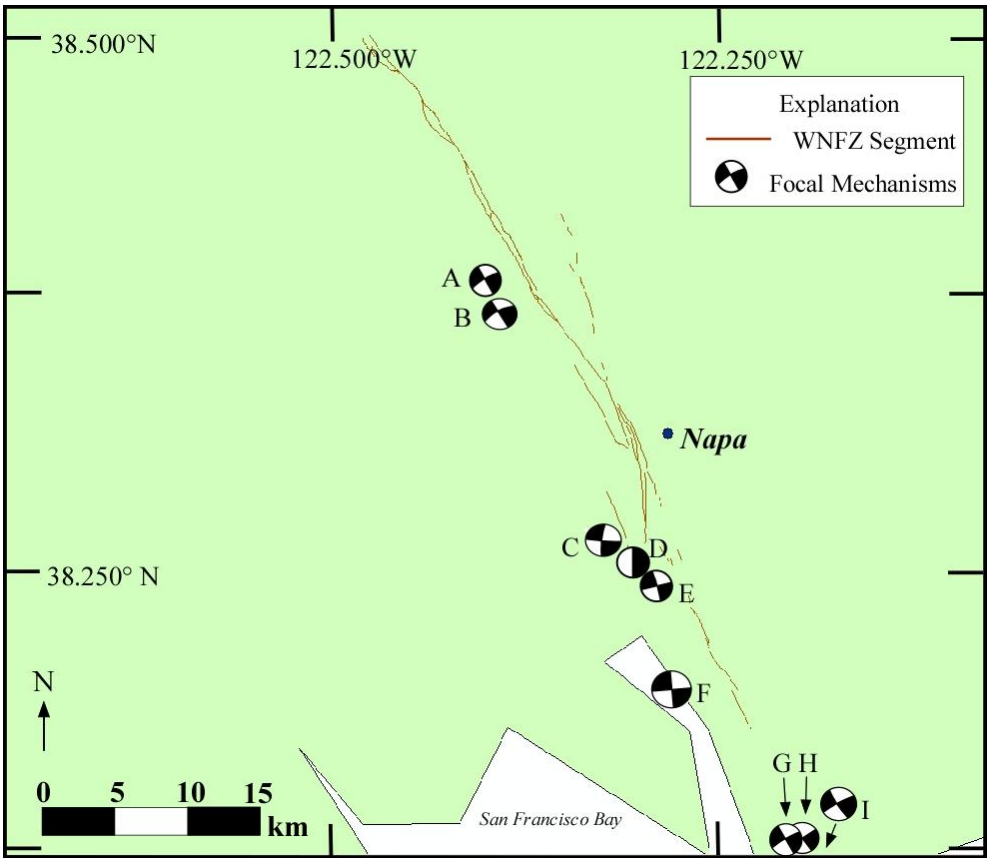

Figure 6. Focal mechanisms for earthquakes in this study. Events were chosen by magnitude and proximity to the sections of the West Napa fault zone. (A) M 4.9 Yountville earthquake of 03 September 2000; (B) M 3.5 earthquake of 11 June 1990; (C) M 3.6 earthquake of 24 August 2014; (D) M 3.81 earthquake of 24 August 2014; (E) M 6.0 South Napa earthquake of 24 August 2014; (F) M 3.9 earthquake of 26 August 2014; (G) M 3.55 earthquake of 16 February 2012; (H) M 3.54 earthquake of 16 February 2012; (I) M 3.5 earthquake of 14 October 1990.

Morelan et al. (2015) conducted a field investigation the morning of the South Napa earthquake and mapped surface ruptures and other earthquake-related deformation. Surface ruptures were mapped along the West Napa fault zone, recording location data, orientations, and photograph evidence. Surface rupture locations and previously known faults from the USGS Quaternary Fault and Fold Database (2015d) were used in both *Google Earth* and *ArcGIS* software for visualization and later compilation of surface ruptures in this project.

Seismo-Lineament Analysis

The Seismo-Lineament Analysis Method has been used to locate faults for events with magnitudes a little as M 2.9. Data required for input into SLAM includes location data for an earthquake hypocenter (latitude, longitude, depth in km, and associated uncertainties), a focal mechanism solution for the event (nodal plane strike, dip, rake, and associated uncertainties), and a DEM of the study area. Appendix B gives an example of the *Microsoft Excel* spreadsheet used as input for the SLAM code in this study.

The uncertainties associated with the vertical and horizontal location of the earthquake hypocenter can be represented in 3D space by an uncertainty ellipsoid (fig. 7). The uncertainties associated with a nodal plane include a dip-angle uncertainty and a strike uncertainty. We simultaneously accommodate all of these uncertainties, for the hypocenter and nodal plane, and find the intersection of all possible nodal planes with the ground surface. That intersection is called a seismo-lineament (fig. 8). Seismo-lineaments with non-zero uncertainties in nodal plane orientation will always appear bow-shaped. The epicenter of the earthquake is located within or adjacent to the thinnest section of the seismo-lineament (Cronin, 2014b). The SLAM code outputs two seismo-lineaments (one for each nodal plane) for an earthquake. For this project, only the north-northwest oriented seismo-lineaments that were produced were studied because of regional trends of fault orientation in the San Andreas fault system. If the hypocenter and focal mechanism are sufficiently accurate, and if the fault is approximately planar and reaches the ground surface, then the ground surface trace of the fault should be located within the seismo-lineament (Cronin, 2014b).

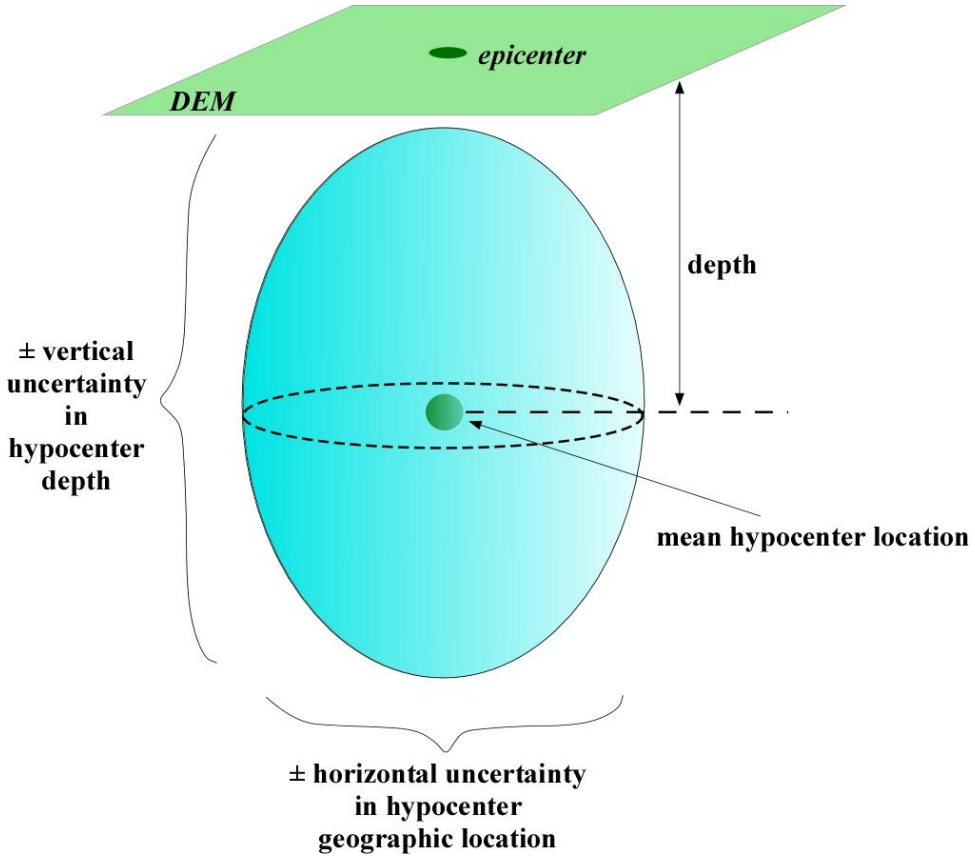

Figure 7. Three-dimensional uncertainty ellipsoid around an earthquake hypocenter, formed with the vertical and horizontal uncertainties in hypocenter location.

Seismo-lineaments were determined for nine events: the M 6.0 earthquake of 24 August 2014, three subsequent earthquakes that occurred very soon after the 24 August 2014 earthquake (ranging from M 3.6 – M 3.9), two M 3.5 events from 2012, the M 4.9 Yountville earthquake, and two M 3.5 events from 1990. The events other than the South Napa earthquake were chosen because of their epicenter location along the approximate trend of the West Napa fault zone.

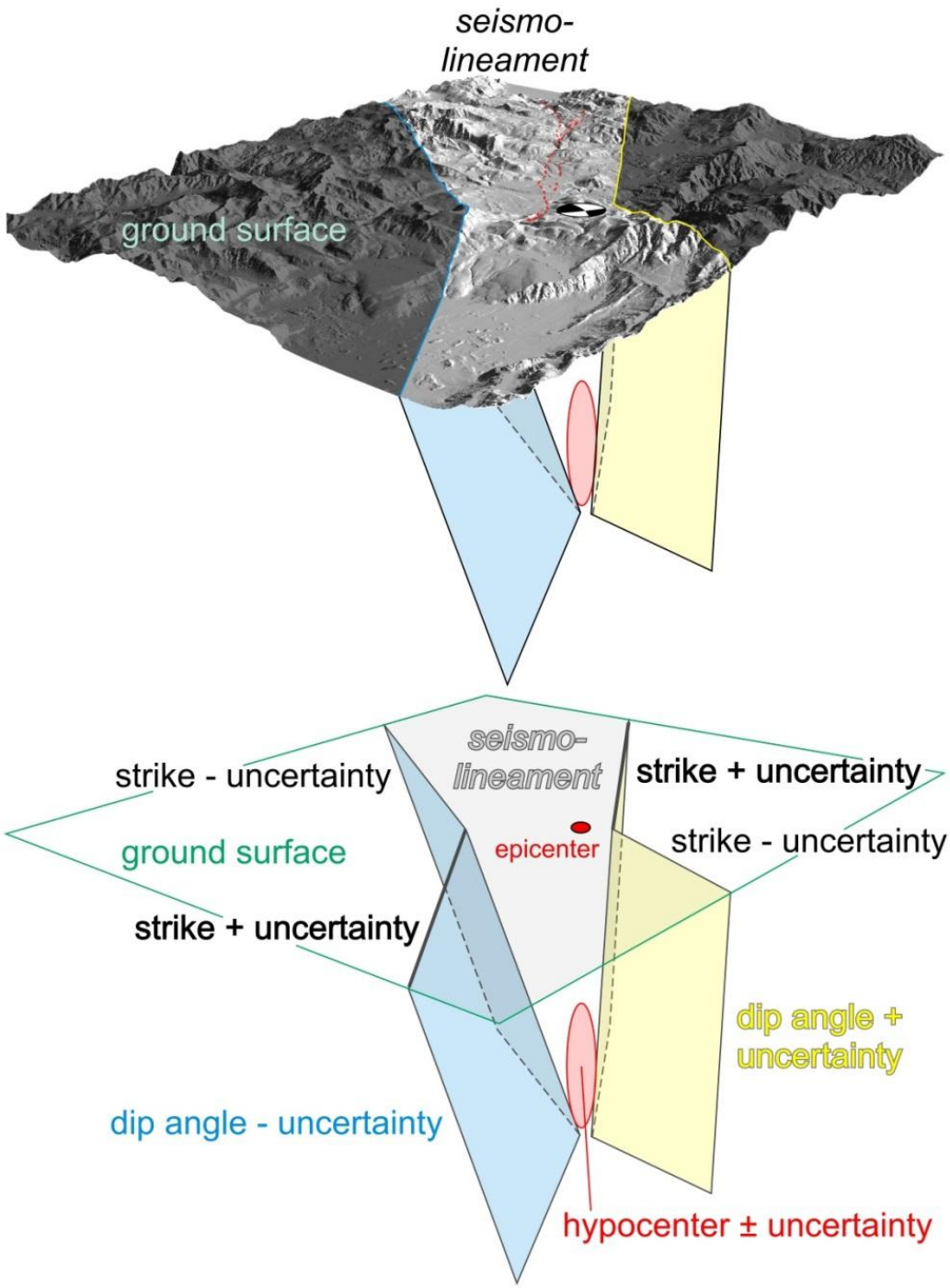

Figure 8. Visualization of the seismo-lineament swath associated with a single nodal plane. The volume between the blue and yellow surfaces contains all possible orientations of that nodal plane, considering the hypocenter location uncertainties and the nodal plain orientation uncertainties. The intersection of this uncertainty volume and the ground surface is the seismo-lineament. This swath represents the ideal area to search for the surface expression of a fault.

Geomorphic Analysis

A geomorphic analysis was conducted within each of the north or northwest-trending seismo-lineaments using a hillshade map created from the full-resolution DEM. Using a hillshade map has several advantages over aerial photography (Cronin et al., 2008). The orientation of light can be manipulated to highlight geomorphic features that might relate to faulting. A hillshade map only contains information about the shape of the land surface and location, and does not include unrelated data that may distract the investigator's eye, such as buildings or roads. The DEM was illuminated at a low angle (~ 15°) orthogonal to the average orientation of the seismo-lineaments (~ 240° from N) to highlight geomorphic features in a north-northwest trend using the *MakeLitHillshade Mathematica* notebook (see Appendix B). The hillshade DEM was then imported into *ArcGIS* v. 10.1.

Features were selected using the guidelines of features distinguishable in aerial imagery described in Cronin et al. (2008). Frequently observed attributes in the study area are characterized in detail in the guidelines described by Cronin et al. (2008):

a. linear trends observed in vegetation;

b. lineations consisting of vegetation or soil formed by local soil moisture variation;

c. variation in the concentration or health of vegetation along a lineation;

d. a combination of soil, rock, or vegetative influence that creates any linear boundary in the tone or texture of the land surface;

e. aligned stream segments of a lower order on opposite sides of a higher-order segment

f. long, linear segments of a stream channel, or aligned segments of a stream channel

g. obvious lateral deflection of a stream channel or a ridge crest

h. ridges that align in an *en echelon* manner

Lineaments were selected in *ArcGIS* by creating a new shapefile, then editing the shapefile to add lines that represent geomorphic lineaments. Lineaments were selected within each seismo-lineament by highlighting linear features that were parallel (± uncertainties) to the mean nodal plane of each seismo-lineament. The geomorphic interpretations were compared to the aerial imagery and confirmed to be unassociated with any man-made features. The geomorphic analysis layer was converted to .kmz format and imported into *Google Earth* for use during field work.

GPS Strain Analysis

The San Francisco Bay area is densely monitored by GPS networks (fig. 9), including instrumentation associated with the EarthScope Plate Boundary Observatory (PBO; UNAVCO, 2014) and the Bay Area Regional Deformation Network. GPS data is available before and after the South Napa earthquake, and is used to compare the change of strain in the Napa area caused by the earthquake.

GPS data has been used to determine the crustal strain of an area in many previous studies (i.e., Caporali, 2003; Kahle et al., 1997; Gan et al., 2000). The Infinitesimal Strain Primer available via Cronin (2014a) describes the process of using GPS data to calculate strain for both 1-, 2-, and 3-dimensional circumstances. GPS velocity data from a triangle of GPS sites are used to calculate average instantaneous crustal strain within the triangle. Recognizing that we are concerned with strike-slip earthquakes, and that the vertical component of GPS velocity is the most poorly

constrained, we follow common practice and only use the horizontal components of velocity to compute crustal strain.

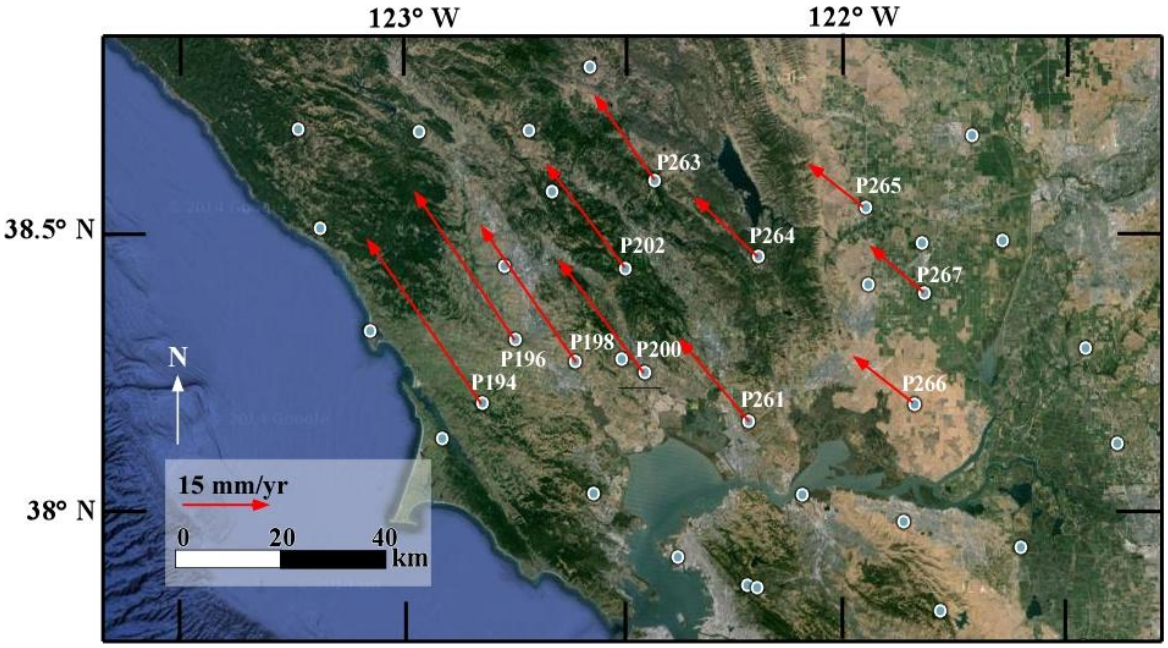

Figure 9. Locations of GPS sites used in this study with GPS velocities recorded prior to the M 6.0 South Napa Earthquake. The sites used in this study are labeled. The GPS velocities recorded are provided in the GPS Strain module packet, available at http://www.unavco.org/education/resources/educational-resources/lesson/majors-gps-strain/napa/napa.html.

Resor et al. (2014) created a new teaching module in conjunction with UNAVCO concerning utilization of publicly-available GPS data to determine strain in the area of the South Napa earthquake. The teaching module provides an activity packet, as well as two spreadsheets containing GPS data of interseismic velocities and coseismic offsets during the South Napa earthquake. Using a strain calculator written in Excel by Cronin (2014a), available via http://www.unavco.org/education/resources/educational-resources/lesson/majors-gps-strain/module-materials/gps-triangle-strain-calculator.xlsx, interseismic deformation (deformation occurring between seismic events) and coseismic deformation (deformation occurring during a seismic event) were computed for five

triangles of GPS sites (fig. 10). Input data were obtained from UNAVCO (2014), and are presented in Appendix C.

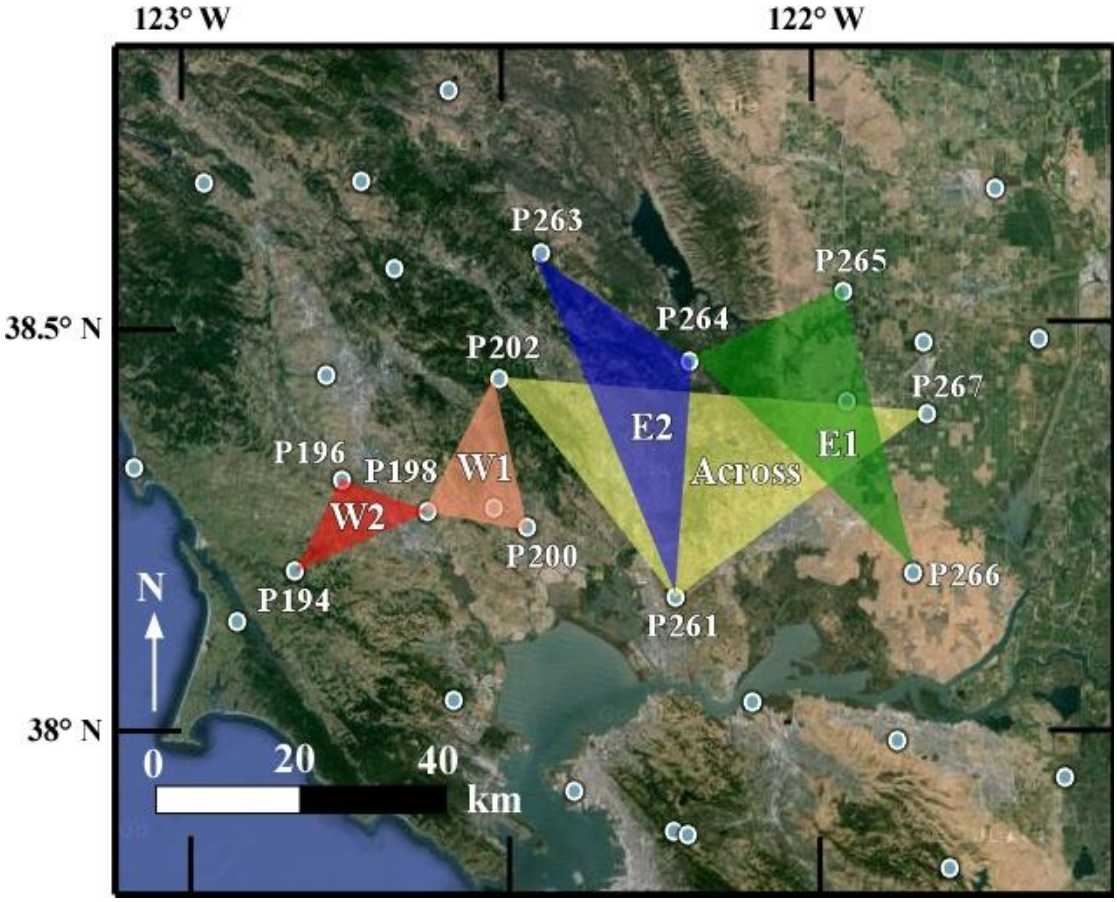

Figure 10. Groups of GPS points used for GPS strain analysis, grouped into sets of three and named by proximity to the West Napa Fault Zone. Groups are labeled by relative orientation to the fault zone (E = East, W = West, Across = Crosses the fault zone.)

Field Work

Field work was conducted in the Napa area from May to June of 2015. Field work in a SLAM study is usually intended to find the surface trace of a fault that is spatially correlated with an earthquake. In this study, the fault that produced the earthquake ruptured the ground surface, and the locations of those ruptures were already known in the early summer of 2015. The goal of field work in this thesis was to examine the previously mapped locations of ground rupture and develop a better understanding of

features to look for in future earthquakes where SLAM is used to identify the area in which to search for the trace of the causative fault.

Geomorphic maps and seismo-lineaments were imported into *Google Earth* for mobile access in the field. Geomorphic lineaments that were identified during the geomorphic analysis were investigated, as were the field sites investigated by Morelan et al. (2015). The majority of data were collected within the urban and suburban areas of Napa, where damage from the South Napa earthquake had not yet been repaired. Rural areas were often privately-owned, and therefore, were inaccessible. For this reason, some data utilized in this study is derived from studies completed immediately after the earthquake, when these locations were inaccessible (Morelan et al., 2015; USGS, 2015b; California Earthquake Clearinghouse, 2015; Boatwright et al., 2015). Information about infrastructure damaged immediately after the earthquake, as well as information about repairs completed in the months following the event, was provided by the City of Napa.

Most of the observed damage was in the form of displaced or folded roads, sidewalks, and curbs, or damaged public buildings, water lines, and private residences. The city of Napa began repairing damage to infrastructure immediately after the South Napa earthquake, and was continuing to do so in June of 2015. Figure 11 gives an example of some of the repairs completed after the South Napa earthquake.

Field equipment included Brunton compasses, measuring tapes, and GPS units. Features that may be useful for identification of an active fault were recorded in the field, and photographs were recorded of all significant sites. All of the features were easily accessible by road or short hike. Due to the extent of private land ownership in the Napa area, it was difficult to investigate geomorphic lineaments in the most northern sections

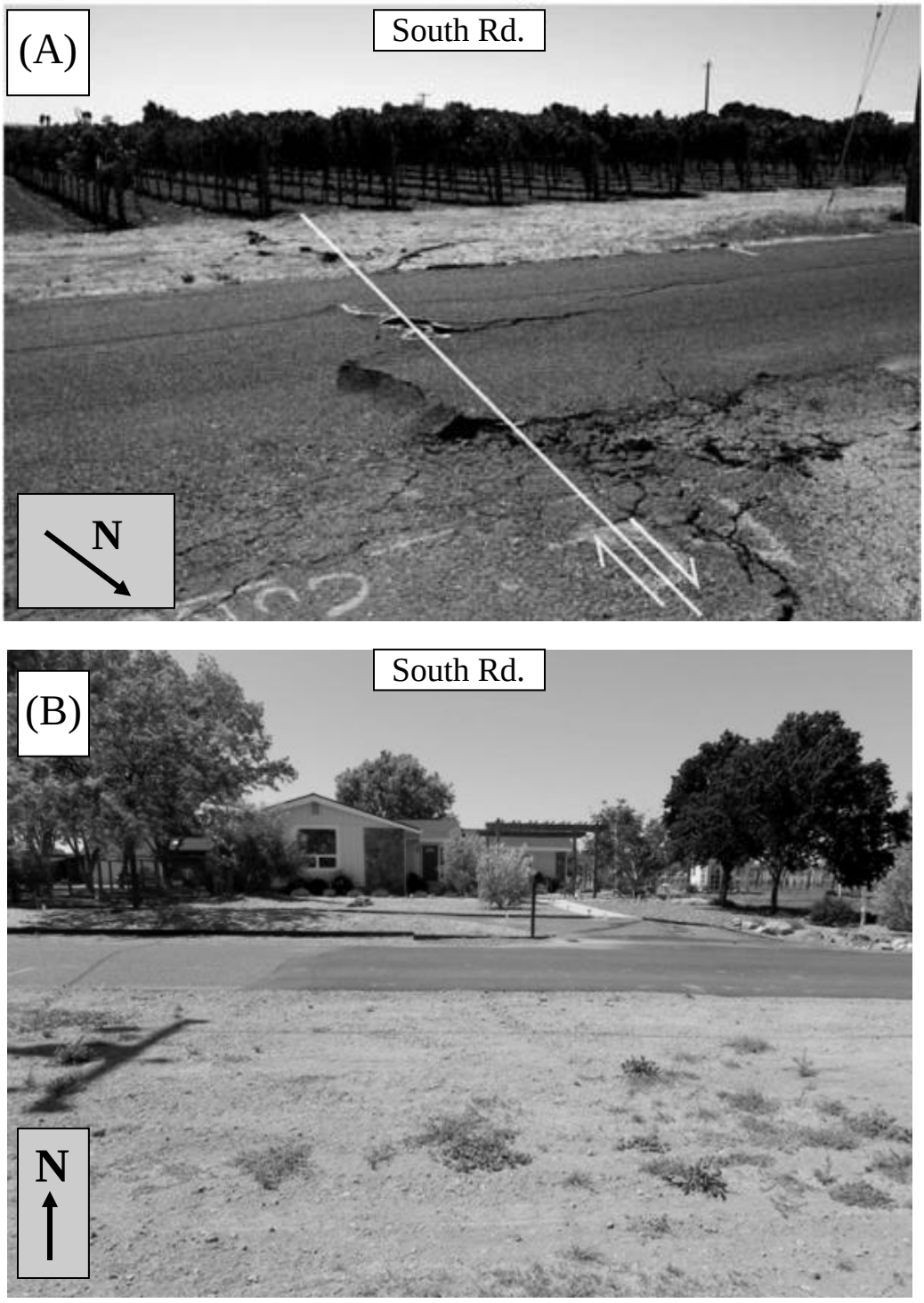

Figure 11. Examples of earthquake damage repaired in the Napa area. (A) Crack across South Road as observed immediately after the South Napa earthquake in August 2014, modified from Morelan et al. (2015). (B) Viewing the area from the opposite side of the road, it is evident that the damaged section of road has been patched. Patching is characteristic of many repairs in the Napa area, and was helpful in identifying areas in the field where rupture could have been seen immediately after the earthquake.

of the study area. Bearings of cracks and other linear fault-related damage were recorded by azimuth. Offsets in roads, sidewalks, and curbs were recorded with offset magnitude and orientation. Because much of the data was located in the suburbs and neighborhoods around Napa, no lithologies were available. Data concerning water line breaks was provided by the city of Napa and was mapped for spatial analysis.

Fisher Statistics

Fisher (1953) established a means of determining an average of a unimodally distributed set of data. Cronin (2008) adapted Fisher's statistical methods to be applied to multiple geologic measurements made on the same geologic surface (i.e., bedding, the vector normal to a fault plane, or shear lineations). Lineament orientations obtained during field work were analyzed using Fisher statistics and computed to a 90% confidence interval in order to maintain consistency with 90% confidence in earthquake data uncertainties (NCEDC, 2015). Appendix D gives an example of a computation of Fisher statistics using data obtained in the field research of this study and a *Mathematica* code for computation (Cronin, 2011).

CHAPTER FOUR

Results

Seismo-Lineaments

The objectives of this seismo-lineament analysis are (1) to test whether a seismo-lineament of the South Napa earthquake encompasses the segments of the West Napa fault that generated the earthquake, and (2) to evaluate whether seismo-lineaments from earthquakes recorded prior to 24 August 2014 might have led to the interpretation that the West Napa fault is seismogenic. Nine seismo-lineaments were created for earthquakes 201408261233, 201408241247, 201408241021, 201408241020, 201202161713, 201202160209, 200009030836, 199010140206, and 199006110907 (Tables 2 and 3). The seismo-lineament solutions for all nine earthquakes in this study are considered spatially correlated to the causative strand of the West Napa fault, and are presented in Figures 12-15.

Each seismo-lineament is displayed on the same DEM basemap so that all solutions can be compared within the study. The colored regions in Figures 12 through 15 mark the seismo-lineament. The trace of the mean nodal plane for each solution is displayed as a black line through the middle of each seismo-lineament. Swath width varies as a function of the dip of the nodal plane and the uncertainties in nodal plane orientation and hypocenter location. Steeper dip and less uncertainty result in thinner seismo-lineaments.

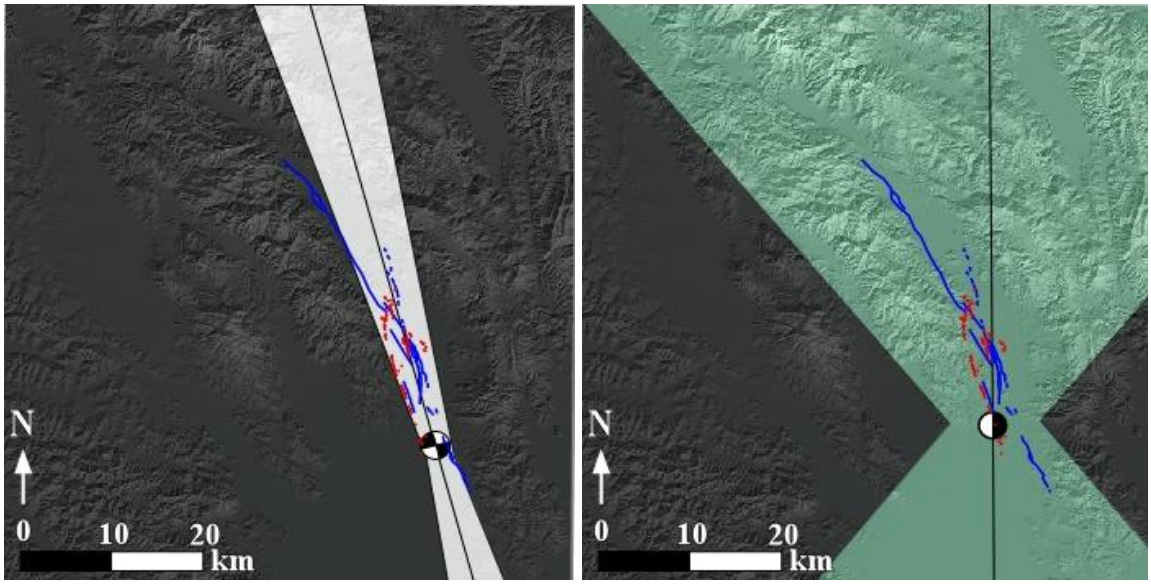

(A) (B)

Figure 12. Seismo-lineament solutions for the (A) M 6.0 South Napa earthquake of 24 August 2014 and (B) M 3.81 earthquake of 24 August 2014. Surface traces of faults in the West Napa fault system are shown in blue (USGS, 2015d). Surface ruptures recorded after the South Napa earthquake are recorded in red (Eidenger, 2015; Morelan et al., 2015).

M 6.0 South Napa Earthquake of 24 August 2014 (201408241020)

The seismo-lineament for the M 6.0 South Napa earthquake is spatially correlated with the West Napa fault zone. All of the surface ruptures recorded along the trace of the West Napa fault after the South Napa earthquake and the majority of the strands in the Browns Valley section of the West Napa fault are within the seismo-lineament for the South Napa earthquake (fig. 12-A). The seismo-lineament is subparallel to the trend of the entire West Napa fault. The uncertainties in nodal plane orientation are small, so the swath is relatively thin.

M 3.81 Earthquake of 24 August 2014 (201408241021)

The seismo-lineament for the M 3.81 event is spatially correlated with both the surface ruptures from the South Napa earthquake and the entire West Napa fault (fig. 12-

B). The focal mechanism solution for the earthquake is not that of a strike-slip fault. This earthquake occurred one minute after the South Napa earthquake, and its mean hypocenter location is just 3.4 km from that of the main shock; however, the focal mechanisms indicate that these earthquakes occurred on different faults. This might indicate that this event occurred because of slip-transfer after the South Napa earthquake. The uncertainties associated with the nodal plane orientations are large, which creates a much wider swath than was observed for the M 6.0 event.

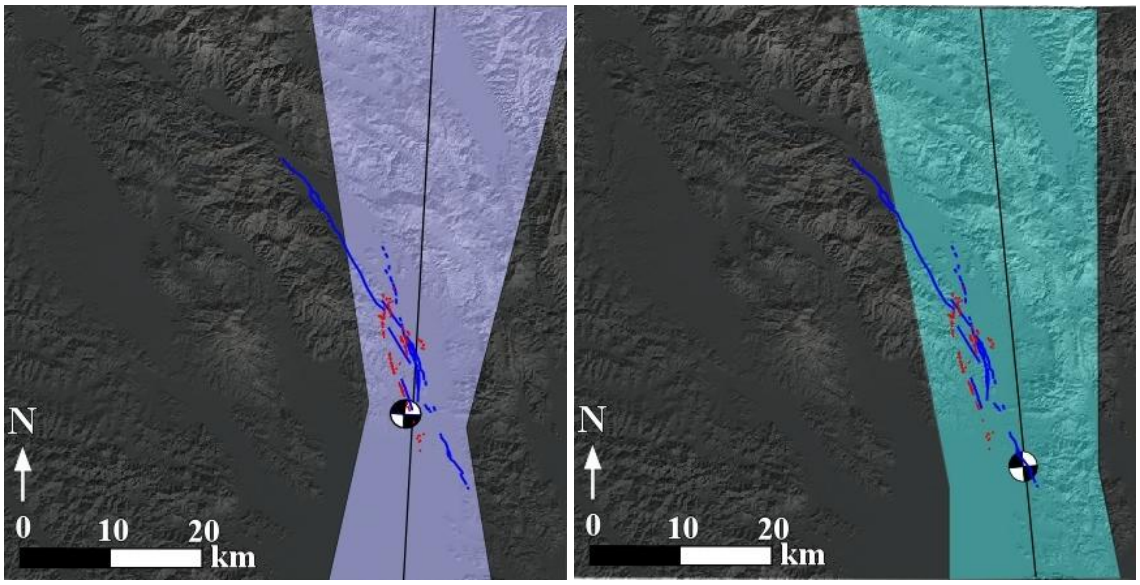

(A) (B)

Figure 13. Seismo-lineament solutions for the (A) M 3.6 earthquake of 24 August 2014 and (B) M 3.9 earthquake of 26 August 2014. Surface traces of faults in the West Napa fault system are shown in blue (USGS, 2015d). Surface ruptures recorded after the South Napa earthquake are recorded in red (Eidenger, 2015; Morelan et al., 2015).

M 3.6 Earthquake of 24 August 2014(201408241247)

The seismo-lineament for the M 3.6 earthquake includes all the surface ruptures from the South Napa earthquake, as well as the majority of the West Napa fault, so the event is considered spatially correlated to the West Napa fault (fig. 13-A). The seismo-

lineament is oblique to the trend of the West Napa fault, which may have affected the utility of this solution for location of the causative fault of the South Napa earthquake. The focal mechanism solution for the event indicates a strike-slip event.

M 3.9 Earthquake of 26 August 2014(201408261233)

All surface ruptures from the South Napa earthquake and most of the West Napa fault are included within the seismo-lineament for the M 3.9 event (fig. 13-B). The seismo-lineament is subparallel to the trend of the West Napa fault. The focal mechanism for the earthquake indicates a strike-slip event. The uncertainties in hypocenter location are larger for this event than for the M 6.0 event, which creates a wider seismo-lineament.

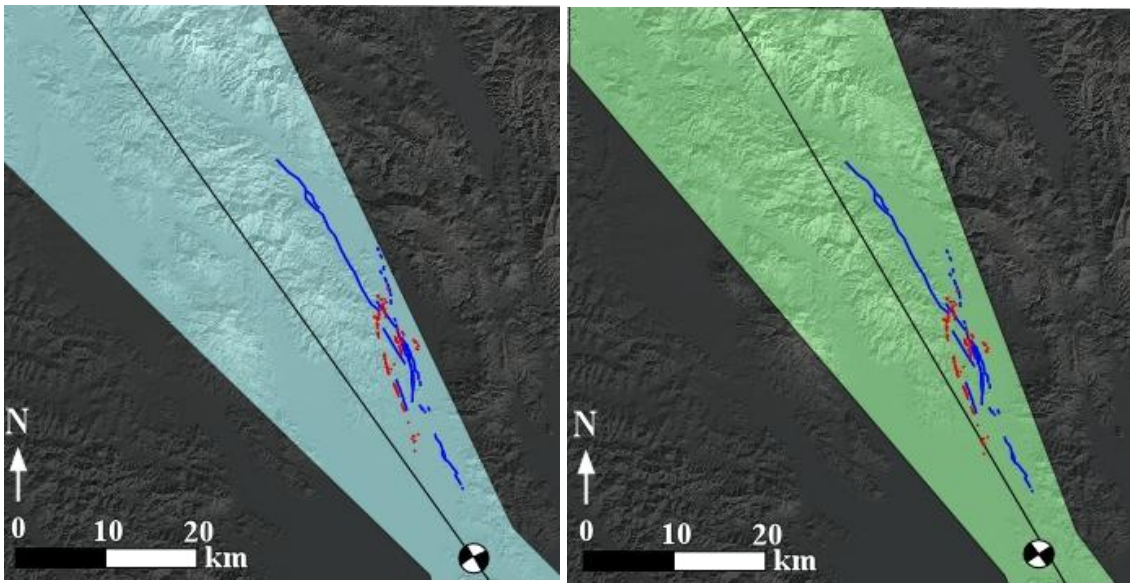

(A) (B)

Figure 14. Seismo-lineament solutions for the (A) M 3.55 earthquake of 16 February 2012 and (B) M 3.54 earthquake of 16 February 2012. Surface traces of faults in the West Napa fault system are shown in blue (USGS, 2015d). Surface ruptures recorded after the South Napa earthquake are recorded in red (Eidenger, 2015; Morelan et al., 2015).

M 3.55 Earthquake of 16 February 2012 (201202160209)

The seismo-lineament for the M 3.55 earthquake of 2012 is sub-parallel to the orientation of the West Napa fault (fig. 14-A). The seismo-lineament includes all of the surface ruptures and the entire length of the West Napa fault, so the solution is considered spatially correlated. The seismo-lineament indicates a strike-slip event, but the epicenter is located considerably further south than the epicenter of the South Napa earthquake.

M 3.54 Earthquake of 16 February 2012 (201202161713)

All of the surface ruptures from the South Napa earthquake and the entire length of the West Napa fault are located within the seismo-lineament for the M 3.54 solution (fig. 14-B). The focal mechanism indicates a strike-slip event, and the epicenter is located considerably further south than the epicenter of the South Napa earthquake. Compared to the seismo-lineament for 201202160209, this seismo-lineament solution trends more parallel to the trend of the West Napa fault.

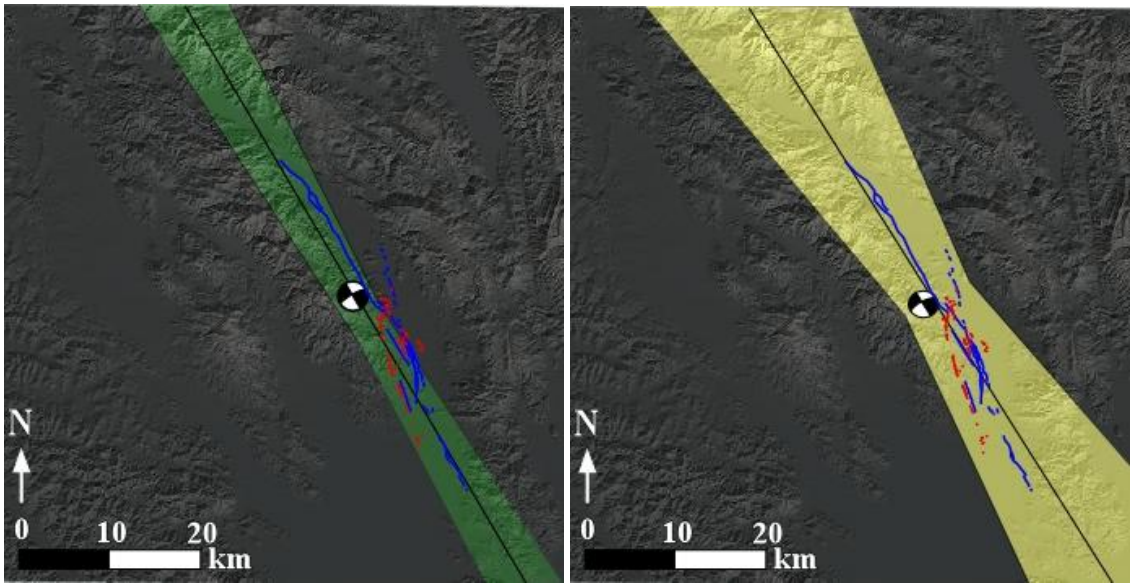

(A) (B)

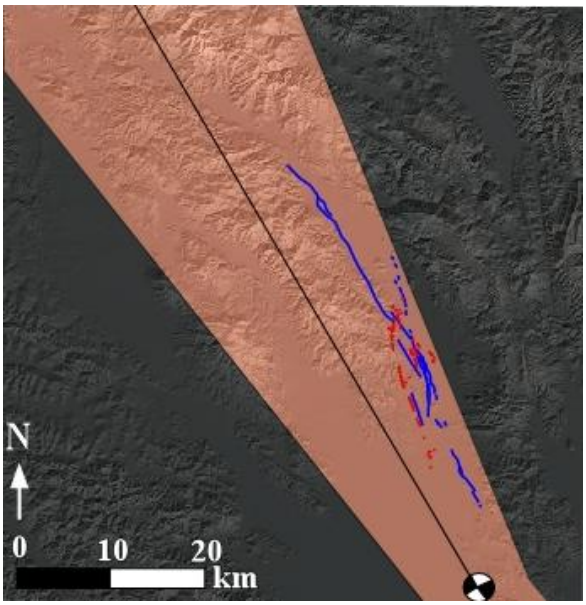

(C)

Figure 15. Seismo-lineament solutions for the (A) M 4.9 Yountville earthquake of 3 September 2000, (B) M 3.5 earthquake of 11 June 1990, and (C) M 3.5 earthquake of 14 October 1990. Surface traces of faults in the West Napa fault system are shown in blue (USGS, 2015d). Surface ruptures recorded after the South Napa earthquake are recorded in red (Eidenger, 2015; Morelan et al., 2015).

M 4.9 Yountville Earthquake of 3 September 2000 (200009030836)

The seismo-lineament for the M 4.9 Yountville earthquake (fig. 15-A) encompasses almost every surface rupture of the South Napa earthquake, and nearly all the sections of the West Napa fault that are also within the seismo-lineament for the South Napa earthquake. The focal mechanism solution for the Yountville earthquake indicates a strike-slip event.

M 3.5 Earthquake of 11 June 1990 (199006110907)

The seismo-lineament solution for the 11 June 1990 earthquake encompasses all of the surface rupture from the South Napa earthquake and the entire West Napa fault (fig. 15-B). The focal mechanism indicates a strike-slip event, and the epicenter is located ~1.5 km from the epicenter of the Yountville earthquake. The trend of the seismo-lineament is parallel to the trend of the West Napa fault.

M 3.5 Earthquake of 14 October 1990 (199010140206)

All surface ruptures from the South Napa earthquake and the entire West Napa fault are located inside the seismo-lineament for the 14 October 1990 earthquake (fig. 15-C). The focal mechanism solution for the event indicates a strike-slip event, but the epicenter is located much further south than that of the South Napa earthquake. The event is considered spatially-correlated with the West Napa fault. The seismo-lineaments for both M 3.5 events of 1990 are shown together in Figure 16. The north-western portion of the seismo-lineament for the M 3.5 earthquake of 11 June 1990 is fully encompassed by the seismo-lineament for the M 3.5 earthquake of 14 October 1990.

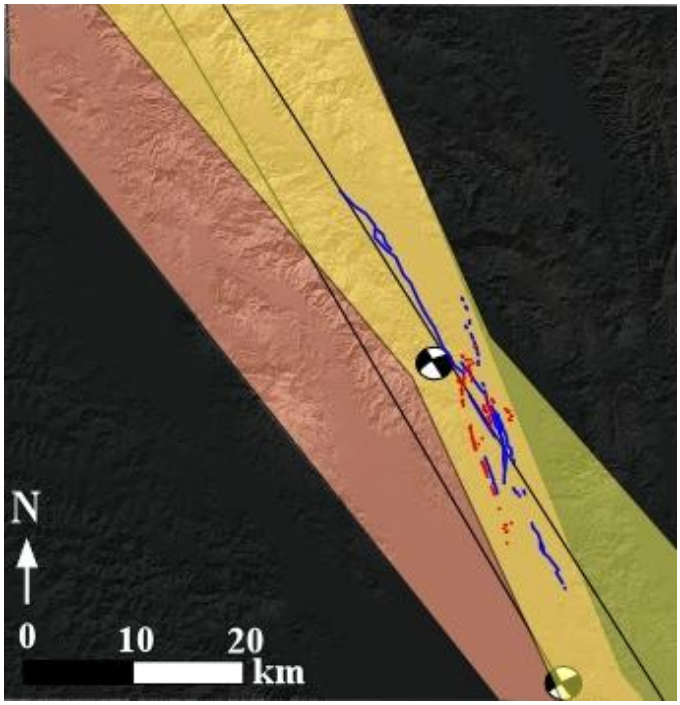

Figure 16. Swaths for the M 3.5 earthquakes of 1990, relative to the West Napa fault zone and surface ruptures (USGS, 2015d; Eidenger, 2015; Morelan et al., 2015).

Geomorphic Analysis

Geomorphic lineaments were identified within each seismo-lineament on a 2-meter resolution hillshade map created from the cropped (but not thinned) DEM for this study. Each seismo-lineament was investigated independently for lineaments that paralleled average nodal plane trend, plus or minus uncertainties. Results were compiled and imported into Google Earth as a .kml file for use during field work. The geomorphic lineaments for each seismo-lineament are presented in Figures 17-19.

The area within each seismo-lineament was examined separately to identify geomorphic lineaments that might be related to active faulting. Many of the geomorphic lineaments identified in the seismo-lineament for the South Napa earthquake (fig. 17-A) are coincident with the West Napa fault (fig. 20). The geomorphic lineaments identified within the swaths for the M 3.81, M 3.6, and M 3.9 earthquakes of 24 and 26 August

2014 extend across broad swaths and display a wide range of strike trends because of the relatively large uncertainties in their respective focal mechanisms (figs. 17-B through D). In Figures 17-B and C, the seismo-lineaments are more oblique than parallel to the West Napa fault. The geomorphic lineaments within these swaths that are less parallel to the orientation of the West Napa fault were not imported for use during field work, as they are representative of the greater errors in each solution.

The geomorphic lineaments identified within each of the other seismo-lineaments vary significantly. The majority of the lineaments identified in the seismo-lineaments for the M 3.5 earthquakes of 2012 (fig. 18-A and B) are the same because the lineaments cover a very similar area and are at nearly parallel orientations. Some seismo-lineament swaths shared a set of geomorphic lineaments, which suggests a relationship between the earthquakes. Figure 21 combines the seismo-lineaments for the Yountville and South Napa earthquakes and highlights the geomorphic lineaments shared between both swaths. All of the geomorphic lineaments identified within the seismo-lineament of the South Napa earthquake can also be identified in the Yountville seismo-lineament (fig. 18-C). The seismo-lineaments for the 1990 earthquakes (fig. 18-D and 19) do not cover the same areas at this scale and do not share as many geomorphic lineaments as the 2012 events.

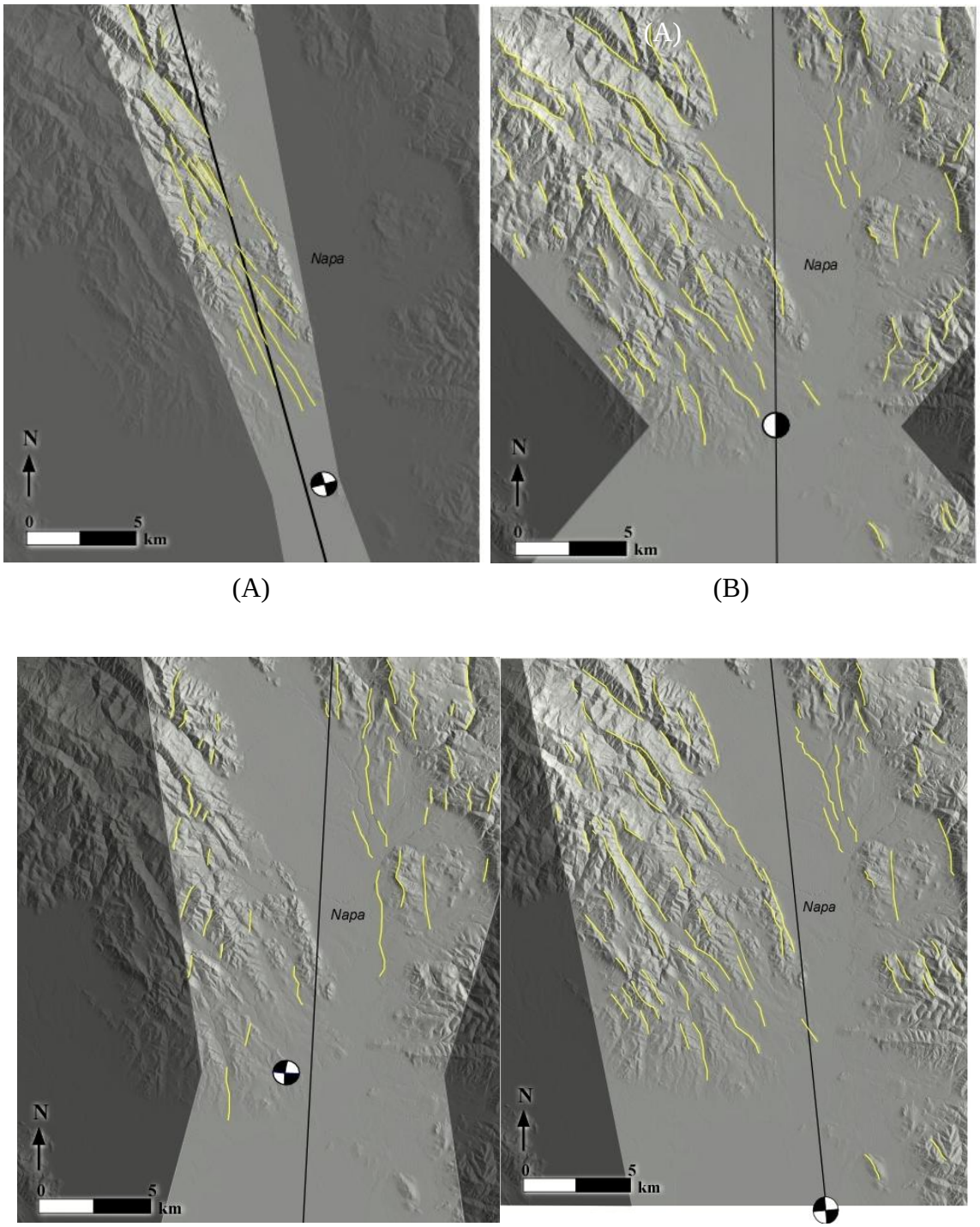

Figure 17. Geomorphic lineaments within the seismo-lineament for the (A) M 6.0 South Napa earthquake of 24 August 2014, (B) M 3.81 earthquake of 24 August 2014, (C) M 3.6 earthquake of 24 August 2014, and (D) M 3.9 earthquake of 26 August 2014.

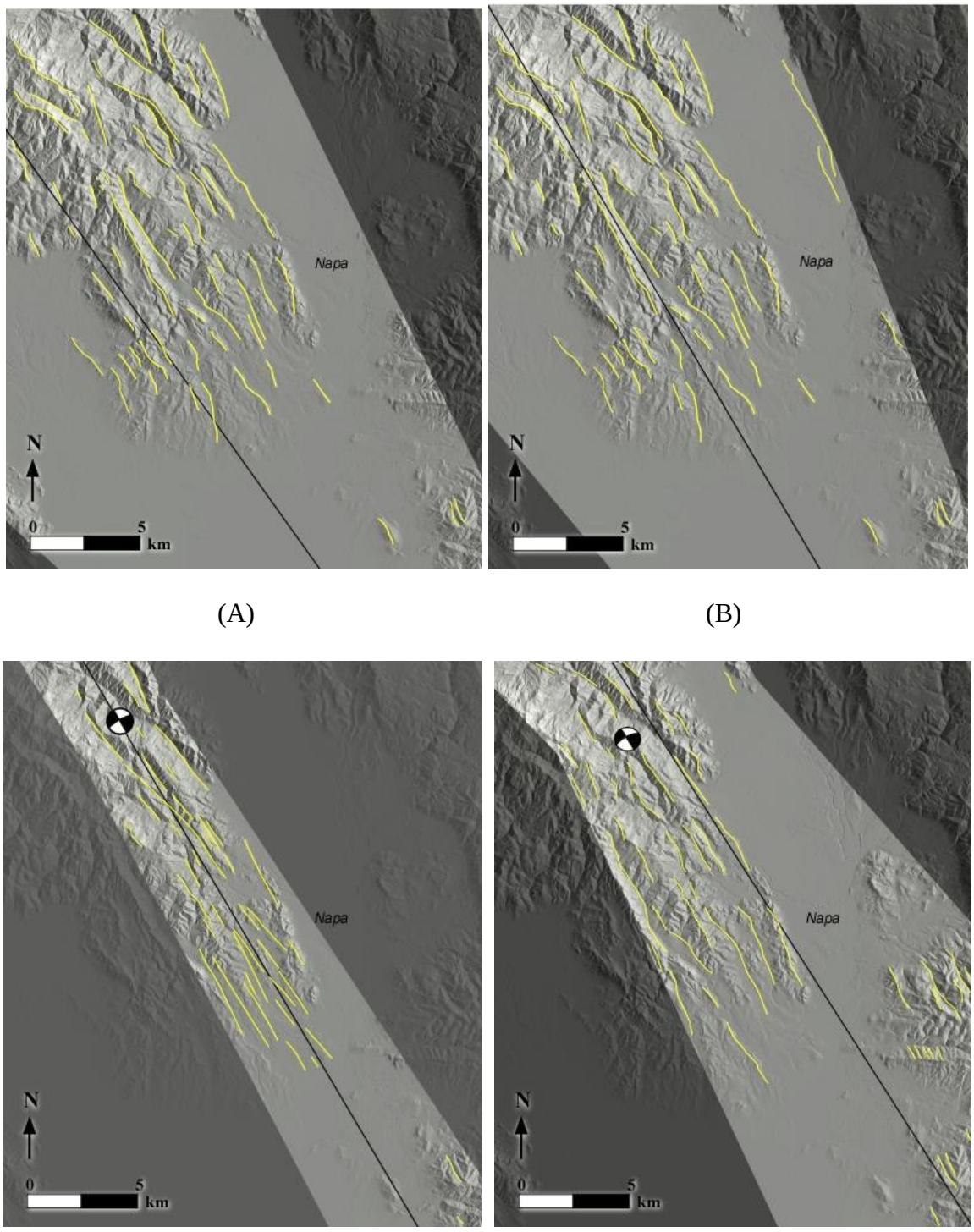

Figure 18. Geomorphic lineaments within the seismo-lineament of the, (A) M 3.55 earthquake of 16 February 2012, (B) M 3.54 earthquake of 16 February 2012, (C) M 4.9 Yountville earthquake of 3 September 2000, and (D) M 3.5 earthquake of 11 June 1990.

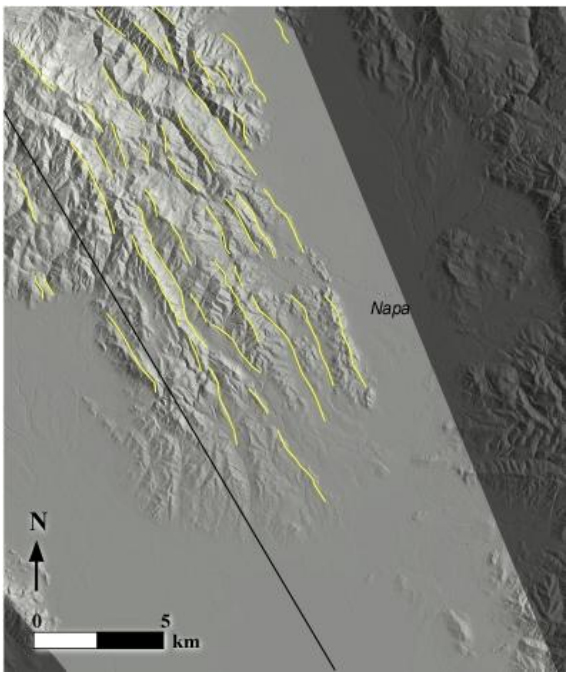

Figure 19. Geomorphic lineaments within the seismo-lineament of the M 3.5 earthquake of 14 October 1990.

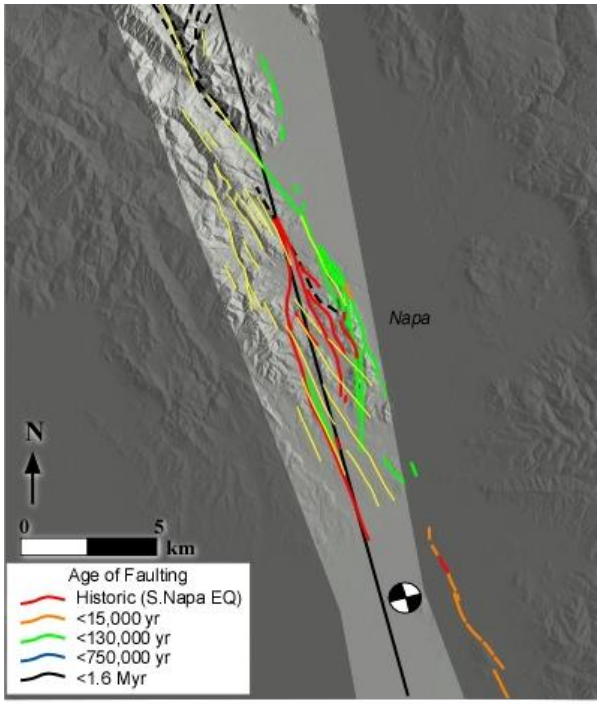

Figure 20. Geomorphic lineaments identified within the seismo-lineament of the South Napa earthquake compared to sections of the West Napa fault, shown with previously mapped sections of the West Napa fault zone (USGS, 2015d) and newly ruptured sections of the West Napa fault zone as of the South Napa earthquake (Brocher et al., 2015).

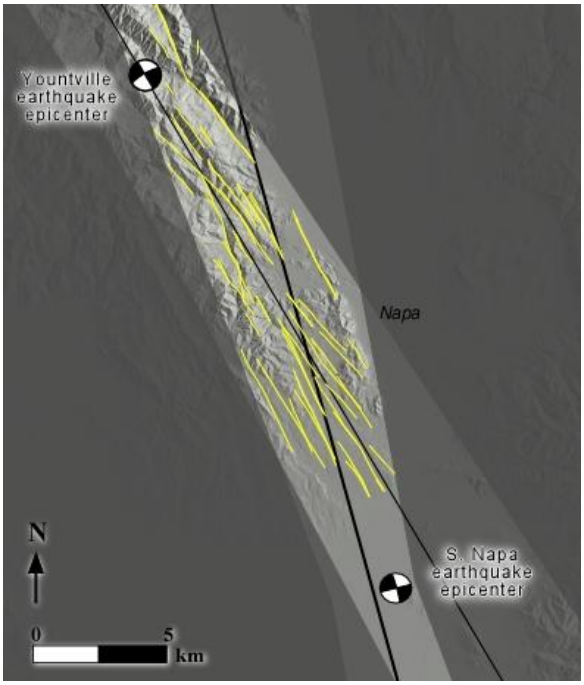

Figure 21. Seismo-lineaments for the M 4.9 Yountville earthquake of 3 September 2000 and the M 6.0 South Napa earthquake of 24 August 2014 with corresponding shared geomorphic lineaments.

Field Work

The majority of fault-related deformation observed in the field was in the form of breaks and cracks in pavement, sidewalks, and curbs (fig. 22). Linear trends in patching of damaged roads and curbs were also considered when original cracks had been repaired. Los Carneros Avenue adjacent to Stone Bridge School was the site of a major road crack (fig. 22-B). City officials were very concerned about the severity of the rupture because of the natural gas pipeline that runs under the property (Kelson and Wesling, 2015). The rupture was marked to record continued offsets (fig. 22-C). The origin of the lines and the dates they were created are unknown. The amount of offset of each mark could be associated with the time at which it was created, but the different colors display varying amounts of offset along the rupture, which complicates dating the marks. Tented sidewalks were very prevalent in the neighborhoods surrounding Napa

(fig. 22-D). The structures were sometimes associated with large trees whose roots had slightly cracked or uplifted the sidewalk before the South Napa earthquake. The damage was amplified during and after the South Napa earthquake.

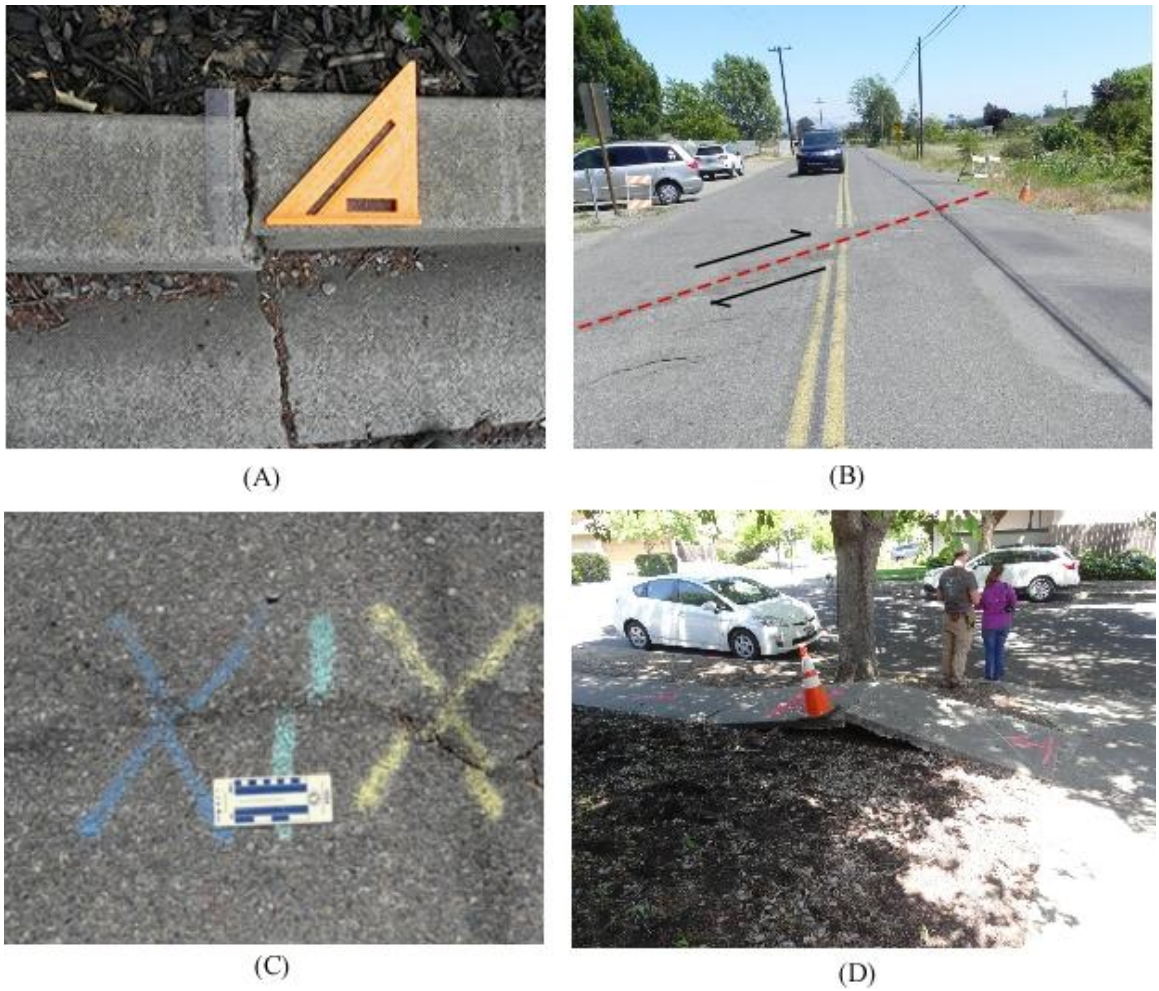

Figure 22. Examples of deformation within suburban areas of Napa. (A) a curb at 3484 Westminster Way offset north, approximately 2 cm; (B) Offset center line on Los Carneros Ave. in front of Stone Bridge School. (C) Marks for tracking continued offset along the ruptured road by Stone Bridge School; (D) Shortening in the form of a tented sidewalk on the western corner of Mason St. and Linda Mesa Way in Napa.

Linear trends in vegetation and animal burrows and tunnels were observed in soft sediment (fig. 23). Linear trends of vegetation (either in color variations or quantity variations) may be caused by preferred orientation of ground water flow because of faulting. Animal burrows and tunnels may be preferentially oriented because of weakened soil in fault-affected areas.

Features identified during field work, such as surface cracks, were located on a map, which demonstrates the regional trends of linear fault-related deformation observed in the field (fig. 24). The locations and bearings of these fault-related cracks are presented in Table 3. The linear features have a mean trend of 352° with an associated 95% confidence interval of ± 9°. The average strike of the Browns Valley section of the West Napa fault is 342°. While the results of the field work in this study suggest there was an increased density of surface ruptures in the Late Quaternary section of the West Napa fault, it must be noted that ruptures that may have been located along the northern section of the WNFZ were not investigated because of private land ownership in the area. Damage observed in this study follows the linear trend of the West Napa fault. The damage observed suggests the area is better characterized as a wide zone of deformation, rather than a linear trend.

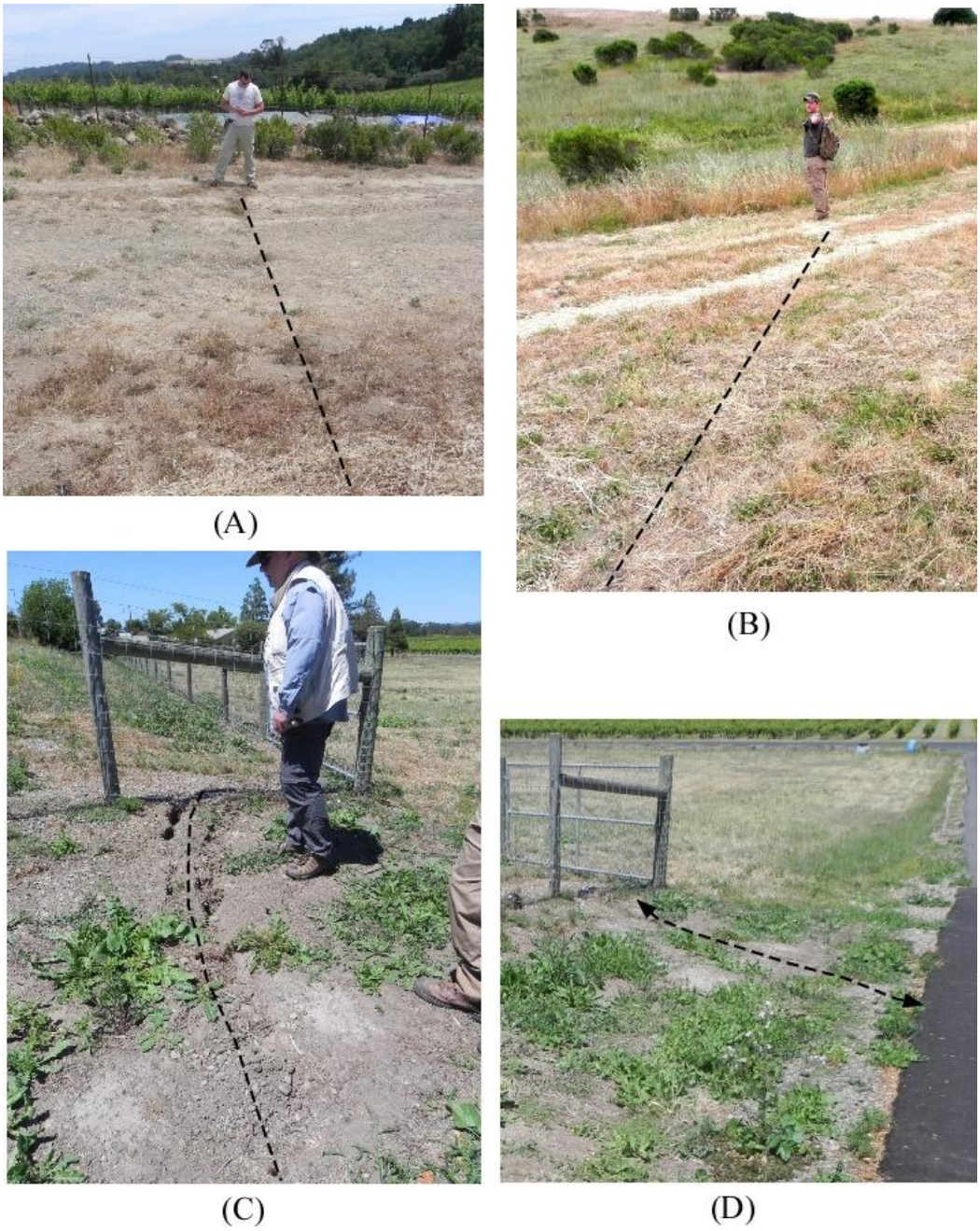

Figure 23. Examples of soft-sediment deformation in Napa. (A) Linear vegetation across a path at Alston Park, collinear with a lineament of gopher holes on the northern end of the line (lat/long: 38.3259°N, 122.3467°W, bearing: 167° +/- 3°); (B) linear array of gopher holes at Alston Park, as indicated by the geologist and the arrow (lat/long: 38.3266°N, 122.3446° W, bearing: 163° +/- 3°); (C) Deep cracks in the soft sediment on the north side of Withers Road (lat/long: 38.2515°, 122.3252°, bearing: 001° +/- 2°). Gopher holes and vegetation in the field on the east side of the fence follow the same trend; (D) Lineations from (C) trend immediately towards the repaired road, where in August 2014, a large crack was observed by Morelan et al. (2015) immediately after the South Napa earthquake.

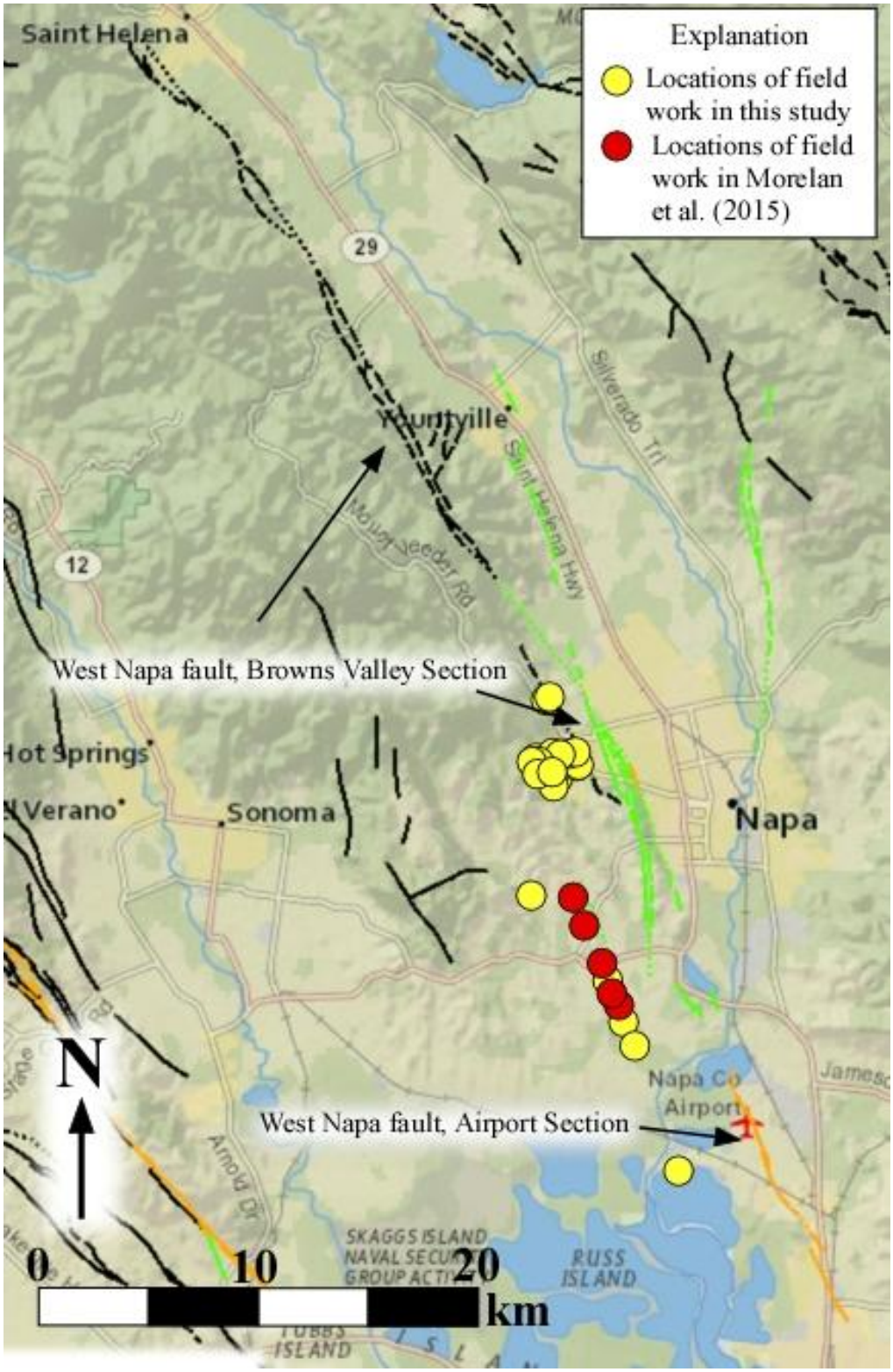

Figure 24. Locations of field work in this study and in Morelan et al. (2015). Basemap is from USGS (2015d).

Table 3. Bearings of linear fault-related deformation observed during field work in Napa, CA

Date	Latitude (°N)	Longitude (°W)	Mean Bearing (° from North)
5/25/2015	38.32600	122.34670	351
5/25/2015	38.32660	122.34465	343
5/25/2015	38.31183	122.34032	354
5/25/2015	38.31166	122.33948	350
5/25/2015	38.31166	122.33948	005
5/25/2015	38.31166	122.33948	006
5/25/2015	38.31162	122.33936	005
5/25/2015	38.31168	122.33893	358
5/25/2015	38.31169	122.33741	348
5/25/2015	38.30395	122.34296	005
5/25/2015	38.31064	122.33892	275
5/25/2015	38.30821	122.33765	001
5/25/2015	38.30732	122.33745	350
5/25/2015	38.32659	122.34444	319
5/25/2015	38.32661	122.34444	307
5/26/2015	38.30241	122.34401	000
5/26/2015	38.30534	122.34252	005
5/26/2015	38.30534	122.34252	332
5/26/2015	38.30470	122.34599	054
5/26/2015	38.30242	122.34415	008
5/26/2015	38.27397	122.35114	045
5/26/2015	38.25154	122.32524	001
5/26/2015	38.24316	122.32081	030
5/26/2015	38.24181	122.32001	008

The assumed uncertainty for a reading on a Brunton compass is ± 2°.

Table 3, continued

Date	Latitude (°N)	Longitude (°W)	Mean Bearing (° from North)
5/26/2015	38.24181	122.32001	340
5/26/2015	38.24181	122.32001	335
5/26/2015	38.23428	122.31647	025
5/26/2015	38.23428	122.31647	006
5/26/2015	38.23428	122.31647	018
5/28/2015	38.42154	-122.41851	014
5/28/2015	38.40621	-122.43829	297
5/28/2015	38.31083	122.34334	004
5/29/2015	38.30627	-122.34554	316
5/29/2015	38.30610	-122.45520	317
5/29/2015	38.30591	-122.34583	325
5/29/2015	38.30591	-122.34583	325
5/29/2015	38.30591	-122.34583	325
5/29/2015	38.30627	-122.34531	330
5/29/2015	38.30627	-122.34531	334
5/29/2015	38.30641	-122.34505	288
5/29/2015	38.30641	-122.34505	287
5/29/2015	38.20129	-122.30199	053
5/29/2015	38.20129	-122.30199	047
5/29/2015	38.32449	-122.34578	347
5/31/2015	38.30117	122.33825	056
5/31/2015	38.30117	122.33825	054
5/31/2015	38.30094	122.33763	320

The assumed uncertainty for a reading on a Brunton compass is ± 2°.

Bearings of linear features observed in the field are compiled on a rose diagram in Figure 25. Nearly all lineaments trended from 315° to 010°. Lineaments in a 315° - 350° range are consistent in orientation with regional fault trends. The most prevalent lineament orientation is from 000°-010°.

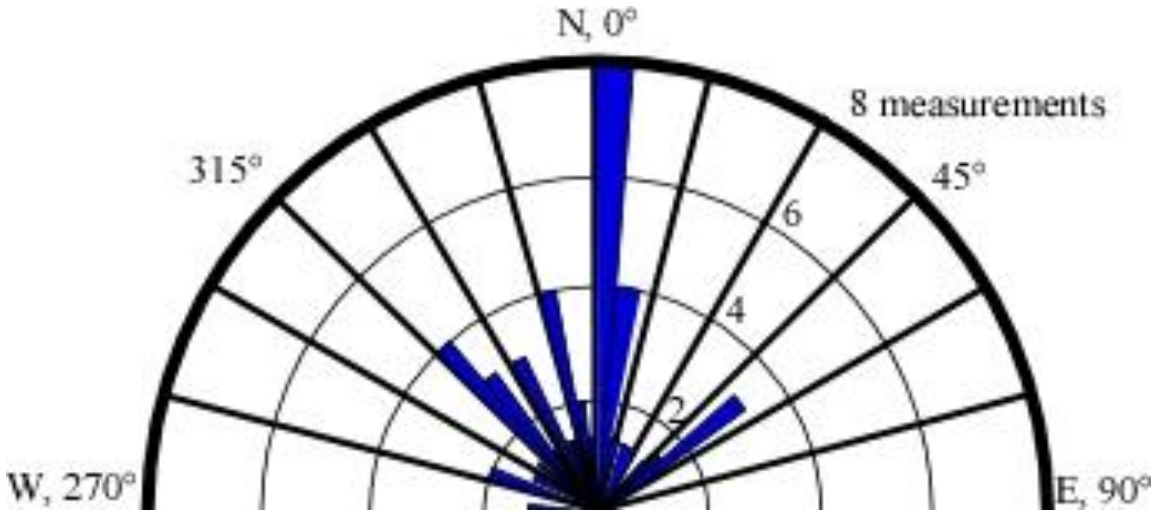

Figure 25. Rose diagram of bearings of fault-related cracks from field work. Note the three primary groupings of data: 000°-010°, 045°-055°, and 315°-350°.

The City of Napa provided information about locations of infrastructure damage, including water line breaks, after the South Napa earthquake. These locations are important because water line breaks indicate areas that underwent significant strain, like a fault trace. The majority of breaks occurred within or adjacent to the West Napa fault zone, but did not follow a particular linear trend (fig. 26). Most recorded water line breaks were located in the urban area of Napa, and while some occurred during the earthquake, many occurred in the following days. This delay in water-line breakage is inferred to be due to slow creep movement and continued stress on the fault. Both main and secondary lines were affected by the earthquake. Repairs began the morning after the earthquake, and continued to be completed until March 2015.

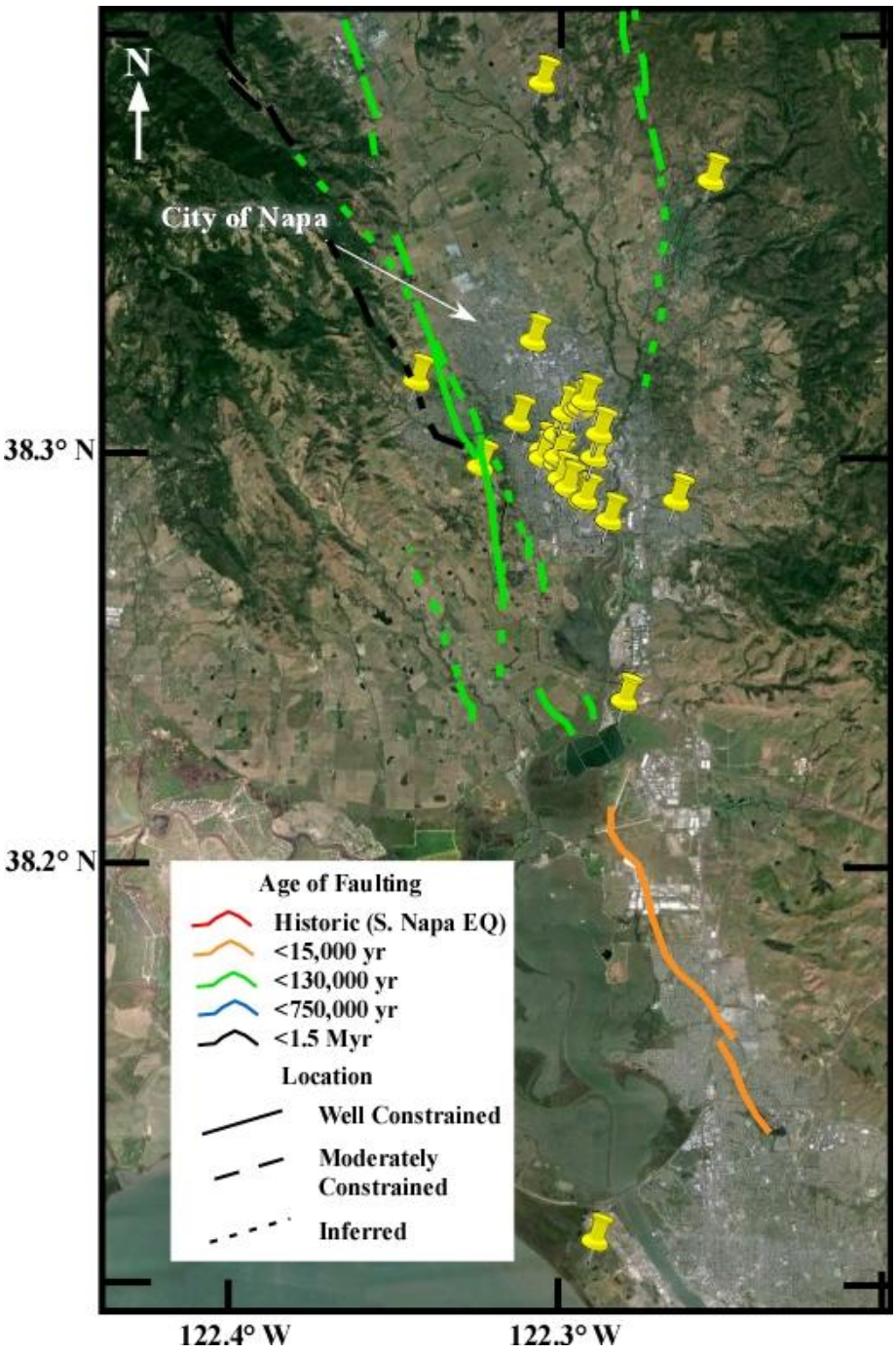

Figure 26. Locations of water line break repairs completed by the City of Napa after the South Napa earthquake. Basemap is from *Google Earth*. Fault data is from USGS (2015d).

GPS Strain Analysis

Interseismic and coseismic GPS strain analyses were completed with results of 11 GPS sites from the PBO monitoring network. The data from the analysis can be used to infer ongoing seismic hazards and changes experienced along the West Napa fault zone because of the South Napa earthquake. Data from the analyses is presented in Tables 4-6 as pre-earthquake interseismic strain, coseismic strain, and post-earthquake interseismic strain.

Table 4. Pre-earthquake interseismic instantaneous horizontal strain, derived from PBO velocities, Napa

Group	Translation Speed ± uncertainty (m/yr)	Translation Azimuth (°)	Rotation Direction	Max. Horiz. Extension (n-strain/yr)	$S1_H$ Azimuth (°)	Min. Horiz. Extension (n-strain/yr)
Across	0.0177 ± 0.0005	319	CCW	349.1998	7.7926	-129.1814
E1	0.0135 ± 0.0006	310.5	CCW	16.0653	38.6898	-29.9524
E2	0.0175 ± 0.0005	319.2	CW	134.4977	118.5902	-179.3208
W1	0.248 ± 0.0005	323.5	CW	180.9922	111.1966	-178.2544
W2	0.031 ± 0.0005	325.5	CW	129.8219	101.5256	-134.6649

Table 5. Coseismic instantaneous horizontal strain, derived from PBO velocities, Napa

Group	Translation Distance ± uncertainty (m)	Translation Azimuth (°)	Rotation Direction	Max. Horiz. Extension (n-strain/yr)	$S1_H$ Azimuth (°)	Min. Horiz. Extension (n-strain/yr)
Across	.0042 ± .0015	124.4	CCW	1271.9802	155.2176	-653.2764
E1	.0012 ± .0009	167.5	CW	15.3330	1.5435	-96.8267
E2	.0117 ± .0015	159	CCW	479.421	151.0779	-1690.5547
W1	0.018 ± .0013	304.3	CCW	34.5594	31.6729	-983.0928
W2	0.0066 ± .0009	291.5	CCW	14.2207	15.0377	-353.9982

Table 6. Post-earthquake interseismic instantaneous horizontal strain, derived from PBO velocities, Napa

Group	Translation Speed ± uncertainty (m/yr)	Translation Azimuth (°)	Rotation Direction	Max. Horiz. Extension (n-strain/yr)	$S1_H$ Azimuth (°)	Min. Horiz. Extension (n-strain/yr)
Across	0.0181 ± 0.0001	321.2	CW	129.6135	121.9564	-84.0838
E1	0.014 ± 0.0001	312.7	CW	-3.8483	81.8964	-92.4498
E2	0.018 ± 0.0001	321.1	CW	147.6428	119.5569	-187.0417
W1	0.0255 ± 0.0001	324.5	CW	178.9712	111.3883	-178.0557
W2	0.0317 ± 0.0010	326.2	CW	133.5673	100.6056	-139.53

The GPS velocity data utilized in this research helps us characterize crustal strain in the Napa area before, during, and after the South Napa earthquake. The horizontal strain axes for the GPS strain analysis are presented in Figure 27. Pre-earthquake interseismic strain results suggest an overall shortening in a north-northeastern orientation, especially on the west of and proximal to the West Napa fault zone. Shortening observed in the triplet that crosses the fault zone (Across) and the most eastern triplet (E1) is oriented in an east-west to northwestern-southeastern direction. This change may be due to complex strain across the fault zone and at an increased distance from the fault. Coseismic strain indicates a sub-orthogonal relationship of strain across the fault zone. Positive extension on the east side of the fault zone parallels fault orientation, while negative extension is sub-parallel to the fault trend on the west side. This may be an indication of increased strike-slip movement of the eastern crust relative to the western crust along the West Napa fault zone. Post-earthquake interseismic strain displays a restoration of clockwise-rotation of primarily north to northeastern negative extension, as was observed in pre-earthquake data.

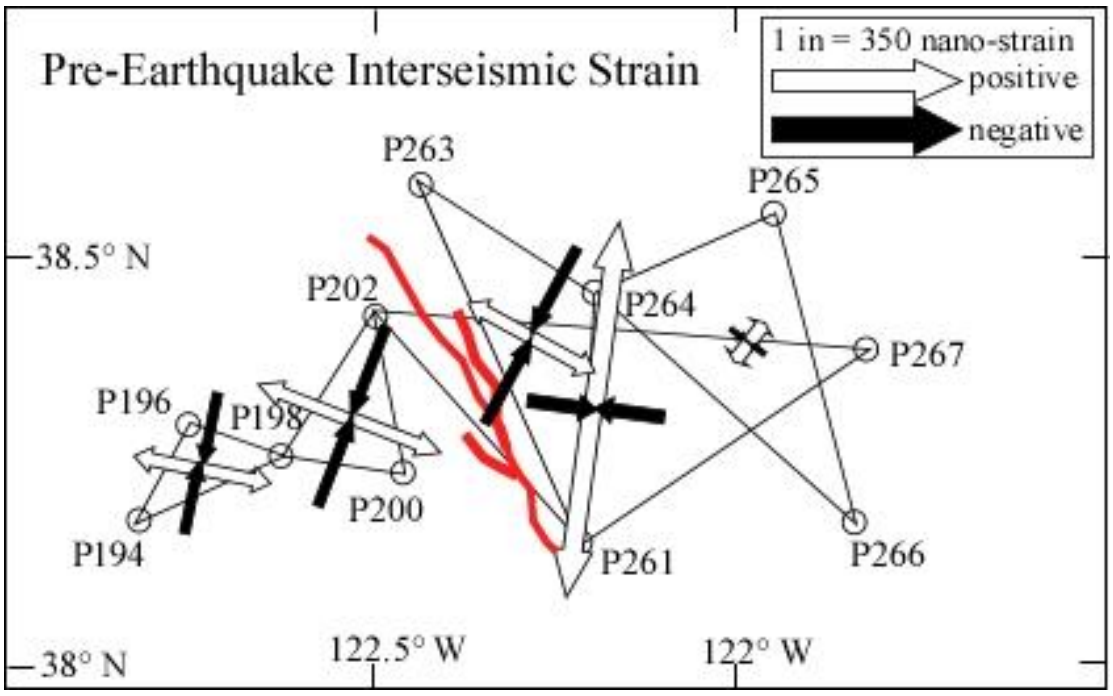

(A)

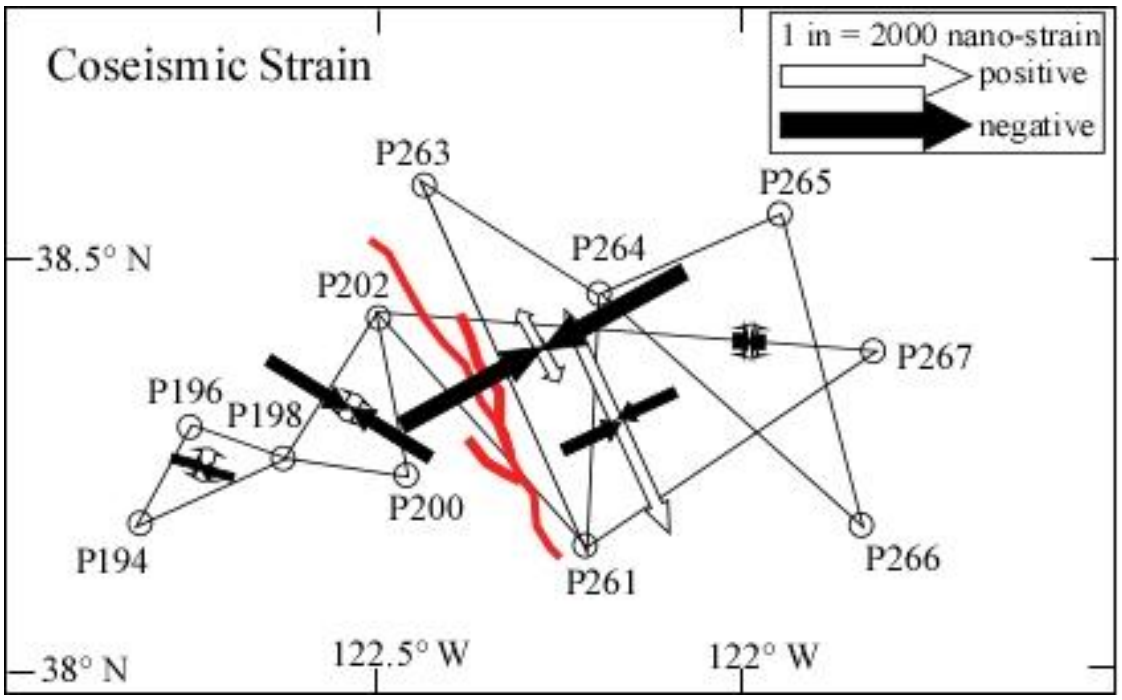

(B)

Figure 27. Horizontal strain axes for (A) pre-earthquake interseismic GPS strain results and (B) coseismic GPS strain results. White arrows indicate positive extension, and black arrows indicate negative extension, or contraction. The West Napa fault zone (WNFZ) is shown in red (USGS, 2015d). Sizes of arrows are relative to extension magnitudes.

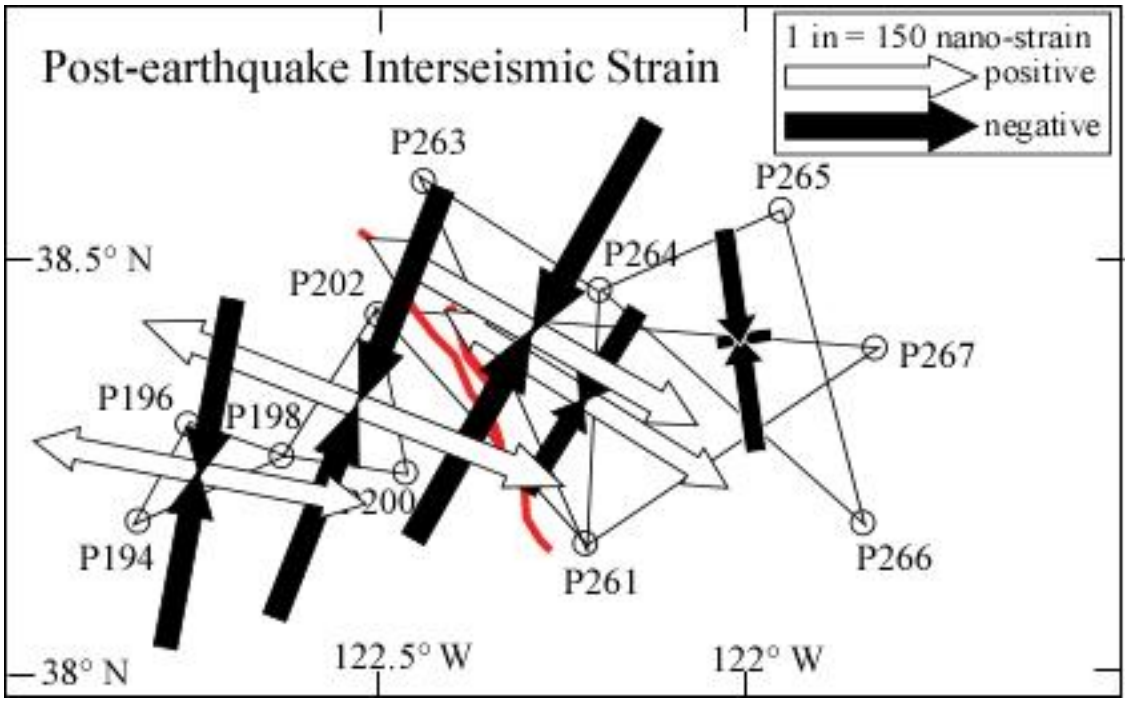

(C)

Figure 27, continued from above. Horizontal strain axes for (C) post-earthquake interseismic GPS strain results. White arrows indicate positive extension, and black arrows indicate negative extension, or contraction. The West Napa fault zone (WNFZ) is shown in red (USGS, 2015d). Sizes of arrows are relative to extension magnitudes.

CHAPTER FIVE

Discussion and Conclusions

Seismo-Lineament Solutions and Geomorphic Analyses

The South Napa earthquake of 24 August 2014, five earthquakes that occurred before the South Napa earthquake, and three earthquakes that occurred immediately after the South Napa event were analyzed using the Seismo-Lineament Analysis Method (figs. 12-15). Geomorphic lineaments that might be related to active faulting were identified within each seismo-lineament.

The NNW-trending seismo-lineament solution for the M 6.0 South Napa earthquake (fig. 12-A) is spatially correlated to the surface ruptures from the South Napa earthquake and to the Browns Valley section of the West Napa fault (fig. 20). Had the seismo-lineament solution for the South Napa earthquake been available immediately after the earthquake, it could have been valuable for field reconnaissance and location of the causative strand of the West Napa fault.

The M 3.81 earthquake of 24 August 2014 (fig. 12-B) is interpreted to be associated with slip on a horizontal detachment fault, perhaps triggered by the South Napa earthquake that occurred just one minute before. While the uncertainties associated with this focal mechanism are significant (±40° in strike, ±25° in dip angle), this earthquake does not appear to have been generated along the West Napa fault.

The M 3.6 earthquake of 24 August 2014 occurred just under two and a half hours after the South Napa earthquake and ~4.5 km to the northwest of the epicenter of the

main shock. While the uncertainties in hypocenter location are small (on the order of tens of meters), uncertainties in the fault plane solution are substantial (±13° in strike, ±35° in dip angle). The Browns Valley segment of the West Napa fault is within the seismo-lineament of the M 3.6 earthquake, as are all of the documented surface ruptures of the South Napa earthquake (fig. 13). The more northerly trend of the fault plane solution of the M 3.6 earthquake, compared with the northwest trend of the fault plane solution of the South Napa earthquake, might indicate that the smaller earthquake occurred along a different strand of the Browns Valley section – perhaps a strand that did not display surface rupture. The M 3.6 earthquake is spatially correlated with the West Napa fault.

The M 3.9 earthquake two days later, on 26 August 2014, occurred ~4.1 km south of the epicenter of the South Napa earthquake. The focal mechanisms of the two earthquakes are quite similar, and their respective seismo-lineaments display significant overlap in the area of the Browns Valley segment of the West Napa fault where surface ruptures associated with the South Napa earthquake were mapped. The epicenter of the M 3.9 earthquake is located within the seismo-lineament of the South Napa earthquake, and vice versa. The M 3.9 earthquake is spatially correlated with the West Napa fault.

The seismo-lineaments for the 2012 events (fig. 14-A and B) overlap the seismo-lineament for the South Napa earthquake. The epicenters for the 2012 events are adjacent to the Franklin fault and other strands of the Contra Costa Shear Zone, which extends from the Northern Calaveras fault with the West Napa fault (fig. 28; Brossy et al., 2010). Some seismic activity recorded after the South Napa earthquake originated at the Franklin fault (Brocher et al., 2015; Barnhart et al., 2015). The results from these seismo-

lineament solutions suggest that there might be a linkage between the Franklin and South Napa faults that should be investigated further.

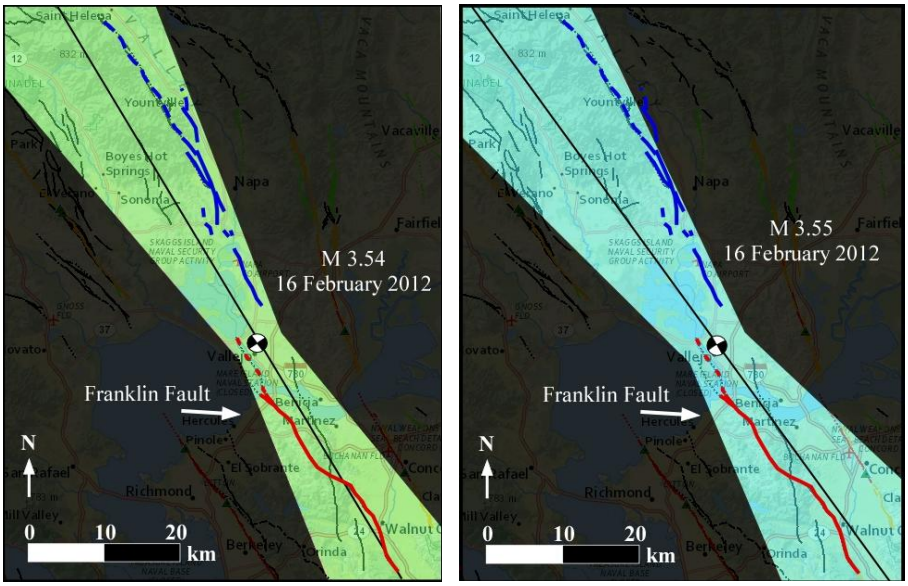

Figure 28. Trends of the 2012 seismo-lineaments relative to the Franklin and West Napa faults. Basemap is from USGS (2015d).

The fault plane solutions for the M 4.9 Yountville earthquake and the M 6.0 South Napa earthquake are oriented parallel to the trend of the West Napa fault (fig. 29). The seismo-lineaments for the 2000 M 4.9 Yountville earthquake (fig. 15-A) and for the 2014 South Napa earthquake (fig. 12-A) have a substantial area of overlap that includes the most if not all of the Browns Valley section of the West Napa fault (fig. 30). This area of overlap includes all of the surface ruptures from the South Napa earthquake. Because geomorphic lineaments identified within the seismo-lineament for the South Napa earthquake lie within the Yountville seismo-lineament (fig. 21), it is reasonable to infer that, had SLAM been applied to data from the Yountville earthquake prior to August 2014, the West Napa Fault might have been recognized as seismogenic.

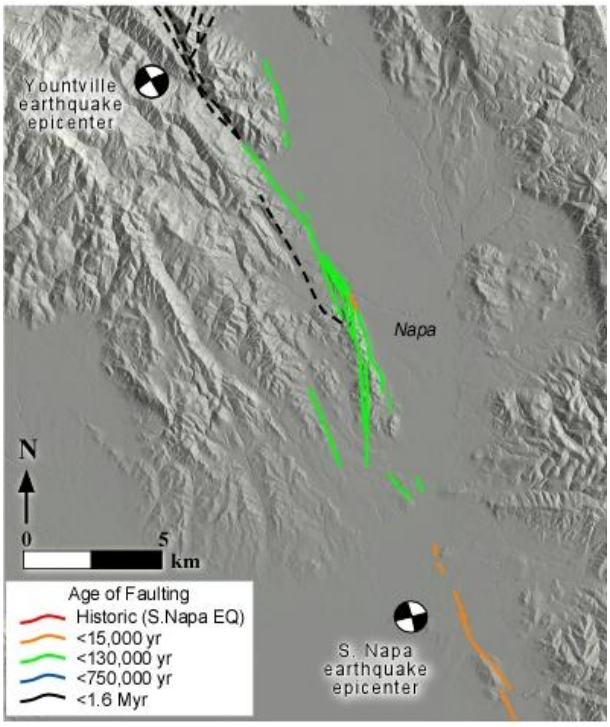

(A)

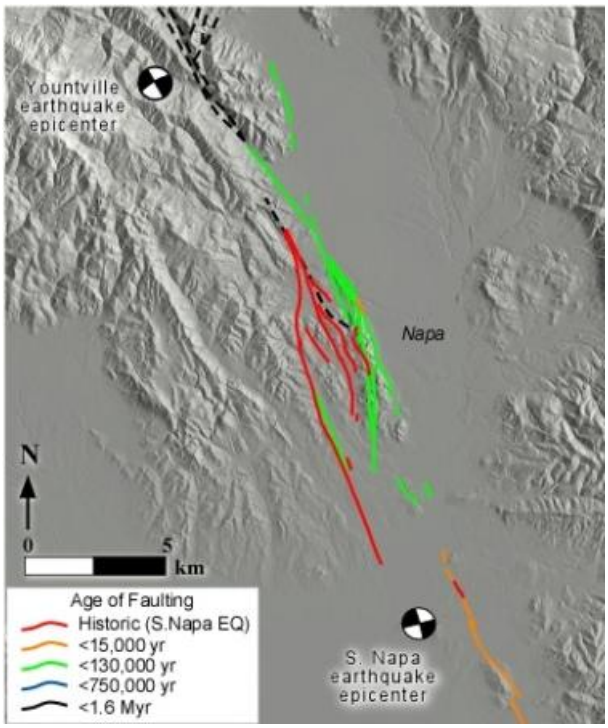

(B)

Figure 29. Epicenters of the M 4.9 Yountville earthquake of 3 September 2000 and the M 6.0 South Napa earthquake of 24 August 2014 relative to the West Napa fault (A) before the South Napa earthquake (USGS, 2015d) and (B) after the South Napa earthquake (Brocher et al., 2015; USGS, 2015d).

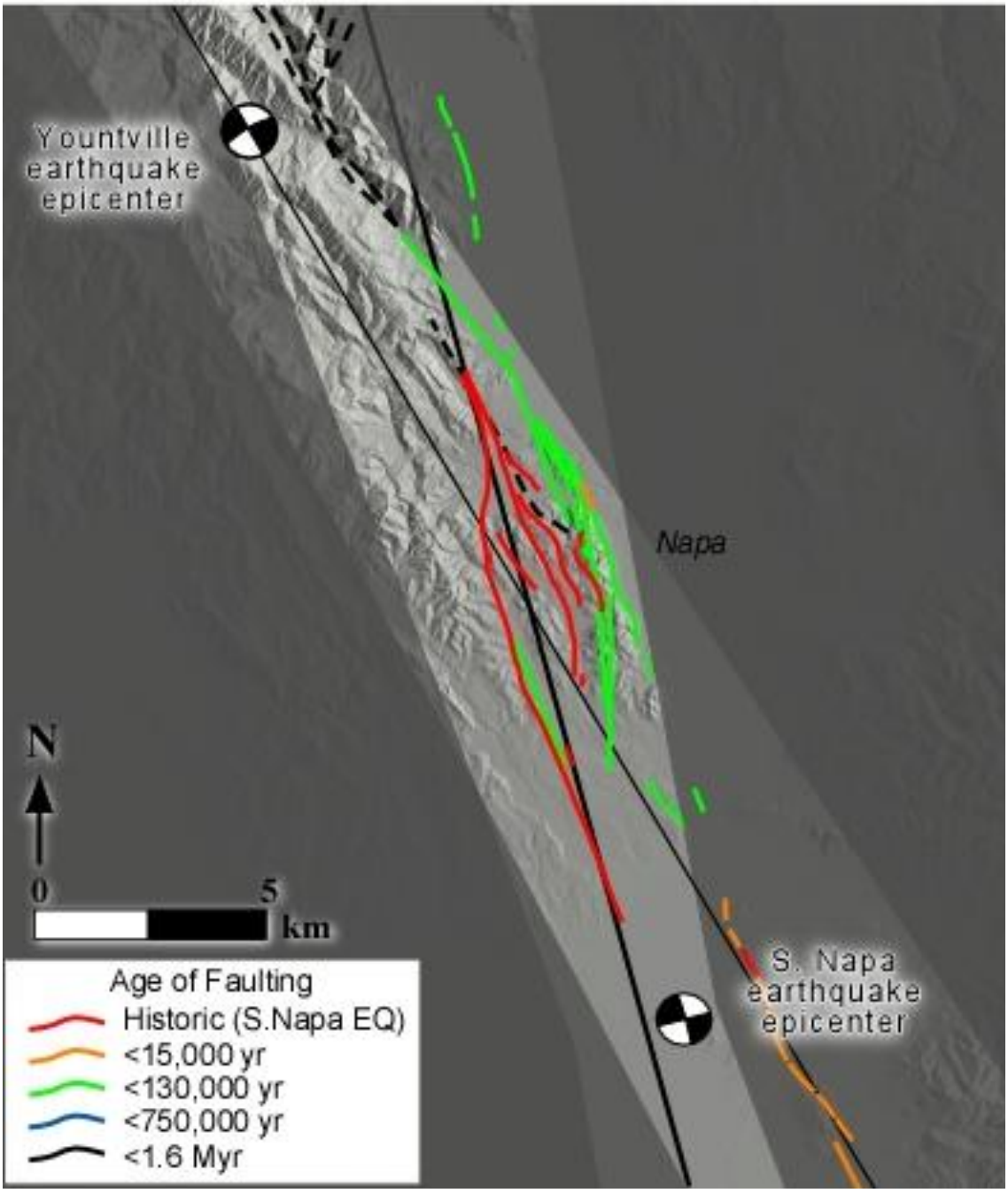

Figure 30. Seismo-lineament solutions for the M 4.9 Yountville earthquake and the M 6.0 South Napa earthquake, shown with previously mapped sections of the West Napa fault zone (USGS, 2015d) and newly ruptured sections of the West Napa fault zone as of the South Napa earthquake (Brocher et al., 2015).

The prevailing interpretation prior to the South Napa earthquake was that the M 4.9 Yountville earthquake of 3 September 2000 occurred along an unnamed fault located ~4.4 km west of the West Napa fault zone (fig. 31; USGS, 2000, 2015d; Miranda and Aslani, 2000). This interpretation was based on an early hypocenter location by the USGS soon after the Yountville earthquake, with an epicenter ~5 km west of the West Napa fault. The current best hypocenter location for the Yountville earthquake was computed using a double-difference relocation method (NCEDC, 2014a), and has an epicenter located ~1.2 km west of the surface trace of the West Napa fault and ~3.6 km east of the closest (unnamed) fault to the west. The seismo-lineament computed using these data and the best available fault-plane solution (NCEDC, 2014b) does not include the closest unnamed fault to the west of the epicenter, but does include the West Napa fault (USGS, 2015d). Hence, the Yountville earthquake is interpreted to have occurred on the West Napa fault, and not on another fault to the west.

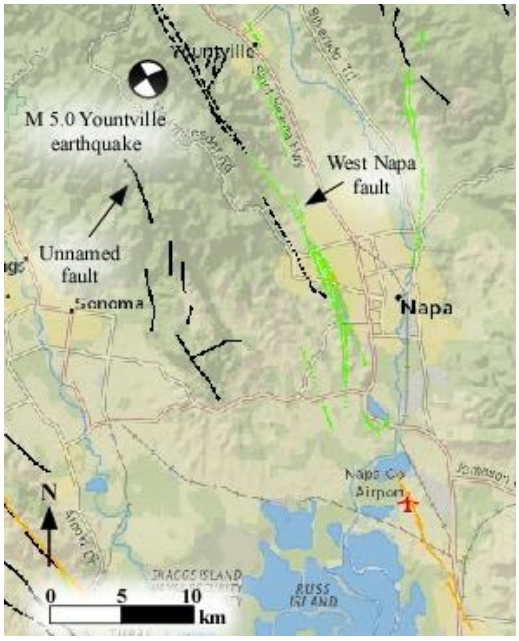

Figure 31. Focal mechanism of the M 4.9 Yountville earthquake of 3 September 2000, shown with sections of the West Napa fault zone and the unnamed fault located west of the West Napa fault. Basemap is from USGS (2015d).

Seismo-lineaments for the M 3.5 earthquakes of 1990 (figs. 15-B & C) are parallel to and encompass the West Napa fault (fig. 16). The seismo-lineament for the earthquake of 14 October 1990 includes several faults between the West Napa fault and the Rogers Creek fault to the west. Seismo-lineaments for both 1990 earthquakes include geomorphic lineaments identified within the South Napa and Yountville earthquake seismo-lineaments, indicating that data from both of the 1990 earthquakes would have been useful identifying the West Napa fault as seismogenic before the South Napa earthquake. Both of the M 3.5 earthquakes that occurred in the Napa area in 1990 are spatially correlated with the West Napa fault, and the correlation for the 11 June 1990 event is particularly strong.

Field Work

No significant fault expression was located in Napa during field work for this thesis that was not already identified by other workers after the South Napa earthquake. The features identified in the field are interpreted as fault-related deformation, and include cracks, breaks, and trends observed in roads, sidewalks, and some soft sediment. The rose diagram in Figure 25 displays primary lineament trends that were observed in the field area. One set of the data trends from 315° - 350° and parallels regional fault trends. The more significant set of data is oriented from 000°-010°. These features are consistent in character with a Riedel array (Tchalenko, 1970). Riedel shears (R-shears, or synthetic shears) were first characterized during ‘clay cake’ experiments of 1928-29 (Cloos, 1928; Riedel, 1929), and have been observed as occurring ~ 15°, en echelon, from the main right-lateral fault trace to which the shears are associated (R-shears occur -15° from left-lateral faults). Riedel shears are produced when the right-or-left-lateral

principal displacement zone (PDZ) creates a fault within the underlying basement rock (fig. 32). R'-shears, or 'antithetic' shears, may appear as connections between Riedel shear zones, and generally occur at an angle of 75° to the main right-lateral fault trace (-75° for left-lateral strike-slip faults) (Davis et al., 2000). Both synthetic R-shears and antithetic R'-shears occur en échelon along the main fault trace. The smallest subset of lineaments observed in this study are oriented at angles of 045°-055°, and may be characterized as R'-shears.

Davis et al. (2000) suggested that Riedel shear zones may appear within a wide zone of deformation and may or may not be associated with an underlying basement fault. In the Napa area, there is an obvious trend of lineaments that parallel regional trends, but the largest group of fractures is oriented in such an attitude to suggest Riedel shearing. These en-echelon, left-stepping shears were also noted by Kelson and Wesling (2015). These shears were predicted by models of slip distribution by the USGS, and confirm suspicions that the West Napa fault ruptured northward. No fault surfaces were located during field work in this study, and the main fault trace of the West Napa fault was not identified. Both the antithetic and synthetic shears and the wide zone of deformation observed in the field indicate that the West Napa fault zone is better characterized by the Riedel array model than a single fault trace.

The water line repairs completed by the City of Napa (fig. 28) are nearly all located adjacent to the West Napa fault zone. The damage was likely caused by the shaking motion of the earthquake, rather than a fault rupture, and cannot be interpreted as an active strand of the West Napa fault.

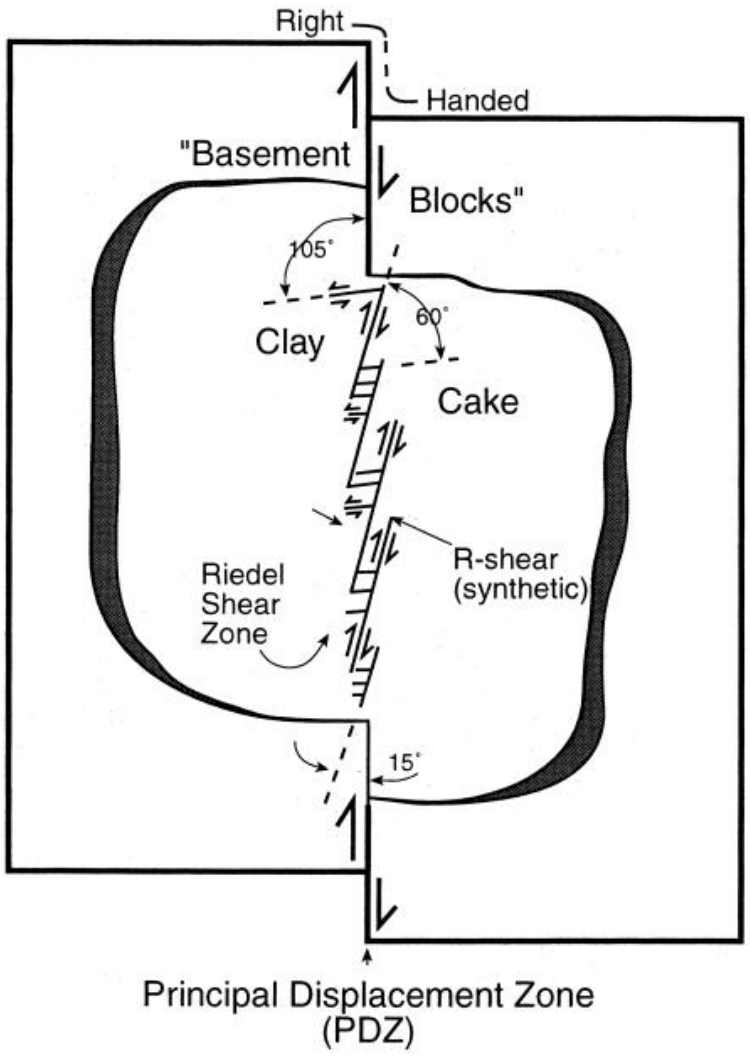

Figure 32. Synthetic and antithetic Riedel shears along a right-lateral strike-slip fault, from Davis et al. (2000).

GPS Strain Analysis

Results from the interseismic and coseismic strain analysis using the PBO GPS velocities support a model of clockwise rotation before the earthquake, increased stress in a dextral strike-slip orientation across the fault, and restoration of the clockwise rotation after the earthquake, which is consistent with regional crustal strain models of the western portion of the North American plate near the San Andreas fault system.

Conclusions

The well documented ground-surface rupture associated with the South Napa earthquake, combined with high-quality seismological data, provided a good opportunity to test the effectiveness of the Seismo-Lineament Analysis Method (SLAM). The purpose of SLAM is to use the focal mechanisms of well-located earthquakes to find the ground-surface trace of faults that spatially correlate with the earthquakes. SLAM is a tool to help identify seismogenic faults.

1. Earthquake focal mechanism and hypocenter-location data, along with their respective uncertainties, related to the M 6.0 South Napa earthquake of 24 August 2014 were used as input to the SLAM code. The resulting seismo-lineament associated with the northwest-striking nodal plane was relatively narrow because of the near-vertical dip of the fault plane and the large quantity of earthquake data available to constrain the focal mechanism and hypocenter location. The Browns Valley segment of the West Napa fault and all of the fault-related ground rupture associated with that earthquake were located within the seismo-lineament. SLAM was able to direct us to the fault that generated the earthquake.

2. Several right-lateral strike-slip earthquakes occurred in the Napa Valley area since early 1990 with magnitudes of 3.5 or more, for which focal mechanisms had been computed. Seismo-lineaments from earthquakes on 16 February 2012 (2 events, both M ~3.5), 3 September 2000 (M 4.9), 14 October 1990 (M 3.5), and 11 June 1990 (M 3.5) all had the West Napa fault within their boundaries. Geomorphic lineaments within the seismo-lineament swaths coincided with the West Napa fault. While none of these events produced surface rupture, all are spatially correlated with the West Napa fault and might

have been generated along one of its splays. The two earthquakes from 2012 and the event of 14 October 1990 also spatially correlate with other Quaternary faults.

3. Focal mechanism data from well-located magnitude 3 and 4 earthquakes, coupled with analysis of geomorphic lineaments within the corresponding seismo-lineaments, were used to identify a seismogenic fault that generated a M 6.0 earthquake. Small earthquakes can be used to identify seismogenic faults capable of producing big earthquakes.

4. SLAM results strongly indicate that the M 4.9 Yountville earthquake of 3 September 2000 was generated along the northern Browns Valley segment of the West Napa fault. Earlier attribution of the Yountville earthquake by the USGS and others to a fault ~5 km west of the West Napa fault is not supported by the SLAM analysis, which is based on our current best understanding of the focal mechanism and hypocenter location of the Yountville earthquake.

The success of this application of SLAM indicates that this methodology might be useful in the immediate aftermath of a large ($M \geq 6$) earthquake to help locate the areas in which to search for areas affected by ground-surface rupture. The boundaries of the seismo-lineament can be available minutes after the first focal-mechanism solution is available, given prior compilation of a suitable DEM data file for the area. SLAM is not dependent upon prior knowledge of the location of fault traces in an area, so it is useful where urbanization, thick soils, vegetation, water, or agricultural modification has buried or obscured the surface trace of faults. Seismo-lineaments can also act as guides for aerial reconnaissance or airborne LiDAR surveys in the immediate aftermath of a large

earthquake, because they map the most likely areas in which to find the ground-surface trace of the fault that generated the earthquake.

APPENDICES

APPENDIX A

Mathematica SLAM codes (Cronin, 2014c)

Cropper for DEM Data

Dataset Cropper for SLAM

Revised September 1, 2014, based on a code begun July 16, 2009.


```
startTime = AbsoluteTime[];
```

Introduction

The purpose of this notebook is to minimize a large DEM dataset so that it can more efficiently be processed in SLAM.

Code

Test file

Change the style of the next line from **Text** to **Input** to test the subsequent code without having to use an external data file. Make sure the code that is normally used to import a data file (in the gray box in the "Input the data file" section below) is disabled during the test -- disable it by converting the **Import** code line from an **Input** style to a **Text** style.

initialDataFile = {{"ncols", 6}, {"nrows", 7}, {"xllcorner", 0}, {"yllcorner", 0}, {"cellsize", 10}, {"NODATA_value", -9999}, {11, 12, 13, 14, 15, 16}, {21, 22, 23, 24, 25, 26}, {31, 32, 33, 34, 35, 36}, {41, 42, 43, 44, 45, 46}, {51, 52, 53, 54, 55, 56}, {61, 62, 63, 64, 65, 66}, {71, 72, 73, 74, 75, 76}};

Choose the percentages of the input DEM to be trimmed off the top, bottom, right and left sides

```
topPercentage = 40;

bottomPercentage = 32;

rightPercentage = 50;

leftPercentage = 35;
```

Input the data file

This code reads an external data file that is in the form of an ASCII DEM file, with the .dat file-type designator. On Vince Cronin's office Macintosh, the Import code would look like the following for a data file named "tahoedem.dat" located on the desktop:

```
initialDataFile = Import["/Users/vince/Desktop/tahoedem.dat"];
```

On the Dell computer in Cronin' s office, the Import code would look like the following for a data file named "tahoedem.dat" located on the C drive in the "TahoeRuns" directory :

```
SetDirectory["C:\TahoeRuns"];
initialDataFile = Import["tahoedem.dat"];
```

Use the appropriate **Import** code below, and make sure it is in the **Input** style.

```
initialDataFile = Import["/Users/vincecronin/desktop/largetahoe.dat"];
```

```
origNcols = initialDataFile[[1, 2]]
```

```
origNrows = initialDataFile[[2, 2]]
```

```
origXLLCorner = initialDataFile[[3, 2]]
```

```
origYLLCorner = initialDataFile[[4, 2]]
```

```
cellsize = initialDataFile[[5, 2]]
```

```
9.3770677923454`
```

```
nodataValue = initialDataFile[[6, 2]]
```

Make the hillshade image

The `adjustContrast` value forces one point of the DEM to have a particular value, which in turn allows the user to adjust the tonal range of the hillshade map.

```
adjustContrast = 0;
```

```
npDipTr = 5;
```

```
demImgFile = Table[initialDataFile[[i + 6, j]] , {i, origNrows}, {j, origNcols}];
elev3 = Table[If[((i > 1) ∧ (j > 1)), demImgFile[[i, j]], adjustContrast], {i, origNrows, 1, -1}, {j, origNcols}];
```

```
npDipTrRad = npDipTr * (π / 180);
```

```
lightDirection = If[npDipTrRad > (3 π / 2), (2 π) - npDipTrRad, (π / 2) - npDipTrRad];
```

```
hillshadeMap1 = ReliefPlot[elev3, ColorFunction -> "GrayTones", LightingAngle -> {lightDirection,
Pi/12}];
Show[hillshadeMap1]
ClearAll[elev3];
```

Extract the reduced data set from the original file

```
initialHeaderData = Table[initialDataFile[[i, j]], {i, 6}, {j, 2}];
```

```
fatDEMdata = Drop[initialDataFile, 6];
```

Take a percentage off the top, bottom and sides

```
haircut = IntegerPart[origNrows * topPercentage * 0.01]

haircutDEM = Drop[fatDEMdata, haircut];

Clear[fatDEMdata];

stripBase = -1 * IntegerPart[origNrows * bottomPercentage * 0.01]

yllcorner = origYLLCorner - (cellsize * stripBase)

stripBaseDEM = Drop[haircutDEM, stripBase];

Clear[haircutDEM];

matrixSize1 = Dimensions[stripBaseDEM];

nrows = matrixSize1[[1]]

stripRight = origNcols - Round[0.01 * rightPercentage * origNcols]

stripLeft = origNcols - Round[0.01 * (100 - leftPercentage) * origNcols]

xllcorner = origXLLCorner + (cellsize * stripLeft)

finalDEM = Table[stripBaseDEM[[i, j]], {i, nrows}, {j, stripLeft, stripRight}];

Clear[stripBaseDEM];

matrixSize2 = Dimensions[finalDEM];

ncols = matrixSize2[[2]]

elev3 = Table[If[((i > 1) ∧ (j > 1)), finalDEM[[i, j]], adjustContrast],
   {i, nrows, 1, -1}, {j, ncols}];

hillshadeMap2 = ReliefPlot[elev3,
   ColorFunction -> "GrayTones", LightingAngle -> {lightDirection, Pi / 12}];

Show[hillshadeMap2]

ClearAll[elev3];

headerData = {{initialHeaderData[[1, 1]], ncols}, {initialHeaderData[[2, 1]], nrows},
   {initialHeaderData[[3, 1]], xllcorner}, {initialHeaderData[[4, 1]], yllcorner},
   {initialHeaderData[[5, 1]], initialHeaderData[[5, 2]]},
   {initialHeaderData[[6, 1]], initialHeaderData[[6, 2]]}};

mergedData = Join[headerData, finalDEM];
```

Export the resultant data file

Choose a name for the resultant data file (different from the name of the original data file) and specify the path to the directory where that file is to be saved. For example, on Vince Cronin' s office Macintosh, the following code will save a resultant file named "thinTahoeDEM.dat" on the desktop :

```
Export["/Users/vince/Desktop/thinTahoeDEM.dat", mergedData];
```

on Vince Cronin' s Dell, the **Export** code would look like the following for a data file named "thinTahoeDEM.dat" located on the C drive in the "TahoeRuns" directory :

```
SetDirectory["C:\TahoeRuns"];
Export["thinTahoeDEM.dat", mergedData];
```

Use the appropriate **Export** code below, and make sure it is in the **Input** style

```
Export["/Users/vincecronin/Desktop/croppedDVFZ.dat", mergedData];
```

How long did this program take to run, in minutes?

```
minutesForProcessing = (AbsoluteTime[] - startTime) / 60
```

Dataset Thinner for SLAM

Revised July 7, 2014, based on a code begun July 16, 2009.


```
startTime = AbsoluteTime[];
```

Introduction

The purpose of this notebook is to minimize a large DEM dataset so that it can more efficiently be processed in SLAM.

Code

Test file

Change the style of the next line from **Text** to **Input** to test the subsequent code without having to use an external data file. Make sure the code that is normally used to import a data file (in the gray box in the "Input the data file" section below) is disabled during the test -- disable it by converting the **Import** code line from an **Input** style to a **Text** style.

initialDataFile = {{"ncols", 6}, {"nrows", 7}, {"xllcorner", 0}, {"yllcorner", 0}, {"cellsize", 10}, {"NODATA_value", -9999}, {11, 12, 13, 14, 15, 16}, {21, 22, 23, 24, 25, 26}, {31, 32, 33, 34, 35, 36}, {41, 42, 43, 44, 45, 46}, {51, 52, 53, 54, 55, 56}, {61, 62, 63, 64, 65, 66}, {71, 72, 73, 74, 75, 76}};

Choose a reduction factor

A reduction factor (`redFactor`) of 2 deletes every other row and column; the resulting matrix begins with the value in the first row, first column of the original matrix. For example, if the initial matrix is a 7x6 matrix, the resulting matrix will be a 4x3 matrix with just under 29% of the values of the original matrix. A reduction factor of 3 deletes two consecutive rows and two columns between values that are retained, resulting in a file that is ~14% of the original size. A reduction factor of 5 deletes 5 consecutive rows and columns after each value it retains (~10% of the original size).

Assign an integer value to the reduction factor below.

```
redFactor = 5;
```

Input the data file

This code reads an external data file that is in the form of an ASCII DEM file, with the .dat file-type designator. On Vince Cronin's office Macintosh, the Import code would look like the following for a data file named "tahoedem.dat" located on the desktop:

```
initialDataFile = Import["/Users/vince/Desktop/tahoedem.dat"];
```

On the Dell computer in Cronin' s office, the Import code would look like the following for a data file named "tahoedem.dat" located on the C drive in the "TahoeRuns" directory :

```
SetDirectory["C:\TahoeRuns"];
initialDataFile = Import["tahoedem.dat"];
```

Use the appropriate **Import** code below, and make sure it is in the **Input** style.

```
initialDataFile =
  Import["/Users/vincecronin/Desktop/Trinidad/PurgatoireThirdDEM.dat"];
```

```
initialDataFile[[1, 1]]
initialDataFile[[1, 2]]
initialDataFile[[2, 1]]
initialDataFile[[2, 2]]
initialDataFile[[3, 1]]
initialDataFile[[3, 2]]
initialDataFile[[4, 1]]
initialDataFile[[4, 2]]
initialDataFile[[5, 1]]
initialDataFile[[5, 2]]
initialDataFile[[6, 1]]
initialDataFile[[6, 2]]
```

Extract the reduced data set from the original file

```
initialHeaderData = Table[initialDataFile[[i, j]], {i, 6}, {j, 2}];
fatDEMdata = Drop[initialDataFile, 6];
thinDEMdata = Take[fatDEMdata, {1, -1, redFactor}, {1, -1, redFactor}];
matrixSize = Dimensions[thinDEMdata];
nrows = matrixSize[[1]];
ncols = matrixSize[[2]];
newCellSize = redFactor * initialHeaderData[[5, 2]];
```

```
yllcorner = (initialHeaderData[[4, 2]] + ((initialHeaderData[[2, 2]] - 1) *
        initialHeaderData[[5, 2]])) - ((nrows - 1) * newCellSize);

headerData = {{initialHeaderData[[1, 1]], ncols}, {initialHeaderData[[2, 1]], nrows},
   {initialHeaderData[[3, 1]], initialHeaderData[[3, 2]]},
   {initialHeaderData[[4, 1]], yllcorner}, {initialHeaderData[[5, 1]], newCellSize},
   {initialHeaderData[[6, 1]], initialHeaderData[[6, 2]]}};

N[headerData]

mergedData = Join[headerData, thinDEMdata];
```

Export the resultant data file

Choose a name for the resultant data file (different from the name of the original data file) and specify the path to the directory where that file is to be saved. For example, on Vince Cronin' s office Macintosh, the following code will save a resultant file named "thinTahoeDEM.dat" on the desktop :

```
Export["/Users/vince/Desktop/thinTahoeDEM.dat", mergedData];
```

on Vince Cronin' s Dell, the **Export** code would look like the following for a data file named "thinTahoeDEM.dat" located on the C drive in the "TahoeRuns" directory :

```
SetDirectory["C:\TahoeRuns"];

Export["thinTahoeDEM.dat", mergedData];
```

Use the appropriate **Export** code below, and make sure it is in the **Input** style

```
Export[
  "/Users/vincecronin/Desktop/Trinidad/thinPurgatoireDEM.dat", mergedData];
```

How long did this program take to run, in minutes?

```
minutesForProcessing = (AbsoluteTime[] - startTime) / 60
```

```
startTime = AbsoluteTime[];
```

Projecting the nodal planes from a focal mechanism solution onto a digital elevation model surface with input records from an Excel spreadsheet

Begun August 5, 2004; Revised May 20, 2014

Introduction

text

Input

Input for the first earthquake in the set

```
counter = 51;
```

Remember to change the names of the output files

General input data

The `eqDataIn` is an Excel (.xls) spreadsheet that contains the earthquake data necessary for the analysis. The first record (row) of the spreadsheet contains words that describe the contents of each column, and each other record (row) contains the data for one earthquake focal mechanism. The data types are as follows, starting with the left-most column (column A): year, month, day, hour, minute, seconds, latitude, longitude, depth, greatest horizontal error (EH1), least horizontal error (EH2), azimuth of EH1 axis, vertical error, earthquake magnitude, Waldhauser's event number, thesis event number, dip direction of nodal plane 1, dip angle of nodal plane 1, rake of hanging-wall slip vector on nodal plane 1, dip direction on nodal plane 2, dip angle on nodal plane 2,

strike uncertainty, dip uncertainty, rake uncertainty, other ID number, solution number (if more than 1 focal mechanism is provided for an earthquake)

```
eqDataIn =
  Import["/Users/vincecronin/Desktop/TahoeDVFZ/Input_EQ_datafile.xls"];
eqData = Flatten[eqDataIn, 1];
```

On Vince' s MacBook Pro, the code is

```
mydata=Import["/Users/vincecronin/Desktop/NTahoeVThin.dat"];
```

On the office Dell workstation, the code is

```
SetDirectory["C:/TylerTahoe"];
mydata = Import["NTahoeVThin.dat"];
```

```
mydata = Import["/Users/vincecronin/Desktop/TahoeDVFZ/thinDVFZCrop.dat"];
```

The **zoneMeridian** is the longitude at the center of the UTM zone that contains the epicentral region. If the epicenter is near a zone boundary, base the UTM grid for this analysis in the zone that is to the west.

```
zoneMeridian = -123;
```

The **gridNorthAdjustment** is the angle between true north and grid north at/near the center of the map area. If grid north is found by a clockwise rotation from true north, the sign of the **gridNorthAdjustment** is negative; otherwise, it is positive. The **gridNorthAdjustment** is approximately equal to (zoneMeridian – (longitude at center of map area))*Sin[latitude at center of map area].

```
gridNorthAdjustment = (zoneMeridian - (-120.15)) * Sin[37.47 Degree]
```

The **epicenterWidth** is the half-width of the square that will be put over the top of the epicenter on the maps generated by this code, in meters

```
epicenterWidth = 250;
```

The **widthFactor** is a multiplier that allows for the adjustment of the half-width of the zone between parallel planes that generate the trace of the mean nodal plane on the maps generated by this code, in meters. A value of 1.5 for the **widthFactor** sets the distance between the planes at 1.5 times the cell size of the DEM.

```
widthFactor = 1.5;
```

The **topoBase** value forces one point of the DEM to have a particular value, which in turn allows the user to adjust the tonal range of the hillshade map.

```
topoBase = 0;
```

The constant **minusOne** is used as input for the pointEvaluator module, in the place for the null value.

```
minusOne = -1;
```

The **meanMultiplier** increases the width of the zone between parallel planes around the mean nodal plane, and is used to simplify interpretation of the seismo-lineament. Care must be taken so that the meanMultiplier value does not become so large that the ground-surface trace of the resulting planes extends beyond the boundaries of the seismo-lineament..

```
meanMultiplier = 1;
```

Some user-defined functions

```
makeVector[plunge_, trend_] := {Cos[plunge Degree] Sin[trend Degree],
   Cos[plunge Degree] Cos[trend Degree], -Sin[plunge Degree]};

vectorNorm[x_] := √x.x ;

unitVector[x_] :=
  {x[[1]] / vectorNorm[x], x[[2]] / vectorNorm[x], x[[3]] / vectorNorm[x]};

vectorAngle[a_, b_] := ArcCos[a.b / (vectorNorm[a] vectorNorm[b])];
```

The lat/long to UTM conversion is after Snyder (1982), and assumes use of the North American Datum of 1927 (NAD27). Another excellent resource for converting from lat/long to UTM and back, using a variety of datums (*e.g.*, NAD27, WGS84 and so on) is provided by Steven Dutch at http://www.uwgb.edu/dutchs/UsefulData/UTM-Formulas.htm, and by an online calculator at http://www.rcn.montana.edu/resources/tools/coordinates.aspx

```
convertToUTM[inLat_, inLong_, centMerid_] :=
  Module[{c1, c2, c3, c4, c5, v1, v2, v3, v4, v5, v6, utmX, utmY}, c1 = 6378206.4;
   c2 = 0.00676866; c3 = 0; c4 = centMerid; c5 = 0.9996; v1 = c2 / (1 - c2);
   v2 = c1 / Sqrt[1 - (c2 * (Sin[inLat Degree]^2))]; v3 = Tan[inLat Degree]^2;
   v4 = v1 * (Cos[inLat Degree]^2); v5 = (Cos[inLat Degree]) * ((inLong - c4) (π / 180));
   v6 = (111132.0894 * inLat) - (16216.94 * Sin[2 * (inLat Degree)]) +
     (17.21 * Sin[4 * (inLat Degree)]) - (0.02 * Sin[6 * (inLat Degree)]);
   utmX = (c5 * v2 * (v5 + (((1 - v3 + v4) * v5^3) / 6) +
          (((5 - (18 * v3) + (v3^2) + (72 * v4) - (58 * v1)) * v5^5) / 120)) + 500000;
   utmY = c5 * (v6 - 0 + (v2 * Tan[inLat Degree] * (((v5^2) / 2) +
            ((((5 - v3 + (9 * v4) + (4 * (v4^2))) * v5^4) / 24) + ((((61 - (58 * v3) + (v3^2) +
                 (600 * v4) - (330 * v1)) * v5^6) / 720))))); {utmX, utmY}];
```

The following module differentiates between points that are within "width" meters from the fault plane and those that are further away. Given unit vector N that is normal to the fault plane that passes through the origin of the coordinate system, the distance from an arbitrary point (whose position vector is P) to that plane is given by |N·P|.

```
pointEvaluator[xCoord_, yCoord_, zCoord_, width_, fltUNrml_, nulData_] :=
  Module[{locVect, distToFlt, result}, locVect = {xCoord, yCoord, zCoord};
   distToFlt = Abs[Dot[fltUNrml, locVect]];
   result = If[(distToFlt ≤ width), 10., nulData]; result];
```

Text

```
epicenterEval[xCoord_, yCoord_, zCoord_, width_, nulData_] :=
  Module[{locVect, distToEpicenter, result}, result = If[(Abs[xCoord] < width),
     If[(Abs[yCoord] < width), zCoord, nulData], nulData]; result];
```

The module `findHalfWidth` is used to determine the half-width of the uncertainty envelope given the lengths of the semi-axes of the triaxial uncertainty ellipsoid around the hypocenter, the azimuth of the greatest horizontal semi-axis, and the dip azimuth and dip angle of a nodal plane. The uncertainty envelope is bounded by parallel planes that are tangent to the uncertainty ellipsoid.

Input Parameters

- `dAz` is the trend or azimuth of the dip vector of the nodal plane, measured in degrees clockwise from north.

All input azimuths are measured relative to the geographic coordinate system. Hence, an azimuth of 90° corresponds to due east.

- `dAng` is the plunge of the dip vector of the nodal plane, measured in degrees down from horizontal. Hence, a dip angle of 90° corresponds to a vertical vector pointing down.
- `hEr1` is the length of the `a` semi-axis of the 95% CI uncertainty ellipsoid surrounding the mean hypocenter, measured in kilometers. Hence, a value of 1 for `hEr1` means that the surface of the 95% CI uncertainty ellipse is 1 km from the mean hypocenter measured horizontally in the direction `hEr1Az`.
- `hEr1Az` is the trend of the `e1h` uncertainty axis (i.e., of the `a` semi-axis of the 95% CI uncertainty ellipsoid surrounding the mean hypocenter), measured in degrees clockwise from north. All input azimuths are measured relative to the geographic coordinate system. Hence, an azimuth of 90° corresponds to due east.
- `hEr2` is the length of the `b` semi-axis of the 95% CI uncertainty ellipsoid surrounding the mean hypocenter, measured in kilometers. Hence, a value of 1 for `hEr2` means that the surface of the 95% CI uncertainty ellipse is 1 km from the mean hypocenter measured horizontally 90° from the direction `hEr1Az`.
- `vEz` is the length of the `c` semi-axis of the 95% CI uncertainty ellipsoid surrounding the mean hypocenter, measured in kilometers. Hence, a value of 1 for `vEz` means that the surface of the 95% CI uncertainty ellipse is 1 km from the mean hypocenter measured vertically.

Local Variables

- `var1` is the angle, in degrees, through which the geographic coordinate system (in which north is {0,1,0} and east is {1,0,0}) is transformed by rotation around the common `z` axis to the coordinate systen that is fixed to the axes of the triaxial uncertainty ellipsoid around the hypocenter (in which the `x` axis coincides with the `a` ellipsoidal axis and with `hEr1`, the `y` axis coincides with the `b` ellipsoidal axis and with `hEr2`, and the `z` axis is vertical and coincides with the `c` ellipsoidal axis and with `vEr`).
- `var2` is the unit vector parallel to the dip vector, in the geographic coordinate system in which north is {0,1,0} and east is {1,0,0}.
- `var3` is the unit vector parallel to the right - hand - rule strike, in the geographic coordinate system in which north is {0,1,0} and east is {1,0,0}.
- `var4` is the 3x3 rotation matrix in which a positive angle results in an anticlockwise rotation around the positive z axis.
- `var5` is the unit vector that is normal to the nodal plane in the geographic coordinate system in which north is {0,1,0} and east is {1,0,0}.
- `var6` is the unit vector that is normal to the nodal plane in the ellipsoid-centered coordinate system that is rotated `var1` degrees around the vertical (z) axis.
- `var7-9` are intermediate values that are ultimately used to compute the value of the Lagrangian multiplier lambda.
- `var10` is the Lagrangian multiplier lambda
- `var11` is the set of components of the location vector to one of the tangent points, expressed in the ellipsoid-centered coordinate system that is rotated `var1` degrees around the vertical (z) axis.
- `var12` is the distance, in km, between the a nodal plane through the hypocenter and a parallel nodal plane through one of the tangent points to the triaxial uncertainty ellipsoid around the hypocenter.

Output

- `result` is the distance, in km, between the a nodal plane through the hypocenter and a parallel nodal plane through one of the tangent points to the triaxial uncertainty ellipsoid around the hypocenter..

```
findHalfWidth[dipAz_, dipAng_, hEr1_, hEr1Az_, hEr2_, vEr_] :=
  Module[{var1, var2, var3, var4, var5, var6,
    var7, var8, var9, var10, var11, var12, result},
   var1 = hEr1Az - 90; var2 = {Cos[dipAng Degree] Sin[dipAz Degree],
     Cos[dipAng Degree] Cos[dipAz Degree], - Sin[dipAng Degree]};
   var3 = {Sin[(dipAz - 90) Degree], Cos[(dipAz - 90) Degree], 0};
   var4 = {{Cos[var1 Degree], - Sin[var1 Degree], 0}, {Sin[var1 Degree],
      Cos[var1 Degree], 0}, {0, 0, 1}}; var5 = Cross[var2, var3];
   var6 = var4.var5; var7 = (1 / hEr1^2) (var6[[1]] (hEr1^2 / 2))^2;
   var8 = (1 / hEr2^2) (var6[[2]] (hEr2^2 / 2))^2;
   var9 = (1 / vEr^2) (var6[[3]] (vEr^2 / 2))^2; var10 = Sqrt[(1 / (var7 + var8 + var9))];
   var11 = {var10 * var6[[1]] * (hEr1^2 / 2), var10 * var6[[2]] * (hEr2^2 / 2),
     var10 * var6[[3]] * (vEr^2 / 2)}; var12 = var6.var11; result = var12];
```

Computations specific to an individual hypocenter, for which there might be multiple focal mechanism solutions available

■ Read and interpret the DEM header information

```
headerData = Table[mydata[[i, j]], {i, 6}, {j, 2}];

ncols = headerData[[1, 2]]

nrows = headerData[[2, 2]]

xllcorner = headerData[[3, 2]]

yllcorner = headerData[[4, 2]]

cellsize = headerData[[5, 2]]

nodataValue = headerData[[6, 2]]
```

■ Read and interpret the hypocenter location data

```
record = counter;

focalLat = eqData[[record, 7]];

focalLong = eqData[[record, 8]];

focalDepthKm = eqData[[record, 9]];
```

The UTM coordinates that specify the horizontal position of the earthquake focus (i.e., the epicenter location) are given in meters. The variable focalDepth gives the depth of the earthquake focus, in meters.

```
focalDepth = focalDepthKm * (-1000)
```

The reported vertical and horizontal uncertainties in the location of the earthquake focus are given in kilome-

ters. The variables horizError and vertError convert these to meters.

```
eh1 = eqData[[record, 10]] * 1000

eh2 = eqData[[record, 11]] * 1000

eh1Azimuth = eqData[[record, 12]]

eh1Az = If[((eh1Azimuth + gridNorthAdjustment) < 0),
    (360 + eh1Azimuth + gridNorthAdjustment),
    If[((eh1Azimuth + gridNorthAdjustment) > 360),
     ((eh1Azimuth + gridNorthAdjustment) - 360),
     (eh1Azimuth + gridNorthAdjustment)]];

ez = eqData[[record, 13]] * 1000
```

Convert the input coordinates of the earthquake focus to the same coordinate system as the DEM data

```
utmCoordinates = convertToUTM[focalLat, focalLong, zoneMeridian];
```

The "focus" is the (x, y, z) coordinates in meters of the reported earthquake focus, in a coordinate system in which the origin is the lower-left (southwest) corner of the DEM at sea level.

```
focusMean = {(utmCoordinates[[1]] - xllcorner),
    (utmCoordinates[[2]] - yllcorner), focalDepth};

rawElevDataM =
  Table[mydata[[i + 6, j]] - focusMean[[3]], {i, nrows}, {j, ncols}];

demImageFileM = Table[rawElevDataM[[i, j]], {i, nrows}, {j, ncols}];
```

Computations specific to the first nodal plane

```
npDipTrend = eqData[[record, 17]]

npDipTr = If[((npDipTrend + gridNorthAdjustment) < 0),
   (360 + npDipTrend + gridNorthAdjustment),
   If[((npDipTrend + gridNorthAdjustment) > 360),
    ((npDipTrend + gridNorthAdjustment) - 360),
    (npDipTrend + gridNorthAdjustment)]]

npDipTrendUncert = eqData[[record, 22]]

npDipPlunge = eqData[[record, 18]]

npDipAngUncert = eqData[[record, 23]]
```

▪ Make the hillshade image

```
rawElevDataInput = Table[mydata[[i + 6, j]] , {i, nrows}, {j, ncols}];
```

```
elev3 = Table[demImageFileM[[i, j]], {i, nrows, 1, -1}, {j, ncols}];

npDipTrRad = npDipTr * (π / 180);

lightDirection =
  If[npDipTrRad > (3 π / 2), (2 π) - npDipTrRad, (π / 2) - npDipTrRad];

hillshadeMap1 = ReliefPlot[elev3, ColorFunction -> "GrayTones",
   LightingAngle -> {lightDirection, Pi / 12}];

ClearAll[elev3];
```

■ Swath 1 of 7: The middle of the road

Convert the fault dip vector from trend and plunge to a unit location vector

```
npDipVect = unitVector[makeVector[npDipPlunge, npDipTr]];
```

Find the strike vector defined using the right-hand rule

```
npStrike = If[(npDipTr < 90), (npDipTr + 270), (npDipTr - 90)];

npStrikeVect = {Sin[npStrike Degree], Cos[npStrike Degree], 0};
```

Find the unit vector that is normal to the fault plane and is directed upwards

```
npNormalVect = unitVector[Cross[npDipVect, npStrikeVect]];

zoneHalfWidthMThin = widthFactor * cellsize * Sin[npDipPlunge Degree];

N[%]

uncertSwath = Table[pointEvaluator[((cellsize * (j - 1)) - focusMean[[1]]),
    ((cellsize * (nrows - i)) - focusMean[[2]]), demImageFileM[[i, j]],
    zoneHalfWidthMThin, npNormalVect, minusOne], {i, nrows}, {j, ncols}];

elevData = Table[uncertSwath[[i, j]], {i, nrows, 1, -1}, {j, ncols}];

traceImgFileMThin = ListContourPlot[elevData, ContourShading -> False,
   AspectRatio -> Automatic, Contours -> {topoBase}];

elevDataTemp1 = elevData;

ClearAll[elevData, uncertSwath];
```

■ Swath 2 of 7: Gentle dip, smaller strike azimuth (GS)

Subtract the dip-angle uncertainty from the mean dip angle (i.e., from the plunge of the mean dip vector)

```
gentleDipAng = If[(npDipPlunge - npDipAngUncert) < 0,
   Abs[(npDipPlunge - npDipAngUncert)], (npDipPlunge - npDipAngUncert)];
```

Subtract the dip-trend uncertainty from the mean dip azimuth (i.e., from the mean dip trend)

```
gentleDipAzS = If[(npDipPlunge - npDipAngUncert) < 0,
    If[((npDipTr - npDipTrendUncert) > 180),
     ((npDipTr - npDipTrendUncert) - 180), ((npDipTr - npDipTrendUncert) + 180)],
    If[((npDipTr - npDipTrendUncert) < 0), 360 + (npDipTr - npDipTrendUncert),
     (npDipTr - npDipTrendUncert)]];
```

Convert the fault dip vector from trend and plunge to a unit location vector

```
dipVectGS = unitVector[makeVector[gentleDipAng, gentleDipAzS]];
```

Find the strike vector defined using the right-hand rule

```
strikeGS = If[(gentleDipAzS < 90), (gentleDipAzS + 270), (gentleDipAzS - 90)];
```

```
strikeVectGS = {Sin[strikeGS Degree], Cos[strikeGS Degree], 0};
```

Find the unit vector that is normal to the fault plane and is directed upwards

```
normalVectGS = unitVector[Cross[dipVectGS, strikeVectGS]];
```

Find the width of the nodal-plane uncertainty zone with the given dip angle, dip azimuth, and triaxial hypocenter uncertainty ellipsoid

```
zoneHalfWidthGS =
  findHalfWidth[gentleDipAzS, gentleDipAng, eh1, eh1Az, eh2, ez];
```

```
N[zoneHalfWidthGS]
```

Find the boundaries of the uncertainty swath as it intersects the ground surface

```
uncertSwath = Table[pointEvaluator[((cellsize * (j - 1)) - focusMean[[1]]),
    ((cellsize * (nrows - i)) - focusMean[[2]]), demImageFileM[[i, j]],
    zoneHalfWidthGS, normalVectGS, minusOne], {i, nrows}, {j, ncols}];
```

```
elevData = Table[uncertSwath[[i, j]], {i, nrows, 1, -1}, {j, ncols}];
```

traceImgFileGS = ListContourPlot[elevData, ContourShading -> False, AspectRatio -> Automatic, Contours -> {topoBase}];

```
elevDataTemp2 = elevData + elevDataTemp1;
```

```
ClearAll[elevData, elevDataTemp1, uncertSwath];
```

▪ Swath 3 of 7: Gentle dip, larger strike azimuth (GL)

Add the dip-trend uncertainty from the mean dip azimuth (i.e., from the mean dip trend)

```
gentleDipAzL = If[(npDipPlunge - npDipAngUncert) < 0,
    If[((npDipTr + npDipTrendUncert) > 180),
     ((npDipTr + npDipTrendUncert) - 180), ((npDipTr + npDipTrendUncert) + 180)],
    If[((npDipTr + npDipTrendUncert) > 360),
     (npDipTr + npDipTrendUncert) - 360, (npDipTr + npDipTrendUncert)]];
```

Convert the fault dip vector from trend and plunge to a unit location vector

```
dipVectGL = unitVector[makeVector[gentleDipAng, gentleDipAzL]];
```

Find the strike vector defined using the right-hand rule

```
strikeGL = If[(gentleDipAzL < 90), (gentleDipAzL + 270), (gentleDipAzL - 90)];

strikeVectGL = {Sin[strikeGL Degree], Cos[strikeGL Degree], 0};
```

Find the unit vector that is normal to the fault plane and is directed upwards

```
normalVectGL = unitVector[Cross[dipVectGL, strikeVectGL]];
```

Find the width of the nodal-plane uncertainty zone with the given dip angle, dip azimuth, and triaxial hypocenter uncertainty ellipsoid

```
zoneHalfWidthGL =
  findHalfWidth[gentleDipAzL, gentleDipAng, eh1, eh1Az, eh2, ez];

N[zoneHalfWidthGL]
```

Find the boundaries of the uncertainty swath as it intersects the ground surface

```
uncertSwath = Table[pointEvaluator[((cellsize * (j - 1)) - focusMean[[1]]),
    ((cellsize * (nrows - i)) - focusMean[[2]]), demImageFileM[[i, j]],
    zoneHalfWidthGL, normalVectGL, minusOne], {i, nrows}, {j, ncols}];

elevData = Table[uncertSwath[[i, j]], {i, nrows, 1, -1}, {j, ncols}];
```

traceImgFileGL = ListContourPlot[elevData, ContourShading -> False, AspectRatio -> Automatic, Contours -> {topoBase}];

```
elevDataTemp1 = elevData + elevDataTemp2;

ClearAll[elevData, elevDataTemp2, uncertSwath];

Dimensions[elevDataTemp1]
```

■ Swath 4 of 7: Steep dip, smaller strike azimuth (SS)

Add the dip-angle uncertainty to the mean dip angle (i.e., from the plunge of the mean dip vector)

```
steepDipAng = If[(npDipPlunge + npDipAngUncert) > 90,
   (180 - (npDipPlunge + npDipAngUncert)), (npDipPlunge + npDipAngUncert)];
```

Subtract the dip-trend uncertainty from the mean dip azimuth (i.e., from the mean dip trend)

```
steepDipAzS = If[(npDipPlunge + npDipAngUncert) > 90,
   If[((npDipTr - npDipTrendUncert) > 180),
    ((npDipTr - npDipTrendUncert) - 180), ((npDipTr - npDipTrendUncert) + 180)],
   If[((npDipTr - npDipTrendUncert) < 0), 360 + (npDipTr - npDipTrendUncert),
    (npDipTr - npDipTrendUncert)]];
```

Convert the fault dip vector from trend and plunge to a unit location vector

```
dipVectSS = unitVector[makeVector[steepDipAng, steepDipAzS]];
```

Find the width of the nodal-plane uncertainty zone with the given dip angle, dip azimuth, and triaxial hypocenter uncertainty ellipsoid

```
zoneHalfWidthSL =
  findHalfWidth[steepDipAzL, steepDipAng, eh1, eh1Az, eh2, ez];
```

```
N[zoneHalfWidthSL]
```

Find the boundaries of the uncertainty swath as it intersects the ground surface

```
uncertSwath = Table[pointEvaluator[((cellsize * (j - 1)) - focusMean[[1]]),
    ((cellsize * (nrows - i)) - focusMean[[2]]), demImageFileM[[i, j]],
    zoneHalfWidthSL, normalVectSL, minusOne], {i, nrows}, {j, ncols}];
```

```
elevData = Table[uncertSwath[[i, j]], {i, nrows, 1, -1}, {j, ncols}];
```

traceImgFileSL = ListContourPlot[elevData, ContourShading -> False, AspectRatio -> Automatic, Contours -> {topoBase}];

```
elevDataTemp1 = elevData + elevDataTemp2;
```

```
ClearAll[elevData, elevDataTemp2, uncertSwath];
```

▪ Swath 6 of 7: Steep dip, mean strike azimuth (SM)

Add the dip-trend uncertainty from the mean dip azimuth (i.e., from the mean dip trend)

```
steepDipAzM = If[(npDipPlunge + npDipAngUncert) > 90,
   If[(npDipTr > 180), (npDipTr - 180), (npDipTr + 180)], npDipTr];
```

Convert the fault dip vector from trend and plunge to a unit location vector

```
dipVectSM = unitVector[makeVector[steepDipAng, steepDipAzM]];
```

Find the strike vector defined using the right-hand rule

```
strikeSM = If[(steepDipAzM < 90), (steepDipAzM + 270), (steepDipAzM - 90)];
```

```
strikeVectSM = {Sin[strikeSM Degree], Cos[strikeSM Degree], 0};
```

Find the unit vector that is normal to the fault plane and is directed upwards

```
normalVectSM = unitVector[Cross[dipVectSM, strikeVectSM]];
```

Find the width of the nodal-plane uncertainty zone with the given dip angle, dip azimuth, and triaxial hypocenter uncertainty ellipsoid

```
zoneHalfWidthSM =
  findHalfWidth[steepDipAzM, steepDipAng, eh1, eh1Az, eh2, ez];
```

```
N[zoneHalfWidthSM]
```

Find the boundaries of the uncertainty swath as it intersects the ground surface

Find the strike vector defined using the right-hand rule

```
strikeSS = If[(steepDipAzS < 90), (steepDipAzS + 270), (steepDipAzS - 90)];

strikeVectSS = {Sin[strikeSS Degree], Cos[strikeSS Degree], 0};
```

Find the unit vector that is normal to the fault plane and is directed upwards

```
normalVectSS = unitVector[Cross[dipVectSS, strikeVectSS]];
```

Find the width of the nodal-plane uncertainty zone with the given dip angle, dip azimuth, and triaxial hypocenter uncertainty ellipsoid

```
zoneHalfWidthSS =
  findHalfWidth[steepDipAzS, steepDipAng, eh1, eh1Az, eh2, ez];

N[zoneHalfWidthSS]
```

Find the boundaries of the uncertainty swath as it intersects the ground surface

```
uncertSwath = Table[pointEvaluator[((cellsize * (j - 1)) - focusMean[[1]]),
     ((cellsize * (nrows - i)) - focusMean[[2]]), demImageFileM[[i, j]],
     zoneHalfWidthSS, normalVectSS, minusOne], {i, nrows}, {j, ncols}];

elevData = Table[uncertSwath[[i, j]], {i, nrows, 1, -1}, {j, ncols}];
```

traceImgFileSS = ListContourPlot[elevData, ContourShading -> False, AspectRatio -> Automatic, Contours -> {topoBase}];

```
elevDataTemp2 = elevData + elevDataTemp1;

ClearAll[elevData, elevDataTemp1, uncertSwath];
```

▪ Swath 5 of 7: Steep dip, larger strike azimuth (SL)

Add the dip-trend uncertainty from the mean dip azimuth (i.e., from the mean dip trend)

```
steepDipAzL = If[(npDipPlunge + npDipAngUncert) > 90,
   If[((npDipTr + npDipTrendUncert) > 180),
    ((npDipTr + npDipTrendUncert) - 180), ((npDipTr + npDipTrendUncert) + 180)],
   If[((npDipTr + npDipTrendUncert) > 360),
    (npDipTr + npDipTrendUncert) - 360, (npDipTr + npDipTrendUncert)]];
```

Convert the fault dip vector from trend and plunge to a unit location vector

```
dipVectSL = unitVector[makeVector[steepDipAng, steepDipAzL]];
```

Find the strike vector defined using the right-hand rule

```
strikeSL = If[(steepDipAzL < 90), (steepDipAzL + 270), (steepDipAzL - 90)];

strikeVectSL = {Sin[strikeSL Degree], Cos[strikeSL Degree], 0};
```

Find the unit vector that is normal to the fault plane and is directed upwards

```
normalVectSL = unitVector[Cross[dipVectSL, strikeVectSL]];
```

```
uncertSwath = Table[pointEvaluator[((cellsize * (j - 1)) - focusMean[[1]]),
     ((cellsize * (nrows - i)) - focusMean[[2]]), demImageFileM[[i, j]],
     zoneHalfWidthSM, normalVectSM, minusOne], {i, nrows}, {j, ncols}];

elevData = Table[uncertSwath[[i, j]], {i, nrows, 1, -1}, {j, ncols}];
```

traceImgFileSM = ListContourPlot[elevData, ContourShading -> False, AspectRatio -> Automatic, Contours -> {topoBase}];

```
elevDataTemp2 = elevData + elevDataTemp1;

ClearAll[elevData, elevDataTemp1, uncertSwath];
```

■ Swath 7 of 7: The middle of the road

Convert the fault dip vector from trend and plunge to a unit location vector

```
npDipVect = unitVector[makeVector[npDipPlunge, npDipTr]];
```

Find the strike vector defined using the right-hand rule

```
npStrike = If[(npDipTr < 90), (npDipTr + 270), (npDipTr - 90)];

npStrikeVect = {Sin[npStrike Degree], Cos[npStrike Degree], 0};
```

Find the unit vector that is normal to the fault plane and is directed upwards

```
npNormalVect = unitVector[Cross[npDipVect, npStrikeVect]];
```

Find the width of the nodal-plane uncertainty zone with the given dip angle, dip azimuth, and triaxial hypocenter uncertainty ellipsoid

```
zoneHalfWidthMean =
  findHalfWidth[npDipTr, npDipPlunge, eh1, eh1Az, eh2, ez];

N[zoneHalfWidthMean]
```

zoneHalfWidthMean = widthFactor*cellsize*Sin[npDipPlunge Degree];

```
uncertSwath = Table[pointEvaluator[((cellsize * (j - 1)) - focusMean[[1]]),
     ((cellsize * (nrows - i)) - focusMean[[2]]), demImageFileM[[i, j]],
     zoneHalfWidthMean, npNormalVect, minusOne], {i, nrows}, {j, ncols}];

elevData = Table[uncertSwath[[i, j]], {i, nrows, 1, -1}, {j, ncols}];
```

traceImgFileMean = ListContourPlot[elevData, ContourShading -> False, AspectRatio -> Automatic, Contours -> {topoBase}];

```
elevDataTemp1 = elevData + elevDataTemp2;

summary = Table[
   If[elevDataTemp1[[i, j]] < 0, minusOne, 1], {i, nrows}, {j, ncols}];

traceImgFileSum = ListContourPlot[summary, ContourShading → False,
   AspectRatio → Automatic, Contours → {topoBase}];
```

```
ClearAll[elevData, elevDataTemp1, elevDataTemp2, uncertSwath];
```

▪ Epicenter

```
epicenterDot = Table[epicenterEval[((cellsize * (j - 1)) - focusMean[[1]]),
    ((cellsize * (nrows - i)) - focusMean[[2]]), demImageFileM[[i, j]],
    epicenterWidth, minusOne], {i, nrows}, {j, ncols}];

elevData = Table[epicenterDot[[i, j]], {i, nrows, 1, -1}, {j, ncols}];

traceImgFileE = ListContourPlot[elevData, ContourShading -> False,
   AspectRatio -> Automatic, Contours -> {topoBase}];

ClearAll[elevData, epicenterDot];

ClearAll[npDipTr, npDipTrend, npDipPlunge, npDipVect, npStrike, npStrikeVect,
  npNormalVect, zoneHalfWidthMean, gentleDipAng, gentleDipAzS,
  dipVectGS, strikeGS, strikeVectGS, normalVectGS, zoneHalfWidthGS,
  gentleDipAzL, dipVectGL, strikeGL, strikeVectGL, normalVectGL,
  zoneHalfWidthGL, steepDipAng, steepDipAzS, dipVectSS, strikeSS,
  strikeVectSS, normalVectSS, zoneHalfWidthSS, steepDipAzL, dipVectSL,
  strikeSL, strikeVectSL, normalVectSL, zoneHalfWidthSL, steepDipAzM,
  dipVectSM, strikeSM, strikeVectSM, normalVectSM, zoneHalfWidthSM];
```

Output

```
outFile1 = Show[hillshadeMap1, traceImgFileMThin, traceImgFileE];

Show[%]

outFile2 = Show[traceImgFileMThin, traceImgFileSum, traceImgFileE];

Show[%]

outFile3 = Show[hillshadeMap1, outFile2];

Show[%]
```

The black square in the "`outFile2`" image marks the epicenter of the earthquake. The length of each side is approximately "`epicenterWidth`" in meters.

```
ClearAll[traceImgFileMean, traceImgFileGS, traceImgFileGL,
  traceImgFileSS, traceImgFileSL, traceImgFileSM, traceImgFileMThin];
```

▪ Export data and image files

The file created in the next line is JPEG image that contains the graphic showing the hillshade image developed from the DEM, curves marking the boundaries of the uncertainty regions, and a circle with 1 km diameter centered on the epicenter.

IMPORTANT NOTE: The user must supply a name for the output file that is different from existing file names, or else the existing files may be over-written.

```
Export[
  "/Users/vincecronin/Desktop/TahoeDVFZ/RyallMS/map1.jpg", outFile1];
```

```
Export[
  "/Users/vincecronin/Desktop/TahoeDVFZ/RyallMS/map2.jpg", outFile2];
```

```
Export[
  "/Users/vincecronin/Desktop/TahoeDVFZ/RyallMS/map3.jpg", outFile3];
```

```
ClearAll[outFile1, outFile3];
```

- **How long did this program take to run to this point, in minutes?**

```
minutesForProcessing1 = (AbsoluteTime[] - startTime) / 60
```

[redacted]

Computations specific to the second nodal plane

```
npDipTrend = eqData[[record, 20]];
```

```
npDipTr = If[((npDipTrend + gridNorthAdjustment) < 0),
    (360 + npDipTrend + gridNorthAdjustment),
    If[((npDipTrend + gridNorthAdjustment) > 360),
     ((npDipTrend + gridNorthAdjustment) - 360),
     (npDipTrend + gridNorthAdjustment)]];
```

```
npDipTrendUncert = eqData[[record, 22]];
```

```
npDipPlunge = eqData[[record, 21]];
```

```
npDipAngUncert = eqData[[record, 23]];
```

- **Make the hillshade image for the second nodal plane**

```
rawElevDataInput = Table[mydata[[i + 6, j]], {i, nrows}, {j, ncols}];
```

```
elev3 = Table[demImageFileM[[i, j]], {i, nrows, 1, -1}, {j, ncols}];
```

```
npDipTrRad = npDipTr * (π / 180);
```

```
lightDirection =
  If[npDipTrRad > (3 π / 2), (2 π) - npDipTrRad, (π / 2) - npDipTrRad];
```

```
hillshadeMap2 = ReliefPlot[elev3, ColorFunction -> "GrayTones",
   LightingAngle -> {lightDirection, Pi / 12}];
```

```
ClearAll[elev3];
```

▪ Swath 1 of 7: The middle of the road

Convert the fault dip vector from trend and plunge to a unit location vector

```
npDipVect = unitVector[makeVector[npDipPlunge, npDipTr]];
```

Find the strike vector defined using the right-hand rule

```
npStrike = If[(npDipTr < 90), (npDipTr + 270), (npDipTr - 90)];

npStrikeVect = {Sin[npStrike Degree], Cos[npStrike Degree], 0};
```

Find the unit vector that is normal to the fault plane and is directed upwards

```
npNormalVect = unitVector[Cross[npDipVect, npStrikeVect]];

zoneHalfWidthMThin = widthFactor * cellsize * Sin[npDipPlunge Degree];

N[zoneHalfWidthMThin]

uncertSwath = Table[pointEvaluator[((cellsize * (j - 1)) - focusMean[[1]]),
    ((cellsize * (nrows - i)) - focusMean[[2]]), demImageFileM[[i, j]],
    zoneHalfWidthMThin, npNormalVect, minusOne], {i, nrows}, {j, ncols}];

elevData = Table[uncertSwath[[i, j]], {i, nrows, 1, -1}, {j, ncols}];

traceImgFileMThin = ListContourPlot[elevData, ContourShading -> False,
   AspectRatio -> Automatic, Contours -> {topoBase}];

elevDataTemp1 = elevData;

ClearAll[elevData, uncertSwath];
```

▪ Swath 2 of 7: Gentle dip, smaller strike azimuth (GS)

Subtract the dip-angle uncertainty from the mean dip angle (i.e., from the plunge of the mean dip vector)

```
gentleDipAng = If[(npDipPlunge - npDipAngUncert) < 0,
   Abs[(npDipPlunge - npDipAngUncert)], (npDipPlunge - npDipAngUncert)];
```

Subtract the dip-trend uncertainty from the mean dip azimuth (i.e., from the mean dip trend)

```
gentleDipAzS = If[(npDipPlunge - npDipAngUncert) < 0,
   If[((npDipTr - npDipTrendUncert) > 180),
    ((npDipTr - npDipTrendUncert) - 180), ((npDipTr - npDipTrendUncert) + 180)],
   If[((npDipTr - npDipTrendUncert) < 0), 360 + (npDipTr - npDipTrendUncert),
    (npDipTr - npDipTrendUncert)]];
```

Convert the fault dip vector from trend and plunge to a unit location vector

```
dipVectGS = unitVector[makeVector[gentleDipAng, gentleDipAzS]];
```

Find the strike vector defined using the right-hand rule

```
strikeGS = If[(gentleDipAzS < 90), (gentleDipAzS + 270), (gentleDipAzS - 90)];

strikeVectGS = {Sin[strikeGS Degree], Cos[strikeGS Degree], 0};
```

Find the unit vector that is normal to the fault plane and is directed upwards

```
normalVectGS = unitVector[Cross[dipVectGS, strikeVectGS]];
```

Find the width of the nodal-plane uncertainty zone with the given dip angle, dip azimuth, and triaxial hypocenter uncertainty ellipsoid

```
zoneHalfWidthGS =
  findHalfWidth[gentleDipAzS, gentleDipAng, eh1, eh1Az, eh2, ez];

N[zoneHalfWidthGS]
```

Find the boundaries of the uncertainty swath as it intersects the ground surface

```
uncertSwath = Table[pointEvaluator[((cellsize * (j - 1)) - focusMean[[1]]),
    ((cellsize * (nrows - i)) - focusMean[[2]]), demImageFileM[[i, j]],
    zoneHalfWidthGS, normalVectGS, minusOne], {i, nrows}, {j, ncols}];

elevData = Table[uncertSwath[[i, j]], {i, nrows, 1, -1}, {j, ncols}];
```

traceImgFileGS = ListContourPlot[elevData, ContourShading -> False, AspectRatio -> Automatic, Contours -> {topoBase}];

```
elevDataTemp2 = elevData + elevDataTemp1;

ClearAll[elevData, elevDataTemp1, uncertSwath];
```

▪ Swath 3 of 7: Gentle dip, larger strike azimuth (GL)

Add the dip-trend uncertainty from the mean dip azimuth (i.e., from the mean dip trend)

```
gentleDipAzL = If[(npDipPlunge - npDipAngUncert) < 0,
   If[((npDipTr + npDipTrendUncert) > 180),
    ((npDipTr + npDipTrendUncert) - 180), ((npDipTr + npDipTrendUncert) + 180)],
   If[((npDipTr + npDipTrendUncert) > 360),
    (npDipTr + npDipTrendUncert) - 360, (npDipTr + npDipTrendUncert)]];
```

Convert the fault dip vector from trend and plunge to a unit location vector

```
dipVectGL = unitVector[makeVector[gentleDipAng, gentleDipAzL]];
```

Find the strike vector defined using the right-hand rule

```
strikeGL = If[(gentleDipAzL < 90), (gentleDipAzL + 270), (gentleDipAzL - 90)];

strikeVectGL = {Sin[strikeGL Degree], Cos[strikeGL Degree], 0};
```

Find the unit vector that is normal to the fault plane and is directed upwards

```
normalVectGL = unitVector[Cross[dipVectGL, strikeVectGL]];
```

Find the width of the nodal-plane uncertainty zone with the given dip angle, dip azimuth, and triaxial hypocen-

ter uncertainty ellipsoid

```
zoneHalfWidthGL =
  findHalfWidth[gentleDipAzL, gentleDipAng, eh1, eh1Az, eh2, ez];

N[zoneHalfWidthGL]
```

Find the boundaries of the uncertainty swath as it intersects the ground surface

```
uncertSwath = Table[pointEvaluator[((cellsize * (j - 1)) - focusMean[[1]]),
    ((cellsize * (nrows - i)) - focusMean[[2]]), demImageFileM[[i, j]],
    zoneHalfWidthGL, normalVectGL, minusOne], {i, nrows}, {j, ncols}];

elevData = Table[uncertSwath[[i, j]], {i, nrows, 1, -1}, {j, ncols}];
```

traceImgFileGL = ListContourPlot[elevData, ContourShading -> False, AspectRatio -> Automatic, Contours -> {topoBase}];

```
elevDataTemp1 = elevData + elevDataTemp2;

ClearAll[elevData, elevDataTemp2, uncertSwath];
```

▪ Swath 4 of 7: Steep dip, smaller strike azimuth (SS)

Add the dip-angle uncertainty to the mean dip angle (i.e., from the plunge of the mean dip vector)

```
steepDipAng = If[(npDipPlunge + npDipAngUncert) > 90,
   (180 - (npDipPlunge + npDipAngUncert)), (npDipPlunge + npDipAngUncert)];
```

Subtract the dip-trend uncertainty from the mean dip azimuth (i.e., from the mean dip trend)

```
steepDipAzS = If[(npDipPlunge + npDipAngUncert) > 90,
   If[((npDipTr - npDipTrendUncert) > 180),
    ((npDipTr - npDipTrendUncert) - 180), ((npDipTr - npDipTrendUncert) + 180)],
   If[((npDipTr - npDipTrendUncert) < 0), 360 + (npDipTr - npDipTrendUncert),
    (npDipTr - npDipTrendUncert)]];
```

Convert the fault dip vector from trend and plunge to a unit location vector

```
dipVectSS = unitVector[makeVector[steepDipAng, steepDipAzS]];
```

Find the strike vector defined using the right-hand rule

```
strikeSS = If[(steepDipAzS < 90), (steepDipAzS + 270), (steepDipAzS - 90)];

strikeVectSS = {Sin[strikeSS Degree], Cos[strikeSS Degree], 0};
```

Find the unit vector that is normal to the fault plane and is directed upwards

```
normalVectSS = unitVector[Cross[dipVectSS, strikeVectSS]];
```

Find the width of the nodal-plane uncertainty zone with the given dip angle, dip azimuth, and triaxial hypocenter uncertainty ellipsoid

```
zoneHalfWidthSS = findHalfWidth[steepDipAzS, steepDipAng, eh1, eh1Az, eh2, ez];
```

```
N[zoneHalfWidthSS]
```

Find the boundaries of the uncertainty swath as it intersects the ground surface

```
uncertSwath = Table[pointEvaluator[((cellsize * (j - 1)) - focusMean[[1]]),
    ((cellsize * (nrows - i)) - focusMean[[2]]), demImageFileM[[i, j]],
    zoneHalfWidthSS, normalVectSS, minusOne], {i, nrows}, {j, ncols}];

elevData = Table[uncertSwath[[i, j]], {i, nrows, 1, -1}, {j, ncols}];
```

traceImgFileSS = ListContourPlot[elevData, ContourShading -> False, AspectRatio -> Automatic, Contours -> {topoBase}];

```
elevDataTemp2 = elevData + elevDataTemp1;

ClearAll[elevData, elevDataTemp1, uncertSwath];
```

▪ Swath 5 of 7: Steep dip, larger strike azimuth (SL)

Add the dip-trend uncertainty from the mean dip azimuth (i.e., from the mean dip trend)

```
steepDipAzL = If[(npDipPlunge + npDipAngUncert) > 90,
   If[((npDipTr + npDipTrendUncert) > 180),
    ((npDipTr + npDipTrendUncert) - 180), ((npDipTr + npDipTrendUncert) + 180)],
   If[((npDipTr + npDipTrendUncert) > 360),
    (npDipTr + npDipTrendUncert) - 360, (npDipTr + npDipTrendUncert)]];
```

Convert the fault dip vector from trend and plunge to a unit location vector

```
dipVectSL = unitVector[makeVector[steepDipAng, steepDipAzL]];
```

Find the strike vector defined using the right-hand rule

```
strikeSL = If[(steepDipAzL < 90), (steepDipAzL + 270), (steepDipAzL - 90)];

strikeVectSL = {Sin[strikeSL Degree], Cos[strikeSL Degree], 0};
```

Find the unit vector that is normal to the fault plane and is directed upwards

```
normalVectSL = unitVector[Cross[dipVectSL, strikeVectSL]];
```

Find the width of the nodal-plane uncertainty zone with the given dip angle, dip azimuth, and triaxial hypocenter uncertainty ellipsoid

```
zoneHalfWidthSL = findHalfWidth[steepDipAzL, steepDipAng, eh1, eh1Az, eh2, ez];

N[zoneHalfWidthSL]
```

Find the boundaries of the uncertainty swath as it intersects the ground surface

```
uncertSwath = Table[pointEvaluator[((cellsize * (j - 1)) - focusMean[[1]]),
    ((cellsize * (nrows - i)) - focusMean[[2]]), demImageFileM[[i, j]],
    zoneHalfWidthSL, normalVectSL, minusOne], {i, nrows}, {j, ncols}];

elevData = Table[uncertSwath[[i, j]], {i, nrows, 1, -1}, {j, ncols}];
```

traceImgFileSL = ListContourPlot[elevData, ContourShading -> False, AspectRatio -> Automatic, Contours -> {topoBase}];

```
elevDataTemp1 = elevData + elevDataTemp2;
```

```
ClearAll[elevData, elevDataTemp2, uncertSwath];
```

▪ Swath 6 of 7: Steep dip, mean strike azimuth (SM)

Add the dip-trend uncertainty from the mean dip azimuth (i.e., from the mean dip trend)

```
steepDipAzM = If[(npDipPlunge + npDipAngUncert) > 90,
   If[(npDipTr > 180), (npDipTr - 180), (npDipTr + 180)], npDipTr];
```

Convert the fault dip vector from trend and plunge to a unit location vector

```
dipVectSM = unitVector[makeVector[steepDipAng, steepDipAzM]];
```

Find the strike vector defined using the right-hand rule

```
strikeSM = If[(steepDipAzM < 90), (steepDipAzM + 270), (steepDipAzM - 90)];
```

```
strikeVectSM = {Sin[strikeSM Degree], Cos[strikeSM Degree], 0};
```

Find the unit vector that is normal to the fault plane and is directed upwards

```
normalVectSM = unitVector[Cross[dipVectSM, strikeVectSM]];
```

Find the width of the nodal-plane uncertainty zone with the given dip angle, dip azimuth, and triaxial hypocenter uncertainty ellipsoid

```
zoneHalfWidthSM = findHalfWidth[steepDipAzM, steepDipAng, eh1, eh1Az, eh2, ez];
```

```
N[zoneHalfWidthSM]
```

Find the boundaries of the uncertainty swath as it intersects the ground surface

```
uncertSwath = Table[pointEvaluator[((cellsize * (j - 1)) - focusMean[[1]]),
     ((cellsize * (nrows - i)) - focusMean[[2]]), demImageFileM[[i, j]],
     zoneHalfWidthSM, normalVectSM, minusOne], {i, nrows}, {j, ncols}];
```

```
elevData = Table[uncertSwath[[i, j]], {i, nrows, 1, -1}, {j, ncols}];
```

traceImgFileSM = ListContourPlot[elevData, ContourShading -> False, AspectRatio -> Automatic, Contours -> {topoBase}];

```
elevDataTemp2 = elevData + elevDataTemp1;
```

```
ClearAll[elevData, elevDataTemp1, uncertSwath];
```

▪ Swath 7 of 7: The middle of the road

Convert the fault dip vector from trend and plunge to a unit location vector

```
npDipVect = unitVector[makeVector[npDipPlunge, npDipTr]];
```

Find the strike vector defined using the right-hand rule

```
npStrike = If[(npDipTr < 90), (npDipTr + 270), (npDipTr - 90)];

npStrikeVect = {Sin[npStrike Degree], Cos[npStrike Degree], 0};
```

Find the unit vector that is normal to the fault plane and is directed upwards

```
npNormalVect = unitVector[Cross[npDipVect, npStrikeVect]];
```

Find the width of the nodal-plane uncertainty zone with the given dip angle, dip azimuth, and triaxial hypocenter uncertainty ellipsoid

```
zoneHalfWidthMean = findHalfWidth[npDipTr, npDipPlunge, eh1, eh1Az, eh2, ez];

N[zoneHalfWidthMean]
```

zoneHalfWidthMean = widthFactor*cellsize*Sin[npDipPlunge Degree];

```
uncertSwath = Table[pointEvaluator[((cellsize * (j - 1)) - focusMean[[1]]),
    ((cellsize * (nrows - i)) - focusMean[[2]]), demImageFileM[[i, j]],
    zoneHalfWidthMean, npNormalVect, minusOne], {i, nrows}, {j, ncols}];

elevData = Table[uncertSwath[[i, j]], {i, nrows, 1, -1}, {j, ncols}];
```

traceImgFileMean = ListContourPlot[elevData, ContourShading -> False, AspectRatio -> Automatic, Contours -> {topoBase}];

```
elevDataTemp1 = elevData + elevDataTemp2;

summary = Table[If[elevDataTemp1[[i, j]] < 0, -1., 1.], {i, nrows}, {j, ncols}];

traceImgFileSum = ListContourPlot[summary, ContourShading → False,
   AspectRatio → Automatic, Contours → {topoBase}];

ClearAll[elevData, elevDataTemp1, elevDataTemp2, uncertSwath];

ClearAll[npDipTr, npDipTrend, npDipPlunge, npDipVect, npStrike, npStrikeVect,
  npNormalVect, zoneHalfWidthMean, gentleDipAng, gentleDipAzS,
  dipVectGS, strikeGS, strikeVectGS, normalVectGS, zoneHalfWidthGS,
  gentleDipAzL, dipVectGL, strikeGL, strikeVectGL, normalVectGL,
  zoneHalfWidthGL, steepDipAng, steepDipAzS, dipVectSS, strikeSS,
  strikeVectSS, normalVectSS, zoneHalfWidthSS, steepDipAzL, dipVectSL,
  strikeSL, strikeVectSL, normalVectSL, zoneHalfWidthSL, steepDipAzM,
  dipVectSM, strikeSM, strikeVectSM, normalVectSM, zoneHalfWidthSM];
```

Output

```
outFile4 = Show[hillshadeMap2, traceImgFileMThin, traceImgFileB];

Show[%]

outFile5 = Show[traceImgFileMThin, traceImgFileSum, traceImgFileB];
```

```
Show[%]

outFile6 = Show[hillshadeMap2, outFile5];

Show[%]

outFile7 = Show[hillshadeMap2, outFile2, outFile5];
```

The black square in the "outFile5" image marks the epicenter of the earthquake. The length of each side is approximately "epicenterWidth" in meters.

```
ClearAll[traceImgFileMean, traceImgFileGS, traceImgFileGL,
  traceImgFileSS, traceImgFileSL, traceImgFileSM, traceImgFileMThin];
```

▪ Export data and image files

The file created in the next line is JPEG image that contains the graphic showing the hillshade image developed from the DEM, curves marking the boundaries of the uncertainty regions, and a circle with 1 km diameter centered on the epicenter.

IMPORTANT NOTE: The user must supply a name for the output file that is different from existing file names, or else the existing files may be over-written.

```
Export[
  "/Users/vincecronin/Desktop/TahoeDVFZ/RyallMS/map4.jpg", outFile4];
```

```
Export[
  "/Users/vincecronin/Desktop/TahoeDVFZ/RyallMS/map5.jpg", outFile5];
```

```
Export[
  "/Users/vincecronin/Desktop/TahoeDVFZ/RyallMS/map6.jpg", outFile6];
```

```
Export[
  "/Users/vincecronin/Desktop/TahoeDVFZ/RyallMS/map7.jpg", outFile7];
```

```
ClearAll[outFine2, outFile4, outFile5, outFile6, outFile7];
```

```
Beep[]

Beep[]

Beep[]
```

Closing

- **How long did this program take to run, in minutes?**

```
minutesForProcessing2 = (AbsoluteTime[] - startTime) / 60
```

References

Colley, S.J., 2002, Vector calculus [2nd edition]: Upper Saddle River, New Jersey, Prentice-Hall, 558 p., (pp. 43-50), ISBN 0-13-041531-6.

Cronin, V.S., and Sverdrup, K.A., 1998, Preliminary assessment of the seismicity of the Malibu Coast Fault Zone, southern California, and related issues of philosophy and practice, *in* Welby, C.W., and Gowan, M.E. [editors], A Paradox of Power--Voices of Warning and Reason in the Geosciences: Geological Society of America, Reviews in Engineering Geology, p. 123-155.

Cronin, V.S., Byars, B.W., and Gammill, T., 2003, Developing techniques for regional structural interpretation using GIS and DEM-based terrain analysis: Geological Society of America, Abstracts with Programs, v. 34, no. 7, p. 261. http://gsa.confex.com/gsa/2003AM/finalprogram/abstract_61851.htm

Cronin, V.S., Millard, M.A., Seidman, L.E., and Bayliss, B.G., 2008, The Seismo-Lineament Analysis Method [SLAM] -- A reconnaissance tool to help find seismogenic faults: Environmental and Engineering Geoscience, v. 14, no. 3, p. 199-219.

Davis, H.F., and Snider, A.D., 1987, Introduction to vector analysis [5th edition]: Boston, Allyn and Bacon, 365 p. (pp. 34-37), ISBN 0-205-10263-8.

Gammill, T., Cronin, V.S., and Byars, B.W., 2004, Combining earthquake focal data and digital map analysis in reconnaissance for active faults, central Santa Monica Mountains and northern Santa Monica Bay, California: Geological Society of America, Abstracts with Programs,v. 36, no. 5, http://gsa.confex.com/gsa/2004AM/finalprogram/abstract_80352.htm

Haneberg, W.C., 2004, Computational geosciences with *Mathematica*: Berlin, Springer-Verlag, 381 p., CD, ISBN 3-540-40245-4.

Snyder, J.P., 1982, Map projections used by the U.S. Geological Survey: U.S. Geological Survey Bulletin 1532, pp. 63-69 and 233-235.

Make hillshade images illumined parallel to the nodal plane dip direction (MakeLitHillshade.nb)

Written July 6, 2014. Last revised July 8, 2014.


```
startTime = AbsoluteTime[];
```

Introduction

The purpose of this notebook is to create hillshade images (from an ASCII DEM) that are illumined in a user-specified direction. The user can also specify the elevation of the illumination, between 0 degrees (at the horizon) and 90 degrees (at the zenith, directly overhead).

Code

Input the data file

This code reads an external data file that is in the form of an ASCII DEM file, with the .dat file-type designator. On Vince Cronin's office Macintosh, the Import code would look like the following for a data file named "tahoedem.dat" located on the desktop:

```
initialDataFile = Import["/Users/vince/Desktop/tahoedem.dat"];
```

On the Dell computer in Cronin' s office, the Import code would look like the following for a data file named "tahoedem.dat" located on the C drive in the "TahoeRuns" directory :

```
SetDirectory["C:\TahoeRuns"];
initialDataFile = Import["tahoedem.dat"];
```

Use the appropriate **Import** code below, and make sure it is in the **Input** style.

```
initialDataFile = Import["/Users/vincecronin/Desktop/thinDVFZCrop.dat"];
```

```
ncols = initialDataFile[[1, 2]];
```

```
nrows = initialDataFile[[2, 2]];
```

```
xllcorner = initialDataFile[[3, 2]]

yllcorner = initialDataFile[[4, 2]]
```

Provide input related to contrast and illumination direction

```
sunAzimuth1 = 302;
```

```
sunElevation = 15;
```

Make the hillshade image

```
demImgFile = Table[initialDataFile[[i + 6, j]] , {i, nrows}, {j, ncols}];

Clear[initialDataFile];

elev1 = Table[demImgFile[[i, j]], {i, nrows, 1, -1}, {j, ncols}];

lightDir1 = sunAzimuth1 * (π / 180);

sunElev = (sunElevation * π) / 180;

hillshadeMap1 = ReliefPlot[elev1,
   ColorFunction -> "GrayTones", LightingAngle -> {lightDir1, sunElev}];

Show[hillshadeMap1]
```

The `gridNorthAdjustment` is the angle between true north and grid north at/near the center of the map area. If grid north is found by a clockwise rotation from true north, the sign of the `gridNorthAdjustment` is negative; otherwise, it is positive. The `gridNorthAdjustment` is approximately equal to (zoneMeridian – (longitude at center of map area))*Sin[latitude at center of map area].

The `zoneMeridian` is the longitude at the center of the UTM zone that contains the epicentral region. If the epicenter is near a zone boundary, base the UTM grid for this analysis in the zone that is to the west.

```
zoneMeridian = -117;

gridNorthAdjustment = (zoneMeridian - (-120.125)) * Sin[39.425 Degree]
```

How long did this program take to run, in minutes?

```
minutesForProcessing = (AbsoluteTime[] - startTime) / 60

ClearAll[nrows, ncols, xllcorner, yllcorner,
  demImgFile, elev1, lightDir1, sunElev, hillshadeMap1];
```

APPENDIX B

An Example of Input to the SLAM Code

The Microsoft *Excel* spreadsheet format as observed in Table B.1 was used as input to the *Mathematica* SLAM code (available at http://croninprojects.org/Vince/SLAM/CurrentBaseCodes.html).

Table B.1 Input to the SLAM Code, in Microsoft *Excel* Format

Year	Month	Day	Hour	Minute	Second	Latitude	Longitude	Depth	EH1	EH2	EH1Az	Ez	Mag
2014	8	26	12	33	16.86	38.17817	-122.30150	12.6	0.1	0.1	1	0.2	3.9

Table B.1, continued from above

Null_ref1	Null_ref2	NP1_DipDir	NP1_DipAng	NP1_Rake	NP2_DipDir	NP2_DipAng	Strike Uncer.	Dip Uncer.	Rake Uncer.
		85	90	180	175	90	5	38	25

Where the headers represent the following:

Year – Year of event

Month – Month of event (1-12)

Day – Day of event (in days of the month)

Hour – Hour of event (1-24)

Minute – Minute of event (0-60)

Second – Second of event (0-60)

Latitude – Latitude of epicenter, in degrees N from equator

Longitude – Longitude of epicenter, in degrees E from prime meridian

Depth – Depth to earthquake hypocenter, in km

EH1- Horizontal error in x-orientation of epicenter location, in km

EH2- Horizontal error in y – orientation of epicenter location, in km

EH1Az – Axis of greatest uncertainty in the horizontal plane, in degrees from N (000°)

Ez – Error in hypocenter depth, in km

Mag – magnitude of the event

Null_ref1 – Placeholder for event reference number (user-preference)

Null_ref2 – Placeholder for event reference number (user-preference)

NP1_DipDir – Dip direction of the first nodal plane (should be the preferred nodal plane), in azimuth from N (000°)

NP1_DipAng – Dip angle of the first nodal plane, in degrees from horizontal (positive input indicates dip down from horizontal)

NP1_Rake – Orientation of slip of the first nodal plane, in degrees from strike (90° from dip direction)

NP2_DipDir – Dip direction of the second nodal plane, in azimuth from N (000°)

NP2_DipAng – Dip angle of the second nodal plane, in degrees from horizontal (positive input indicates dip down from horizontal)

Strike Uncer. – Uncertainty in the dip direction of nodal planes, in degrees

Dip Uncer. – Uncertainty in the dip angle of nodal planes, in degrees

Rake Uncer. – Uncertainty in the rake of nodal plane slip, in degrees

APPENDIX C

GPS Strain Data, derived from Cronin (2014a) and UNAVCO (2014), relative to the North American plate.

Table C.1 Pre-Earthquake GPS strain data, with associated errors

Station	Lat (deg)	Long (deg)	Orientation to WNFZ	Pre- N Vel (mm/yr)	Pre - N Err (mm/yr)	Pre - E Vel (mm/yr)	Pre - E Err (mm/yr)
P194	38.18571777	-122.8162587	West	28.22	0.634	-19.368	0.496
P196	38.29814522	-122.7464297	West	25.248	0.652	-17.129	0.499
P198	38.259875899	-122.607451546	West	23.147	0.64	-16.213	0.494
P200	38.239832642	-122.451703296	West	19.059	0.674	-14.555	0.514
P202	38.423581928	-122.496001317	West	17.663	0.643	-13.492	0.493
P261	38.152961137	-122.217540135	South	14.35	0.657	-11.962	0.548
P263	38.577695190	-122.429176865	North	14.93	0.644	-11.494	0.512
P264	38.442154700	-122.19533064	East	10.379	0.744	-10.724	0.579
P265	38.530186117	-121.954195540	East	7.754	0.666	-9.88	0.516
P266	38.183968807	-121.843527331	East	8.21	1.05	-10.209	0.791
P267	38.380336146	-121.823235255	East	8.031	0.875	-9.317	0.699

Table C.2 Coseismic GPS strain data, with associated errors

Station	Coseimsic-N offset(mm)	Coseismic-N Err (mm)	Coseismic-E offset (mm)	Coseismic-E Err (mm)
P194	0.8	0.9	-3.3	0.8
P196	2	1.1	-5.7	1.1
P198	4.5	0.9	-9.5	1.4
P200	17.3	1.7	-19.1	2.1
P202	8.7	1.4	-16.1	1.8
P261	-14.6	1.8	25.7	3
P263	-1.3	0.8	-2.1	0.8
P264	-16.8	2.2	-10.8	1.4
P265	-2	1.1	-3.1	1
P266	-0.4	1	2.9	1.1
P267	-1.2	1.3	1	1.3

Table C.3 Post-Earthquake GPS strain data, with associated errors

Station	Post - N Vel (mm/yr)	Post - N Err (mm/yr)	Post - E Vel (mm/yr)	Post - E Err (mm/yr)	Post - Z Vel (mm/yr)	Post - Z Err (mm/yr)
P194	29.01	3	-19.5	0.05	-0.57	0.38
P196	26.04	0.04	-17.22	0.06	-0.72	0.23
P198	23.9	0.1	-16.22	0.17	-0.93	0.52
P200	19.84	0.07	-14.59	0.08	-2.48	0.27
P202	18.45	0.06	-13.57	0.13	-0.4	0.32
P261	15.09	0.2	-11.09	0.26	-0.54	0.35
P263	15.66	0.05	-12.03	0.12	-1.27	0.3
P264	11.21	0.06	-10.77	0.11	0.89	0.27
P265	8.53	0.09	-9.86	0.07	-2.63	0.15
P266	8.85	0.07	-10.3	0.08	-0.96	0.19
P267	8.78	0.12	-9.36	0.12	-2.68	0.17

APPENDIX D

Fisher Statistics Example

The code for this computation is available via http://croninprojects.org/Vince/Codes/FisherStats.nb (Cronin, 2011).

This computation is an example of a Fisher statistics calculation using strike and dip measurements of bedding obtained at Alston Park in Napa (lat/long: 38.32661° N, 122.34444° W). Data is input as an excel spreadsheet of strike and dip measurements with the first column representing the right-hand-rule strike azimuth in degrees, and the second column as the dip angle in degrees.

Table D.1 Input for Fisher Statistics Calculations, in Microsoft *Excel* Format

Strike (Right-hand-rule, degrees)	Dip angle (degrees West)
124	42.5
121	39
119	44
134	39
132	41
135	36
125	35

The output of the notebook provides values for: mean dip azimuth (meanDipAzimuth), mean strike (meanStrike), uncertainty in the strike value (strikeUncertainty), mean dip angle (meanDipAngle), the angular radius of the cone of the 95% confidence interval around the mean vector, in radians (alphaNinetyFive), and the precision parameter, k

(precisionparameterK, larger numbers indicate increasingly colinear vectors). For this example, results are output as:

Output

The numerical output below is rounded to the nearest integer value. All angles and azimuths are expressed in degrees.

```
In[135]:= meanDipAzimuth
Out[135]= 217

In[136]:= meanStrike
Out[136]= 127

In[137]:= strikeUncertainty
Out[137]= 6

In[138]:= meanDipAngle
Out[138]= 40

In[139]:= alphaNinetyFive
Out[139]= 4

In[140]:= precisionParameterK
Out[140]= 185
```

The code also generates a lower-hemisphere equal area projection of statistics for the calculated values:

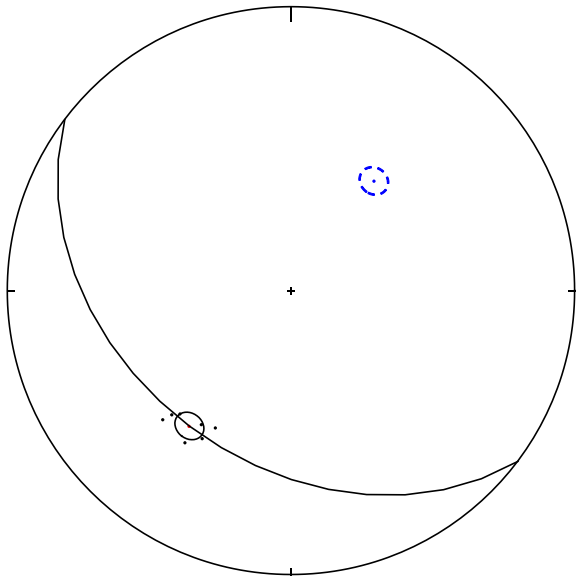

The mean dip vector (red dot) is displayed inside a small circle with the radius of alphaNinetyFive, which represents the 95% confidence interval of that value. The dip vectors are overlain as black dots to show accuracy and precision of dip angle values. A

great circle trace of the average plane strike runs through the mean dip vector, and the pole of the average plane (blue dot) is shown with 95% confidence interval (dashed blue circle).

REFERENCES CITED

Atwater, T., 1970, Implications of plate tectonics for the Cenozoic tectonic evolution of western North America: Geological Society of America Bulletin, v. 81, p. 3513-3536.

Barnhart, W.D., Murray, J.R., Yun, S.H., Svarc, J.L., Samsonov, S.V., Fielding, E.J., Brooks, B.A., and Milillo, P., 2015, Geodetic constraints on the 2014 M 6.0 South Napa Earthquake: Seismological Research Letters, v.86, no. 2A, p. 335-343, doi:10.1785/0220140210.

Bayliss, B.G., 2007, Test of a method for recognizing unmapped seismogenic faults [M.S. thesis]: Waco, Baylor University, 79 p.

Boatwright, J., Blair, J.L., Aagaard, B.T., and Wallis, K., 2015, The distribution of red and yellow tags in the city of Napa: Seismological Research Letters, v. 86, no. 2A, doi: 10.1785/022014023.

Brocher, T.M. et al., 2015, The M 6.0 24 August 2014 South Napa Earthquake: Seismological Research Letters, v. 86, no. 2A, p. 309-326, doi: 10.1785/0220150004.

Brossy, C., Kelson, K., and Ticci, M., 2010, Digital compilation of data for the Contra Costa Shear Zone for the Northern California Quaternary Fault Map Database: Final technical report, collaborative research with William Lettis & Associates, Inc., and the U.W. Geological Survey, available on the world wide web, accessed 1 April 2016 at http://earthquake.usgs.gov/research/external/reports/07HQGR0063.pdf.

Bryant, W.A., compiler, 2000a, Fault number 36a, West Napa fault, Browns Valley section, *in* Quaternary Fault and Fold Database of the United States: U.S. Geological Survey on the world wide web, accessed March 2016, at http://earthquakes.usgs.gov/hazards/faults.

———, 2000b, Fault number 36b, West Napa fault, Napa County Airport section, *in* Quaternary Fault and Fold Database of the United States: U.S. Geological Survey on the world wide web, accessed March 2016, at http://earthquakes.usgs.gov/hazards/faults.

Bryant, W.A. and Hart, E.W., 2007, Fault-rupture hazard zones in California: California Department of Conservation, California Geological Survey, Special Publication 42, 42 p.

California Department of Conservation, 2015, 2002 California fault parameters available on the world wide web, accessed February 2016, at http://www.conservation.ca.gov/cgs/rghm/psha/fault_parameters/htm/Pages/ca_flt_parameters_sfbay1.aspx#West%20Nap.HTM.

California Earthquake Clearinghouse, 2015, South Napa, USA Clearinghouse on the world wide web, accessed September 2014, at http://www.eqclearinghouse.org/2014-08-24-south-napa/.

California Geological Survey (CGS), 2015, Quaternary and pre-Quaternary faults of California: ArcGIS data on the world wide web, accessed September 2015, at http://www.arcgis.com/.

Caporali, A., 2003, Average strain rate in the Italian crust inferred from a permanent GPS network – I. Statistical analysis of the time-series of permanent GPS stations: Geophysics Journal International, v. 155, p. 241-53.

Cloos, H., 1928, Experiments on inner structure (Tectonics): Centralblatt for Mineral. Geol. Und Palaontol., (West Germany), p. 609-621.

Cronin, V.S., 2008, Finding the mean and 95 percent confidence interval of a set of strike-and-dip or lineation data: Environmental and Engineering Geoscience, v. 14, no. 2, p. 113-119.

———, 2011, Fisher Statistics, Trend & Plunge Version: available on the world wide web, accessed September 2015, at http://croninprojects.org/Vince/Codes/FisherStats.nb.

———, 2014a, Infinitesimal strain analysis using GPS data: Module for structural geology or geophysics course, available on the world wide web, accessed March 2015, at https://www.unavco.org/education/resources/educational-resources/lesson/majors-gps-strain/majors-gps-strain.html#extension.

———, 2014b, Seismo-Lineament Analysis Method (SLAM), Using Earthquake Focal Mechanisms to Help Recognize Seismogenic Faults, *in* Proceeding of the 5th International INQUA Meeting on Paleoseismology, Active Tectonics and Archeoseismology, 21-27 September 2014, Busan, Korea: Seoul, Republic of Korea, The Geological Society of Korea, p. 28-31 (available on the world wide web at http://www.croninprojects.org).

———, 2014c, SLAM Workflow: available on the world wide web, accessed September 2014, at http://croninprojects.org/Vince/SLAM/SLAMWorkflow.html.

Cronin, V.S., Millard, M., Seidman, L., and Bayliss, B., 2008, The Seismo-Lineament Analysis Method (SLAM): A reconnaissance tool to help find seismogenic faults: Environmental and Engineering Geoscience, v. 14, no. 3, p. 199-219, doi: 10.2113/gseegeosci.14.3.199.

Davis, G.H., Bump, A.P., Garcia, P.E., and Ahlgren, S.G., 2000, Conjugate Riedel deformation band shear zones: Journal of Structural Geology, v. 22, p. 169-190.

EERI, 2014, M 6.0 South Napa earthquake of August 24, 2014: EERI Special Earthquake Report, October 2014, 27 pp.

Eidinger, J., ed., 2015, South Napa M 6.0 Earthquake of August 24, 2014: G&E Engineering Open-File Report: available on the world wide web, accessed January 2016, at http://www.geengineeringsystems.com/ewExternalFiles/NAPA%202014%20Rev%201.pdf.

Environmental Systems Research Institute (ESRI), 2015, Data for geographic basemaps: available on the world wide web, accessed September 2015, at http://www.arcgis.com/.

Figuers, S., 1991, The tectonics of western Solano County *in* Figuers, S., Prince, R., Eppink, J., Erskine, M., Baldwin, R., Crane, R., Halliday, J., and Crane, K., eds., Field Trip Guide to the Geology of Solano County: Northern California Geological Society and Association of Engineering Geologists Field Trip, October 12, Pleasanton, CA, p. 160-171.

Fisher, R.A., 1953, Dispersion on a Sphere: Proceedings of the Royal Society of London. Series A, Mathematical and Physical Sciences, v. 217, no. 1130, p. 295-305.

Galehouse, J.S. and Lienkaemper, J.J., 2003, Inferences drawn from two decades of alinement array measurements of creep on faults in the San Francisco Bay region: Bulletin of the Seismological Society of America, v. 93, no. 6, p. 2415-2433.

Gan, W., Svarc, J.L., Savage, J.C., and Prescott, W.H., 2000, Strain accumulation across the Eastern California Shear Zone at latitude 36°30'N: Journal of Geophysical Research, v. 105, no. B7, p. 16,229-16,236.

Geomatrix Consultants, Inc. (Geomatrix), 1998, Final Report, Walnut Creek Water Treatment Plant Expansion, Seismic Study – Phase II: Unpublished consulting report prepared for East Bay Municipal Utility District, October 30, 63 pp.

Helley, E.J. and Herd, D.G., 1977, Map showing faults with Quaternary displacement, northeastern San Francisco Bay region, California: U.S. Geological Survey Miscellaneous Field Studies Map MF-881, 1 sheet, scale 1:125,000.

Jennings, C.W., Strand, R.G., Rogers, T.H., and California Department of Conservation, 1977, Geologic Map of California: Division of Mines and Geology, Digital Map, available on the world wide web, accessed October 2015, at http://www.conservation.ca.gov/cgs/cgs_history/Pages/2010_ faultmap.aspx.

Jennings, C.W., 1994, Fault activity map of California and adjacent areas with locations and ages of recent volcanic eruptions: California Geological Survey Geologic Data Map No. 6, scale 1:75,000, Department of Conservation.

Kahle, H., Straub, C., Reilinger, R., McClusky, S., King, R., Hurst, K., Veis, G., Kastens, K., and Cross, P., 1997, The strain rate field in the eastern Mediterranean region, estimated by repeated GPS measurements: Tectonophysics, v. 294, p. 237-52.

Kelson, K.I., Unruh, J.R., and Baldwin, J.N., 2005, Late Quaternary deformation in the northeastern East Bay hills, San Francisco Bay region (abs): Geological Society of America, Abstracts with Programs, v. 37, no. 4, p. 106.

Kelson, K., and Wesling, J., 2015, Appendix B.1: Preliminary observations of surface cracking within the epicentral area of the M 6.0 South Napa earthquake of August 24, 2014 *in* August 24, 2014 South Napa, California Earthquake: GEER Report GEER-037, available on the world wide web, accessed February 2016, at http://www.geerassociation.org/GEER_Post%20EQ% 20Reports/SouthNapa_2014/.

Lancaster, D.S., 2011, Correlation of earthquakes with seismogenic faults along the Northern Arizona Seismic Belt, southwestern margin of the Colorado Plateau [M.S. thesis]: Waco, Baylor University, 107 p.

Lawson, A.C., Gilbert, G.K., Reid, H.F., Branner, J.C., Fairbanks, H.W., Wood, J.F., Hayford, J.F., Baldwin, A.L., Omori, F., Leuschner, A.O., Davidson, G., Matthes, F.E., Anderson, R., Louderback, G.D., Holway, R.S., Eakle, A.S., Crandall, R., Hoffman, G.F., Warring, G.A., Hughes, E., Rogers, F.J., Baird, A., and others, 1908, The California earthquake of April 18, 1906 -- Report of the State Earthquake Investigation Commission in two volumes and atlas: Washington, D.C., The Carnegie Institution, Publication No. 87; available on the world wide web, accessed February 2016, at http://publicationsonline.carnegiescience.edu/publications_online/earthquake_volume/.

Lindsay, R.D., 2012, Seismo-Lineament Analysis of selected earthquakes in the Tahoe-Truckee area, California and Nevada [M.S. thesis]: Waco, Baylor University, 159 p.

Millard, M.A., 2007, Linking onshore and offshore data to find seismogenic faults along the Eastern Malibu coastline [M.S. thesis]: Waco, Baylor University, 147 p.

Miller, C., 2014, Napa Quake Forces Redrawing of Fault Maps: KQED Science: available on the world wide web, accessed September 2014, at http://ww2.kqed.org/science/2014/09/02/napa-quake-forces-redrawing-of-fault-maps/.

Miranda, E. and Aslani, H., 2000, Brief report on the September 3, 2000 Yountville/Napa, California earthquake: Pacific Earthquake Engineering Research (PEER) Open-File Report, Berkeley, CA, available on the world wide web, accessed September 2015, at http://peer.berkeley.edu/publications/yountville-napa_sep-2000.html.

Morelan, A.E., Trexler, C.C., and Oskin, M.E., 2015, Surface-rupture and slip observations on the day of the 24 August 2014 South Napa earthquake: Seismological Research Letters, v. 86, no. 4, p. 1-9.

NCEDC, 2014a, Northern California Earthquake Catalog search, double-difference catalog 1984 to present: Northern California Earthquake Data Center, UC Berkeley Seismological Laboratory, Dataset, doi:10.7932/NCEDC, available on the world wide web, accessed 1 April 2016, at http://www.ncedc.org/ncedc/catalog-search.html.

———, 2014b, Northern California Earthquake Catalog search, mechanism catalog 1968 to present: Northern California Earthquake Data Center, UC Berkeley Seismological Laboratory, Dataset, doi:10.7932/NCEDC, accessed 1 April 2016, at http://www.ncedc.org/ncedc/catalog-search.html.

———, 2015, Northern California Earthquake Data Center, UC Berkeley Seismological Laboratory, Dataset, doi:10.7932/NCEDC.

Reed, T.H., 2014, Spatial correlation of earthquakes with two known and two suspected seismogenic faults, North Tahoe-Truckee area, California [M.S. thesis]: Waco, Baylor University, 105 p.

Resor, P.G., Cronin, V.S., Hammond, W.C., Pratt-Sitaula, B., and Olds, S.E., 2014, A Teachable Moment in Earth Deformation: An Undergraduate Strain Module Incorporating GPS Measurement of the August 24, 2014 M 6.0 South Napa Earthquake, presented at 2014 Fall Meeting, American Geophysical Union, San Francisco, California, 15-19 December 2014, Abstract S33F-4951 (documents available via UNAVCO on the world wide web, accessed October 2015, at http://www.unavco.org/education/resources/educational-resources/lesson/majors-gps-strain/napa/napa.html).

Riedel, W., 1929, Zur mechanic Geologischer Brucherscheinungen: Zentralblatt fur Mineralogie, Geologie und Palaontologie B., p. 354-368.

SCEDC, 2013, Significant Earthquakes and Faults: Fort Tejon Earthquake: available on the world wide web, accessed January 2016, at http://scedc.caltech.edu/significant/forttejon1857.html.

Seidman, L.E., 2007, Seismo-Lineament Analysis of the Malibu Beach Quadrangle, Southern California [M.S. thesis]: Waco, Baylor University, 106 p.

Tchalenko, J.S., 1970, Similarities between shear zones of different magnitudes: Geological Society of America Bulletin, v. 81, p. 1625-1640.

UNAVCO, 2014, PBO Network Monitoring: available on the world wide web, accessed March 2015, at http://www.unavco.org/instrumentation/networks/status/pbo.

Unruh, J.R., Kelson, K.I., and Barron, A., 2002, Critical evaluation of the northern termination of the Calaveras fault, eastern San Francisco Bay area, California: Final Technical Report, U.S. Geological Survey, National Earthquake Hazards Reduction Program Award No. 00-HQ-GR-0082, July, 72 p.

U.S. Geological Survey (USGS), 2000, The September 3, 2000 Yountville earthquake: U.S. Geological Survey Earthquake Hazards Program, available on the world wide web, accessed March 2016, at http://www.strongmotioncenter.org/NCESMD/data/yountville_03sep2000/eqinfo.htm.

———, 2012, Earthquake Hazards Program: The Great 1906 San Francisco Earthquake: available on the world wide web, accessed January 2016, at http://earthquake.usgs.gov/regional/nca/1906/18april/index.php.

———, 2015a, Earthquake Hazards Program: Earthquake Archives: available on the world wide web, accessed September 2014, at http://earthquake.usgs.gov/earthquakes/search/.

———, 2015b, M6.0 – South Napa Earthquake: available on the world wide web, accessed October 2014, at http://earthquake.usgs.gov/earthquakes/eventpage/nc72282711#general_summary.

———, 2015c, The National Map Viewer: available on the world wide web, accessed September 2014, at http://viewer.nationalmap.gov/viewer/.

———, 2015d, Quaternary Fault and Fold Database for the United States: available on the world wide web, accessed September 2014, at http://earthquake.usgs.gov/hazards/qfaults/.

———, 2015e, South Napa Earthquake – One Year Later: available on the world wide web, accessed March 2016, at http://www.usgs.gov/blogs/features/usgs_top_story/south-napa-earthquake-one-year-later/.

Waldhauser, F., 2015, Real-time double-difference earthquake locations for Northern California (1984 – 2011): available on the world wide web, accessed February 2016, at http://ddrt.ldeo.columbia.edu/DDRT/index.html.

Weaver, C.E., 1949, Geology and mineral deposits of an aera north of San Francisco Bay, California: California Division of Mines Bulletin 149, p. 135.

Wesling, J.R. and Hanson, K.L., 2008, Mapping of the West Napa fault zone for input into the Northern California Quaternary Fault Database: USGS Final Technical Report, External Grant No. 05HQAG0002, 61 p., available on the world wide web, accessed October 2015, at http://earthquake.usgs.gov/research/external/reports/05HQAG0002.pdf.

Williams, J., Verdin, T., Leff, L., Thanawala, S., and Bonnell, C., 2014, Napa earthquake is area's strongest in 25 years: KCRA News, available on the world wide web, accessed March 2016, at http://www.kcra.com/news/usgs-60-earthquake-shakes-northern-california/27703718.